PHYSICAL AND CHEMICAL INTERACTIONS OF LUBRICANTS IN HYBRID BEARING SYSTEMS

By

ROBERT SABIA

A DISSERTATION PRESENTED TO THE GRADUATE SCHOOL
OF THE UNIVERSITY OF FLORIDA IN PARTIAL FULFILLMENT
OF THE REQUIREMENTS FOR THE DEGREE OF DOCTOR OF PHILOSOPHY

UNIVERSITY OF FLORIDA

1997

Dedicated in loving memory of my father, Raffaele Sabia.

ACKNOWLEDGMENTS

Funding for this work was provided by the Air Force Office of Scientific Research, Grant No. F49620-93-1-0349DEF. Experiments were performed at the University of Florida's Department of Materials Science and Engineering, Department of Chemistry, Major Analytical Instrumentation Center (MAIC), and at the United Technologies Pratt & Whitney location in West Palm Beach, Florida.

The author wishes to acknowledge the guidance and support of various faculty, staff, and student members of the Department of Materials Science and Engineering and Department of Chemistry. The inspiration and direction of Dr. James H. Adair was essential in the successful completion of this work. The guidance of Dr. Paul H. Holloway, Dr. John J. Mecholsky, Dr. E. Dow Whitney, and Dr. James D. Winefordner was most appreciated. Further instruction and assistance was received from Dr. David Allen, Dr. Michael Kaufman, and Dr. Ben Smith.

From Pratt & Whitney in West Palm Beach, Florida, special thanks is given to Susan C. Brown and Dr. Herbert Chin for their assistance in the development of my understanding of gas turbine engine operation and lubricant performance. With respect to experiments performed in the Fuels and Lubricants Laboratory at Pratt & Whitney, thanks is given to the laboratory staff for technical assistance.

With regards to the development of UV/VIS absorption spectrometry as a technique for oil monitoring, special recognition is given to Dr. Joseph Simmons and Kevin Powers for their help in data analysis and interpretation. Further help was also received from Robin Russell and Dr. Benjamin W. Smith.

With regards to laboratory assistance, David Mitchell and Ken Shannon are recognized for sample preparation and equipment operation. For assistance with infrared spectrometry analysis, Dr. Jim Kunetz and Guy La Torre (currently of US Biomaterials Corporation) are thanked. For assistance with molecular weight analysis, gratitude is given to Michael Zamora and Ahmad R. Hadba. Helpful discussion and direction were also received from Dr. Sridhar Venigalla, Dr. Tuo Li, Dr. Robert Chodelka, Craig Habeger, Tom Miller, Jeff Kerchner, Paul Demkowicz, and Dr. Melanie Carasso.

Finally, the author would like to thank his wife, Yi, for her love and support throughout his graduate career. Especially during the last few months, her strength and encouragement have endured and are the greatest reason for the successful completion of this dissertation. Support from his family throughout his education is greatly appreciated.

TABLE OF CONTENTS

ACKNOWLEDGEMENTS iii

LIST OF TABLES viii

LIST OF FIGURES ix

ABSTRACT xiii

CHAPTERS

1. INTRODUCTION 1

- 1.1. Overview 1
- 1.2. Motivation 2
- 1.3. Chapter Summaries 3
  - 1.3.1. Introduction to Ball Bearing Systems 3
  - 1.3.2. Oil Degradation and Resulting Effects on Friction and Wear 3
  - 1.3.3. A Kinetic Study of Oil Degradation 4
  - 1.3.4. The Use of UV/VIS Spectrometry for Oil Monitoring 5

2. LITERATURE REVIEW 7

2.1 Introduction 7
- 2.2. The Gas Turbine Engine 7
- 2.3. Lubrication System and Environment 9
- 2.4. Bearing Materials 10
  - 2.4.1. M-50 Steel 11
  - 2.4.2. Silicon Nitride 11
  - 2.4.3. Synthetic Lubricants 14
  - 2.4.4. Synthetic Ester Lubricants 16
  - 2.4.5. Perfluoropolyethers 17
- 2.5. Bearing Design 21
- 2.6. Failure Behavior 25
- 2.7. Oil Analysis 29
- 2.8. Summary 30

3. EFFECTS OF OIL DEGRADATION ON THE FRICTION AND WEAR PROPERTIES OF SILICON NITRIDE/M-50 STEEL SLIDING COUPLES 32

- 3.1. Introduction 32
- 3.2. Background 32

3.2.1. Bearing Design 33
3.2.2. Wear of Bearing Components 34
3.2.3. Behavior of Lubricants 34
3.2.4. Oil Monitoring 35
3.2.5. Oil Degradation Mechanisms 37
3.2.6. Objective 39
3.3. Materials and Methods 39
3.4. Results and Discussion 44
3.4.1. Rheological Analysis 44
3.4.2. Water Content Analysis 50
3.4.3. Spectroscopic Analysis 45
3.4.4. Molecular Weight Analysis 54
3.4.5. Tribological Analysis 56
3.5. Conclusions 57

4. A KINETIC STUDY ON THE DEGRADATION EFFECTS OF VARIOUS ENVIRONMENTAL PARAMETERS 62

4.1. Introduction 62
4.2. Background 63
4.2.1. Oil Degradation Mechanisms 63
4.2.2. Current Oil Monitoring Techniques 65
4.2.3. Previous Kinetic Studies 67
4.2.4. Objective 69
4.3. Materials and Methods 69
4.4. Results and Discussion 74
4.4.1. Rheological Analysis 75
4.4.2. Chemical Analysis 75
4.4.3. Molecular Weight Analysis 80
4.4.4. Peak Analysis 86
4.4.5. Analysis of the Volatiles 93
4.4.6. Rate of Degradation 98
4.5. Conclusions 105

5. THE USE OF UV/VIS SPECTROMETRY FOR OIL MONITORING 108

5.1. Introduction 108
5.2. Background 108
5.2.1. Oil Monitoring Techniques 109
5.2.2. Ultraviolet/Visible Absorption Spectrometry 110
5.2.3. Objective 112
5.3. Materials and Methods 112
5.4. Results and Discussion 117
5.4.1. Sample Characterization 118
5.4.2. Total Loss Edge Analysis 119

        - 5.4.3. Variations in Total Loss Edge Values in Chapters 3 and 5.............124
        - 5.4.4. Absorption Behavior of the Degraded Oil Samples..........................125
        - 5.4.5. Absorption Behavior and Degradation Product Concentration 129
        - 5.4.6. Degradation Product Concentration Versus Particle Volume........134
        - 5.4.7. Association of Absorbance Peaks 135
        - 5.4.8. Comparison of Peak Area and Total Loss Edge Analysis...............136
    - 5.5. Conclusions 142

6. CONCLUSIONS AND SUGGESTED FUTURE WORK..145

- 6.1. Overview 145
- 6.2. Conclusions 146
    - 6.2.1. Oil Degradation and Resulting Effects on Friction and Wear........146
    - 6.2.2. A Kinetic Study of Oil Degradation 147
    - 6.2.3. The Use of UV/VIS Spectrometry for Oil Monitoring.....................149
- 6.3. Suggested Future Work..151
    - 6.3.1. Effects of Oil Degradation on Wear Properties.................................151
    - 6.3.2. Confirmation of Polycondensation Reaction Mechanism................152
    - 6.3.3. UV/VIS Absorption Spectrometry for Oil Monitoring....................153
- 6.4. Summary..154

LIST OF REFERENCES...155

BIOGRAPHICAL SKETCH..163

LIST OF TABLES

Table page

2-1. Physical properties of M-50 steel, magnesia doped silicon nitride, and yittria/alumina doped silicon nitride [Ara88,Bla92,Can91,Gal92,Luc92]............... 12

2-2 Critical properties of lubricants for conventional turbine engines [courtesy of Susan C. Brown, United Technologies Pratt & Whitney]....................................... 16

3-1 Physical data determined for samples from three heating schedules. “Sch” refers to schedule number and “hrs” refers to hours tested.. 45

3-2. Tribological data generated for the oil samples using a pin-on-disk apparatus. “Sch” refers to schedule number and “hrs” refers to hours tested.. 55

4-1. List of degradation experiments for the kinetic study.. 70

4-2. List of correlation coeffiencents and slopes for plot of Growth Factor versus test time shown in Figure 4-17(a).. 99

4-3. List of values for fractional particle volume (ϕ) calculated for the oil samples using Eq. 4-3.. 101

5-1. List of degradation experiments used for UV/VIS spectrometry testing................ 113

5-2. List of concentrations (weight percent) and normalized absorbance peak areas (given in percent change) for OX12NC 13 hour test sample diluted in as-received oil.. 127

5-3. List of values for fractional particle volume (ϕ) calculated for the oil samples using Eq. 5-4.. 135

5-4. List of correlation coefficients and slopes for linear regression analysis performed on absorbance versus time plots shown in Figure 5-11.......................... 142

LIST OF FIGURES

Figure page

2-1. Cross-sectional schematic of the Pratt & Whitney F-100 gas turbine engine (courtesy of United Technologies Pratt & Whitney) .8

2-2. Schematic of a standard gas turbine engine showing each of the different compartments [Uni88]. .8

2-3. Structures for pentaerythritol ester (a) and 1,1,1-trimethylolpropane ester with minimum molecular weights of 374 and 302 respectively [Bak92]. 19

2-4. Structure of tricresylphosphate [Sha94] 19

2-5. Schematic showing the intermolecular disproportionation process, also refereed to as acid catalyzed cleavage [Del94,Kas91a,Kas91b,Kas92]. 20

2-6. Schematic of the structure for Krytox [Dup95,Kas91a,Kas91b,Kas92] 20

2-7. Schematic of a ball bearing system and the elastic deformation between the rolling element and raceway at the contacts, as expected under elastohydrodynamic lubricating conditions [Jac91] 23

2-8. Graphical representation of how the contact angle in a bearing changes during operation. β_o and β_i indicate changes in the contact angles with respect to each raceway [Ham94] 23

3-1. Heating schedules for oil degradation experiments. Error bars reflect standard deviation 40

3-2. Assembly for degradation experiments 40

3-3. UV/VIS spectrometry data for samples run according to heating schedule 1 46

3-4. UV/VIS spectrometry data for samples run according to heating schedule 2 47

3-5. UV/VIS spectrometry data for samples run according to heating schedule 3 48

3-6. Total loss edge versus change in viscosity, showing a linear relationship with the correlation coefficient r^2=0.96 49

3-7. Infrared spectra for the as-received sample of ETO 2380 (MIL-L-23699) 51

3-8. GPC data for schedule 1. Arrows indicate direction of changes with test time.....52

3-9. GPC data for schedule 2. Arrows indicate direction of changes with test time.....52

3-10. GPC data for Schedule 3. Arrows indicate direction of changes with test time. (note: Molecular weight range differs from previous figures)..........53

3-11. Coefficient of friction data for oil samples plotted versus molal concentration of the degradation product (Eq. (3-2)). Lines refer to a linear regression fit with m= 0.023 and corresponding 95% confidence intervals..........58

3-12. Rate of wear data for pin surfaces given in weight loss versus sliding distance (picograms/meters) plotted against molal concentration of the degradation product for oil the samples (Eq. (3-2))..........59

3-13. Rate of wear data for disk surfaces given in increasing track width versus sliding distance (microns/meters) plotted against molal concentration of the degradation product for oil the samples (Eq. (3-2))..........60

4-1. Assembly for degradation experiments. Water bubbler, presence of M-50 bearing balls placed in the beaker, and gas type dependent on individual test description..........71

4-2. Changes in viscosity as a function of test time for all test series..........76

4-3. Changes in antioxidant content as a function of test time for all test series..........78

4-4. Changes in total acid number as a function of test time..........79

4-5. FTIR spectra for the 13 hours sample from test OX12NC..........81

4-6. Comparison of molecular weight chromatogram and fitted data for the IN12NC 3 hour sample (r^2= 0.999) (a) and peak fit curves generated for the as-received sample (b)..........83

4-7. Comparison of molecular weight chromatogram curves for tests IN12NC (a) and OX12NC (b)..........84

4-8. Comparison of 1050 and 225 molecular weight curves for tests IN12NC, (a) and (b), and for OX12NC, (c) and (d)..........85

4-9. Viscosity changes versus changes in percent area of peak 1. Plotted lines correspond to oxidative environments ($y = 5.11 \cdot 10^{-6} \cdot x^{3.95}$) with r^2=0.82 and non-oxidative environments ($y = 0.019 \cdot x - 1.75$) with r^2=0.94..........88

4-10. Changes in total acid number versus changes in percent area for peak 1. Plotted lines correspond to oxidative environments ($y = 5.43 \cdot 10^{-7} \cdot x^{3.66}$) with r^2=0.75 and non-oxidative environments ($y = 2.95 \cdot 10^{-4} \cdot x^{1.77}$) with r^2=0.92. 89

4-11. Changes in antioxidant content versus normalized height for peak 5. Fitted line reflects $y = 33.04 \cdot x^{0.23}$ with r^2=0.98. 90

4-12. Changes in viscosity versus normalized height for peak 5. 91

4-13. Changes in normalized height of peak 5 versus test time for all test series 92

4-14. FTIR spectrums for volatile phases condensed from test OX12NC. The denser phase (a) consists of a water solution, and the less denser phase (b) consists of an ester. 95

4-15. Molecular weight distribution for condensed volatiles from test OX12NC at 3 and 7 hour test times. 96

4-16. Water content for tests performed in oxidative environments 97

4-17. Rate of growth for high molecular weight degradation species (a) and viscosity versus growth of the high molecular weight species following parabolic equation $y = 0.036 - 1.82 \cdot x + 4.51 \cdot x^2$ (b) 103

4-18. Changes in molecular weight distribution versus molecular weight and corresponding radius of gyration values for the high MW degradation product 104

5-1. Assembly for degradation experiments. Water bubbler, presence of M-50 bearing balls placed in the beaker, and gas type dependent on individual test description 114

5-2. UV/VIS spectra for tests IN12NC (a) and OX12NC (b), plotted as % transmittance versus Wavelength. 121

5-3. Total loss edge versus changes in viscosity. Lines reflect oxidative ($y = 482.91 \cdot x^{0.10}$) and non-oxidative environments ($y = 8.11 \cdot x + 515.13$) with correlation coefficients of r^2=0.96 122

5-4. Total acid number results versus antioxidant content (a) and antioxidant content versus viscosity changes (b). Dotted lines indicate onset of chemical degradation in the oil samples 123

5-5. Absorbance spectra for tests IN12NC (a) and OX12NC (b) 126

5-6. Changes in the absorbance spectra for the OX12NC, 13 hour sample as a function of concentration of degraded oil diluted in as-received oil (a), and changes in intensities for 355, 415, and 500 nm peaks with changes in concentration (b) 128

5-7. Absorbance values for peaks 2 and 3 as a function of concentration for the OX12NC 13 hour sample diluted in as-received oil. Linear regression coefficients and slopes for peaks 2 and 3 are r^2=0.99, m=4.07 and r^2=0.98, m=4.16 respectively 131

5-8. Changes in absorbance (a) for peak 2 ($y = 0.86 \cdot x^{1.34}$) area and peak 3 ($y = 0.14 \cdot x^{1.68}$) area with correlation coefficients of r^2=0.93 and 0.95 respectively , and changes in viscosity (b) versus changes in area of the high moleular weight species. with coefficients of r^2=0.82 and 0.93 for the oxidative and inert environments respectively 132

5-9. Changes in absorbance peak 2 and 3 areas versus changes in growth factor for the high molecular weight degradation species with correlation coefficients of r^2=0.96 133

5-10. Relative concentration of high molecular weight species versus particle volume for absorbance peak 2 (a) where r^2=0.93 and m=1.34, and for peak 3 (b) where r^2=0.92 and m=1.55 137

5-11. Changes in absorbance peaks 2 and 3 as a function of test time with linear regression for each test series. 139

5-12. Total loss edge versus test time for degraded oil samples 140

5-13. Total loss edge versus absorbing peaks 2 and 3 areas. Fitted curves reflect ($y = 190.59 \cdot x^{0.16}$) for peak 2 and ($y = 273.68 \cdot x^{0.14}$) for peak 3 with correlation coefficients of r^2=0.98 and 0.99 respectively 141

Abstract of Dissertation Presented to the Graduate School
of the University of Florida in Partial Fulfillment of the
Requirements for the Degree of Doctor of Philosophy

PHYSICAL AND CHEMICAL INTERACTIONS OF LUBRICANTS IN HYBRID BEARING SYSTEMS

By

Robert Sabia

May, 1997

Chairman: James H. Adair
Major Department: Materials Science and Engineering

Experiments designed to evaluate the effects of oil degradation on bearing performance were carried out on a commercial synthetic lubricant (MIL-L-23699) at temperatures between 200-300°C. Characterization included analysis of coking and preliminary analysis using UV/VIS spectroscopy as a technique for oil monitoring. Tribological experiments were performed using a pin-on-disk test machine with yttria/alumina doped silicon nitride and M-50 steel test materials with hardness and surface finish indicative of bearing grade materials. Results showed a general increase in friction with decreasing oil condition, and results from wear testing showed no correlation with oil condition.

A kinetic study of the effects of various environmental parameters on oil degradation was performed at 250°C. Environmental parameters included testing in oxidative and non-oxidative environments and investigating the presence of M-50 steel as a catalyst material at both low and high relative humidity. Analysis included changes in the rates of degradation for the various environmental parameters, as well as analysis of antioxidant removal and subsequent effects on the formation of high molecular weight degradation products. Results showed that the presence of M-50 steel acted to increase the rate of oil degradation while high humidity lowered the rate of degradation. Water was also found to be a primary degradation products. From the beneficial affect of high humidity and from the generation of water as a byproduct, the mechanism for the formation of high molecular weight degradation products is proposed to be a polycondensation reaction. Furthermore, diffusion is proposed to be rate limiting for this process .

An investigation into the use of ultraviolet/visible absorption spectrometry as a technique for oil monitoring was carried out on oil samples generated at 250°C. Analysis included determining the mechanism for spectral changes and determining effects of environmental parameters on associated changes. Results showed spectral changes with degradation to be the result of changes in intensity for absorption peaks which represented the base stock and degradation products. The behavior of these absorption peaks followed the Beer-Lambert law and can be used to represent the concentration of degradation product.

CHAPTER 1

INTRODUCTION

1.1. Overview

Increasing requirements in the performance characteristics of load bearing systems call for a better understanding of system behavior. Specifically for applications under extreme environments, understanding the interactions between various components is critical. Without advances in the knowledge of how such systems operate and fail, improvements in design and implementation are limited.

For bearing systems used in gas turbine engines, increasing demands include greater thrust-to-weight ratios and longer lifetimes A significant step was made in achieving these goals when silicon nitride materials were implemented for the rolling elements in hybrid bearing systems [Han88,Sil90,Ste90,Wed87]. This achievement allowed for bearing systems with lower weights and resulting centripetal forces, helping to achieve both of the previously mentioned demands. However, the requirement for further improvements still exists and is being pursued.

Work presented in this thesis is the direct result of endeavors motivated by the lack of understanding in the failure behavior of hybrid bearing systems utilized in gas turbine engines. The approach was specifically designed to develop a more complete understanding of performance and failure characteristics through the analysis of the lubrication systems employed with these bearings. Objectives included developing an understanding of how the lubricants degrade, determining the influences of degradation on the performance characteristics of bearing systems, and developing a means of monitoring performance and predicting failure.

Oil degradation experiments were performed using Exxon turbine oil ETO 2380, a commercially available ester-based synthetic lubricant meeting military specifications MIL-L-23699. Advantages to using a conventional lubrication system include the direct application to industry. Disadvantages result from the proprietary nature of the base stock, additives, and mixing ratios, resulting in limited interpretation of chemical changes which result from degradation.

1.2. Motivation

Results of oil analysis from fatigue testing performed by MRC Bearings, Inc.[1] using V-groove test machines suggested competing degradation mechanisms. Chemical analysis performed using infrared spectroscopy yielded inconclusive results. Peak broadening effects could not be attributed to the generation of any specific structure, as new ester, carboxylic acid, or ketone molecules were all possibilities. Evident from molecular weight analysis was the formation of high molecular weight species (MW>2500), which subsequently disappeared upon further testing. This observation was attributed to coking, the formation of a high molecular weight structures which typically sediment from the oil and coat engine components. By nature, either transesterification, the formation of acids, or the formation of ketones would result from an oxidation reaction, while coking would result from a reduction reaction. Due to the amount of air which is introduced into the lubrication systems, results suggest that tribochemical reactions which take place on highly active surfaces promoted the coking behavior.

1.3. Chapter Summaries

1.3.1. Introduction to Ball Bearing Systems

Chapter 2 serves as an introduction to the gas turbine engine and ball bearing system. Topics covered include engine description, bearing materials, bearing design, failure behavior, and oil analysis. Specific attention is given to the different classes of and to the failure behavior of lubricants. Through description of the turbine engine and lubrication system, the importance of each component to performance and failure is shown.

1.3.2. Oil Degradation and Resulting Effects on Friction and Wear

The objective for the initial work performed in Chapter 3 was to generate laboratory experiments which would either support or disprove the observations and hypotheses of coking behavior from the preliminary research. This was accomplished by thermally degrading samples of the ETO 2380 conventional turbine oil (MIL-L-23699) for various durations at extreme temperatures (>200°C). Samples were analyzed for degradation behavior and the formation of high molecular weight species which might reflect coking. Further information as to the influences oil degradation has on bearing

---

[1] MRC Bearings Division of SKF Aerospace Bearings, USA, Inc., Jamestown, NY 14702

performance was measured by using the degraded oil samples for friction and wear testing performed on a pin-on-disk test machine.

Results show the successful generation of higher molecular weight species which reflect coking. A linear relation is also shown between total loss edge data and percent change in viscosity, suggesting a possible method for oil characterization. Tribology testing performed using the oil samples show increasing coefficient of friction with increasing degradation. Wear experiments show no correlation with oil degradation.

1.3.3. A Kinetic Study of Oil Degradation

Preliminary research raised questions as to how the individual effects of oxidative and tribochemical degradation mechanisms affect performance characteristics of the turbine oils. Answering these questions is the first step in developing methods for monitoring oil condition in an effort to determine engine lifetime. As a result, the objectives for Chapter 4 were to separate the individual effects of various degradation parameters and mechanisms. Oil degradation experiments were performed under both inert and oxidative atmospheres, promoting thermal degradation mechanisms and a combination of thermal and oxidative degradation mechanisms respectively. Further parameters introduced to these experiments were the presence of a catalyst material in the form of M-50 tool steel, and low and high humidities introduced through the gas source. In this manner, characterization performed on the generated oil samples yielded insight as to the individual affects of these four parameters.

Results show negligible difference in physical and chemical changes with respect to humidity and catalyst effects for samples tested in non-oxidative environments.

Results from experiments performed under oxidative environments show the presence of catalyst material to increase the rate of degradation and the presence of high humidity to decrease the rate of degradation. Furthermore, significant degradation is shown to occur only after the depletion of antioxidant, and the rate of reaction after antioxidant depletion is shown to be diffusion limited.

From the results, the mechanisms for the formation of high molecular weight degradation products are proposed. During the initial stages of testing, degradation is attributed to the formation of free radicals which promote the generation of primary degradation products before being rendered inactive by the antioxidant. After antioxidant depletion, the primary degradation products undergo a polycondensation reaction which is promoted by the free radicals and generates water as a product.

1.3.4. The Use of UV/VIS Spectrometry for Oil Monitoring

Interest in developing a technique for monitoring oil performance during engine operation was one of the main goals for this research endeavor. In Chapter 3, results are presented which suggest that absorption characteristics in the ultraviolet/visible region of the electromagnetic spectrum can be used to predict physical changes resulting from degradation. In order to pursue this concept, values for total loss edge data was determined for each of the test samples generated in Chapter 4 and compared with results from physical and chemical characterization of the samples.

Results show spectra changes to be the result of absorbance peaks located at 355, 415, and 500 nm. The 355 nm peak represents absorption behavior of the as-received oil, whereas the 415 and 500 nm peaks represent the high molecular weight degradation product. Changes in absorbance peak intensities are shown to dictate the total loss edge, thus both absorbance and loss edge values are representative of oil degradation. However, absorbance changes for the 500 nm peak are shown to be the best representation of oil condition.

CHAPTER 2

LITERATURE REVIEW

2.1. Introduction

The need for continual improvements in load bearing applications has resulted in the increasing replacement of metal components with those made of various ceramic materials. More specifically, advances in design and processing have resulted in the replacement of all-metal bearings with hybrid bearings for aerospace applications. However, little is known of the failure behavior of these materials, therefore limiting further advances which could be possible due to design improvements and failure prediction. The need to understand the failure behavior of these devices includes analysis of all components involved, i.e., rolling elements, raceways, and lubricants. This chapter summarizes various aspects of bearing design and operation. Topics include operating environment, materials, design, failure, and oil monitoring.

2.2. The Gas Turbine Engine

In order to determine the wear behavior of these bearing systems, it is important to understand typical operating environments and conditions encountered. Figure 2-1 shows a schematic of the F-100 gas turbine engine which was developed by Pratt & Whitney and currently incorporates hybrid bearings. This engine operates as follows (see Figure 2-2 for compartment locations) [Uni88]. Air drawn in through the air inlet duct is

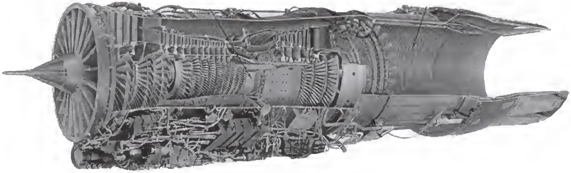

Figure 2-1. Cross-sectional schematic of the Pratt & Whitney F-100 gas turbine engine (courtesy of United Technologies Pratt & Whitney).

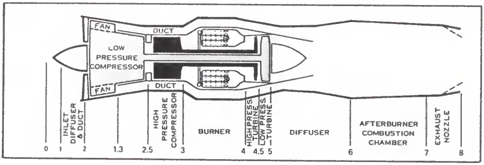

Figure 2-2. Schematic of a standard gas turbine engine showing each of the different compartments.[Uni88]

increased to 315°C in the low pressure compression chamber by the compressive effect of the air inlet, then further increased to 538°C in the high pressure compression chamber. The air stream then passes through the combustor, where fuel is injected into the stream and ignited to generate temperatures reaching 2100°C. The air stream is then cooled to 1425°C by air vented into the chamber after the combustor, thus producing a temperature withstandable by the turbine. Passing through the turbine section, the air stream then forces rotation of the turbine blades before exiting the engine and generating thrust. The turbine blades are split into two sections, each of which are attached to individual shafts that connect the turbine blades to the low and high pressure compressor blades. The forced rotation of the turbine blades therefore forces the rotation of the compressor blades and eliminates the need to mechanically rotate any of these systems aside from startup. The main bearings are located along the shafts which connect the turbine and compressor blades.

2.3. Lubrication System and Environment

The purpose of the lubrication system of a gas turbine engine is to lubricate, cool, and clean the bearings, gearbox, and accessory drives [Uni88]. The system supplies oil from a common tank to each location, first circulating the oil through filters to remove contaminants and debris. In the case of the main bearings, correct oil pressure is achieved by bleeding air into the oil, and subsequently removing most of the air before returning the oil to the tank. Through this cycle, oil used for all components is subjected to pressures and temperatures common to each engine part, and the oil absorbs any detrimental constituents contained in the air [Uni88]. These constituents can include unburned fuel, burnt fuel products (e.g., water vapor), and oxidants [Dan91].

The most extreme environment for the oil is found in the main bearings located along the shafts which connect the compressor and turbine blades. Bearings in conventional gas turbine engines operate between 2-3 million DN (bore radius × RPM), with oil flow rates on the order of 80,000 cc/min, and a Hertzian contact stress of 2.1 GPa (300,000 psi) [Ara88]. Although bulk bearing operating temperatures range between 75-150°C, frictional heating between rolling elements and raceways result in temperatures up to 350°C at the contacts [Kla85,Kla91]. These temperatures well exceed the degradation limits for conventional lubricants.

2.4. Bearing Materials

Failure of bearing systems under high temperature, pressure, and speed conditions is most commonly attributed to the fatigue of raceways and rolling elements. This behavior results as stresses generated by high centrifugal forces and gyroscopic moments initiate subsurface cracking, leading to failure [Ara88,God95,Wed87]. To reduce the occurrence of true fatigue oriented failure and to limit the creation of stress concentrators, requirements for bearing materials include high yield strength, fracture strength, hardness, toughness, corrosion resistance, and low thermal conductivity, at both low and high operating temperatures [Kat90,Luc92,Wak74]. Structural and dimensional stability are important for producing a product which will perform consistently. The development and use of adequate lubricants tailored to specific applications is also critical in designing a bearing system for optimum performance.

2.4.1 M-50 Steel

Over the past few decades, one of the most commonly used metals for aerospace applications has been VIMVAR (Vacuum Induction Melt Vacuum Arc Remelt) M-50 steel [Braz92,Galb92,Wed87]. This specialty steel consists of 0.8-0.85% carbon, 0.15-0.35% manganese, 0-0.25% silicon, 4-4.25% chromium, 0.9-1.1% vanadium, and 4-4.5% molybdenum [Braz92,Boh93]. The final, through-hardened product has a Vickers Hardness of 800-1000 kg/mm^2, with a microstructure consisting of large, elongated carbides. The finishing procedure consists of soft grinding prior to heat treatment followed by hard grinding after heat treatment, both performed using SiC abrasives [Galb92]. Physical properties of the final product are shown in Table 2-1. Application of M-50 steel is limited to temperature conditions not exceeding 300°C, corrosive environments of hydrocarbons, and lubrication using hydrocarbons and some fluorocarbons only [Luc92]. Processing improvements have included removal of O_2 contamination, eliminating hard oxide inclusions which act as stress concentrators [Galb92].

2.4.2 Silicon Nitride

Due to the need to improve bearing performance and efficiency by developing systems with higher speed and temperature limits, ceramic materials have been investigated. From materials such as Al_2O_3, ZrO_2, SiAlON, TiC, and SiC, silicon nitride (Si_3N_4) has proven far superior due to the best combination of properties. Table 2-1 shows the most relevant physical properties for silicon nitride. Performance improvements over M-50 steel include higher operating speeds, higher service temperature, better corrosion resistance, better rigidity, lower torque, lower heat-up, lower wear, no magnetism, no electrical conductivity, and no seizing, all of which translate to longer service life [Luc92,Ste90]. Also beneficial is the flexibility of lubricants eligible to be used in conjunction with Si_3N_4, which include hydrocarbons, water, steam, solid lubricants, refrigerants, and transfer films [Galb92]. This broad variety is made possible due to silicon nitride's thermodynamic instability in air, which allows the generation of inert surface layers which protect the material from corrosion [Jah94,Kop75].

Table 2-1. Physical properties of M-50 steel, magnesia doped silicon nitride, and yttria/alumina doped silicon nitride [Ara88,Bla92,Can91,Galb92,Luc92].

Material Property	M-50 Steel	MgO-Si_3N_4	Y_2O_3-Al_2O_3-Si_3N_4
Density (g/cc)	7.8	3.16	3.23
Poisson's Ratio	0.3	0.26	0.29
Elastic Modulus (GPa)	207	320	308
Vickers Hardness (GPa)	8-10	16.6	14-16
Coefficient of Thermal Expansion ($x10^{-6}$/K)	12	2.9	2.9-3.2
Specific Heat (J/kg×K)	450	800	800
Thermal Conductivity (W/m×K)	30	29.3	18-25
High Temperature use (K)	600	1300	1300
Fracture Toughness (MPa×$m^{1/2}$)	>16	4.1	6-8

Fabrication of silicon nitride components typically includes consolidation of the powder using such techniques as slip casting. Preparation of stable suspensions is of vital importance in generating homogeneous forms appropriate for further processing. Dispersion of silicon nitride for slipcasting applications typically incorporates water as the solvent. Silicon nitride is very soluble in water, as amine (Si-NH_2) and secondary amine (Si_2=N-H) surface groups react to form hydroxide (Si-O-H) and oxide surfaces (SiO_2) [Ada96,And84,Ber89,Gala95,Gee94,Kop75,Lyc91]:

$$@\ pH<9,\quad Si_3N_{4(s)} + 6H_2O_{(l)} \rightleftharpoons 3SiO_{2(s)} + 4NH_{3(g)} \qquad [2.1]$$

$$@\ pH>9,\quad SiNH_{2(s)} + H_2O_{(l)} \rightleftharpoons SiOH_{(aq)} + NH_{3(g)} \qquad [2.2]$$

Reaction [2.1] does not proceed to completion. The SiO_2 surface layer acts to passivate the core of the Si_3N_4 particle, thus protecting from further degradation. The aforementioned surface groups can also significantly affect powder processing behavior. For example, the isoelectric point for α-Si_3N_4 powder in water can vary between pH 3 and pH 9, depending on the ratio of amine to silanol surface groups, and the extent of oxidation [Ber90,Lut94].

As well as being advantageous for stabilization in aqueous environments, the resulting SiO_2 surface layer is also beneficial during heat treatment, as reaction with dopants aids in the formation of a silicon-oxynitride (Si_2ON_2) liquid phase at elevated temperatures [Han88,Zut94]. This glassy, intergranular phase acts as a solvent for silicon nitride, allowing for the dissolution of α- Si_3N_4 and reprecipitation of β- Si_3N_4. Viscosity of the liquid phase is governed by the additive types and concentrations, thus determining appropriate sintering temperatures and maximum working temperatures of the final parts.

The most commonly used sintering aids are MgO, Al_2O_3, and Y_2O_3. MgO is preferred as the main additive for bearing grade materials, due to the fact that MgO promotes a glassy, intergranular phase which has a lower viscosity at sintering temperatures [Han88,Ste90]. This ensures the attainability of 100% dense structures. The lower viscosity at elevated temperatures also lowers the maximum working temperature of the material, however this temperature is well above the operating temperatures for both liquid and solid lubrication techniques.

Processing of bearing grade silicon nitride involves mechanical mixing of constituents under clean room conditions to minimize contamination, cold forming to 50-70% theoretical density, and then hot isostatic pressing (HIPing) at 1800°C and 30,000 psi to 100% theoretical density. Finishing techniques consist of lapping with diamond abrasives [Fag90,Galb92]. The resulting microstructure consists primarily of elongated β-Si_3N_4 grains less than 0.5 μm in size, with high aspect ratios. Mechanical properties are isotropic, with the elongated grains leading to high fracture energy and grain pullout [Han88,Zut94].

Physical properties of the final material are strongly influenced by phase composition and processing. As stated earlier, the final density is influenced by types of sintering additives used. Less than 100% dense materials will contain inclusions which become stress raisers, particularly under rolling contact. Grain size and morphology also play a significant influence on the physical properties of the final product. The large aspect ratio of the reprecipitated β-Si_3N_4, as well as the percent conversion of α to β and the amount of silicon oxynitride phase present, dictate properties such as mechanical strength and toughness [Han88,Zut94]. Further influencing the performance of silicon nitride is the formation of a protective oxide surface layer on the final product.

2.4.3 Synthetic Lubricants

Two main categories of lubricants exist for load bearing applications: liquid and solid lubricants. Liquid lubricants offer advantages over solid lubricants primarily from ease of handling, self-replenishing capabilities, cooling capabilities, lower temperature applications, and the ability to form a seperatory film between surfaces, with the main limitation being high temperature capabilities [But90,Sek92,Wed87]. Applications under increasingly adverse environments have resulted in the development of synthetic oils, which offer advantages over conventional petroleum-based oils primarily due to easy addition and mixing of additives resulting in the ability to tailor lubricant composition based on desired performance [Gun62,Sek92]. Examples of performance advances include increased fire resistance, low viscosity-temperature coefficients, and low vapor pressure [Kla85,Sek92]. Even more essential, synthetic oils do not oxidize as rapidly at extreme temperatures as petroleum oils and, therefore, are suitable for higher temperature applications. Table 2-2 lists some of the more critical properties of synthetic lubricants and resulting impacts on performance characteristics. Applications under high temperature, pressure, and speed conditions call for the use of solid lubricants, which are presently being investigated and developed for future application [Sli92].

Synthetic oils used for extreme applications include those composed of organic esters, polyglycols, synthetic hydrocarbons, phosphates, silicones, and fluorocarbons [Kir85]. Additives for ester based and other synthetic oils are categorized as polymers, polar compounds, and compounds with active elements and are identified as polymers, antioxidants, lubricity additives, metal deactivators, detergents, and dispersants [Fei92,Kla85]. Understanding the degradation behavior of these oils is essential for improving system behavior and extending system lifetime. Thermal instability, metallic corrosion, and lubricant oxidation are the primary sources of breakdown for oil lubricants [Jon85a,Kla85].

Table 2.2. Critical properties of lubricants for conventional turbine engines [courtesy of Susan C. Brown, United Technologies Pratt & Whitney].

Property	Significance/Influences
Viscosity	Heat generation Elastohydrodynamic film and bearing life Lubricant system pressure Component size Pumpability
Density	Lubricant system pressure Component size System Weight
Vapor Pressure	Component pressure and operability Fluid loss Pump performance
Thermal and Oxidative Stability	Bearing operating temperatures Coking System weight
Autoignition Temperature	Bearing component operating temperature System weight
Specific Heat	Heat exchanger size
Thermal Conductivity	Heat exchanger size
Load Carrying Capacity	Gear system (speeds and sizes)

2.4.4. Synthetic Ester Lubricants

Conventional gas turbine engines use synthetic oils which meet military specifications MIL-L-7808 and MIL-L-23699. The synthetic base esters are composed of pentaerythritol ester and 1,1,1-trimethylolpropane ester (Figure 2-3), which are generated by the estrification of pentrerythritol and trimethylpropane alcohols with various acids [Bak92,Jon85a]. Examples of the MIL-L-23699 specification include Mobil Oil Corporation's Mobil Jet II[1] and Exxon Corporation's ETO 2380 synthetic oils[2]. Research performed using these lubricants is complicated by proprietary nature of the lubricant formulations with respect to base oil, additives, and mixing ratios. Determining the oil's chemistry is a difficult task, which includes separation of components and individual identification using a number of analytical techniques. Of particular importance are additives which inhibit wear of surfaces and the oxidative degradation of the base stock.

---

[1] Mobil Oil Corporation, Fairfax, VA. 22037.

[2] Exxon Company USA, A Division of of the Exxon Corporation, Houston, TX 77252.

The antiwear additive for these lubricants is known to be tricresylphosphate (TCP). The chemical structure for TCP is shown in Figure 2-4. TCP acts to prevent hybrid bearing system failure by reacting with the surface of M-50 steel to generate a protective surface layer of $FePO_4$ by specific reaction of the phosphate atom with iron sites on the surface [Gat91]. This hard surface film increases resistance to wear and therefore can extend system lifetime. However, removal of this surface film in the form of debris can be detrimental by promoting failure via overrolling.

Antioxidants act to prevent degradation of the lubricant and therefore extend bearing lifetime. Current understanding of the mechanisms for degradation of these oils shows that degradation results from a free radical chain mechanism [Bak92,Hsu86,Hun93a,Kau95a,Kla85]. The antioxidant acts to eliminate this propagation mechanism by donating a proton to satisfy the free radical. This process results in creating a free radical antioxidant unit, which is self-satisfied by resonance. In this manner, antioxidants act to delay the free radical chain mechanism of degradation until depleted [Kau95a].

2.4.5. Perfluoropolyethers

Perfluoropolyethers (PFPE), also known as perfluoroalkylethers (PFAE) or perfluoropolyalkylethers (PFPAE), are a category of lubricants which have been recently considered for application in ball bearing systems. Significant advantages over conventional ester based lubricants include a larger liquid-phase temperature range, low vapor pressure, small temperature dependence of viscosity, higher thermal stability, and low chemical reactivity [Kas91a,Kas91b,Kas92]. Of particular emphasis is a thermal stability, as high as 350°C, and the inability of these materials to ignite. However, limitations and disadvantages of these materials do exist.

The structure of PFPE's include trifluoromethyl groups connected in chains between ether linkages. Also present in some structures, acetal groups ($-O-CF_2-O-$) play important roles in determining stability at elevated temperatures. Degradation at elevated temperatures in the presence of metals can occur at temperatures as low as 185°C, when metal surfaces act as catalysts in breaking the structure at the acetal linkage via an intermolecular disproportionation process referred to as acid catalyzed cleavage (see Figure 2-5) [Dup95,Kas91a,Kas91b,Kas92]. Reaction products between oil and steel surfaces such as FeF_3 act as Lewis acids and form a bidentate linkage with oxygens from two ether linkages [Car86,Mor89]. A fluorine atom transfer then occurs between an adjacent $-CF_2-$ group and the acetal group, resulting in a scission in the chain. For the case of PFPE's which do not have acetal groups but rather ether linkages with longer chains between, this type of degradation is also possible. However, differences can include an increased resistance to acid catalyzed cleavage due to chain length, which separates ether linkages and dictates cis or trans positioning, and a lower rate of degradation because the scission process occurs closer to the ends of the structures.

Emphasis in this research has fallen one on particular type of PFPE. Krytox (Figure 2-6) is composed of 21.6% carbon, 9.4% oxygen, and 69.0% fluorine, and is identified in the Chemical Abstracts Index as oxirane, trifluoro (trifluoromethyl)-, homopolymer with a CAS Registry Number 60164-51-4 [Dup95,Kas91a,Kas91b,Kas92].

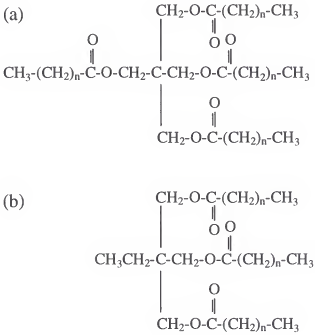

Figure 2-3. Structures for pentaerythritol ester (a) and 1,1,1-trimethylolpropane ester with minimum molecular weights of 374 and 302 respectively [Bak92].

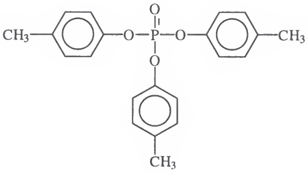

Figure 2-4. Structure of tricresylphosphate [Sha94].

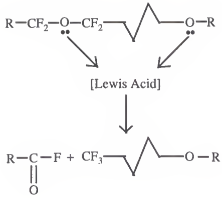

Figure 2-5. Schematic showing the intermolecular disproportionation process, also refereed to as acid catalyzed cleavage [Del94,Kas91a,Kas91b,Kas92].

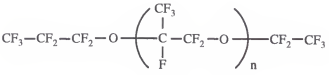

$$CF_3-CF_2-CF_2-O\left(\underset{F}{\overset{CF_3}{C}}-CF_2-O\right)_n-CF_2-CF_3$$

where n = 10 to 60

Figure 2-6. Schematic of the structure for Krytox [Dup95,Kas91a,Kas91b,Kas92].

The structure includes ether linkages which are separated by chains two carbon units long. This even number of carbons dictates that oxygen atoms from the ether linkages will be in trans positions relative to one another. Further shielding occurs due to pendant CF_3 groups. These effects result in better thermal stability of Krytox in comparison to other PFPE's.

The degradation behavior of Krytox varies upon environment [Del94,Dup95]. Normally stable in air to temperatures above 350°C, the presence of various metals (e.g.: M-50) and metal oxides initiate degradation at temperatures as low as 288°C. Degradation products of Krytox in air include perfluoroacetylfluoride (CF_3COF) and carbonyl fluoride (COF_2). In the presence of moisture, both of these degradation products can hydrolyze to form hydrogen fluoride.

Further disadvantages of using this category of synthetic lubricants has recently become evident for silicon nitride systems [Yoa95]. The presence of fluorine has been shown to accelerate subcritical crack growth, leading to premature failure. However, this observation has only been shown for yittria doped silicon nitride, raising the question of whether or not fluorinated lubricants may be used with magnesia doped materials.

2.5. Bearing Design

Ball bearings (Figure 2-7) are designed to allow the ball elements to roll along the inside of the raceway, generating subsurface tensile stresses which ultimately should lead to spalling along either component as the source of failure [Jac91]. Conventional design incorporates materials with high elastic moduli, such as metals and ceramics, and the use of liquid lubricants which reflect Newtonian behavior to generate a contact area which are consistent with elastohydrodynamic lubrication (EHL) [Den95,Ham85,Jac91,Wak74].

With ideal rolling contact and EHL behavior, the ball and outer raceway elastically deform under high pressures within the contact region, generating a larger contact area. Oil is drawn into the contact region under hydrodynamic lubrication. The high pressure increases the lubricant viscosity, creating a film which separates the ball and raceway, allowing the ball to roll with only a small degree of sliding [Jac91,Wak74]. The higher the viscosity, the thicker the film and, therefore, the better protection against wear [Lin94]. However, non-ideal behavior does exist within rolling bearing systems [Jac91]. Larger amounts of slip and spin result as centripetal forces and gyroscopic moments separate the contact angle between raceways (Figure 2-8), increasing torque and breaking down the EHL layer [Den95,Gen94,Jac91,Sli94]. Surfaces come into contact, generating high wear rates and increased temperatures. Further deviations from ideal behavior occur as the high centripetal forces increase the Hertzian contact zone on the outer raceway and decrease the zone on the inner raceway, resulting in the specific breakdown of the EHL layer on the inner raceway. The combination of these non-ideal behaviors result in the generation of other modes of lubrication, namely those characteristic of dry lubrication and boundary lubrication, in which surface wear and tribochemical reactions occur to a much greater extent [Wak74]. This combination of lubricating modes requires the understanding of not just fatigue lifetime testing, but also friction and wear testing.

Hybrid bearings consisting of silicon nitride rolling elements and M-50 steel raceways offer advantages over all-metal systems by exhibiting lower wear rates and longer lifetimes due to lower density rolling elements and other physical properties shown for silicon nitride in Table 2-1. Primary benefits over all-metal bearings include higher temperature applications, higher corrosion resistance, higher thermal shock resistance,

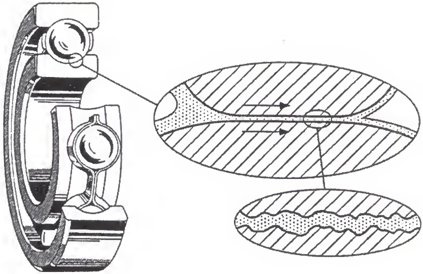

Figure 2-7. Schematic of a ball bearing system and the elastic deformation between the rolling element and raceway at the contacts, as expected under elastohydrodynamic lubricating conditions [Jac91].

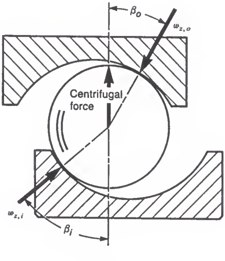

Figure 2-8. Graphical representation of how the contact angle in a bearing changes during operation. β_o and β_i indicate changes in the contact angles with respect to each raceway [Ham94].

lower weight, non-magnetic behavior, and electrical resistance.[Han88,Ste90] Furthermore, hybrid bearings improve lubricant performance due to nongalling behavior and improved surface finish, therefore allowing higher speeds and accelerations [Ara88,Sil90]. The high temperature limitations of conventional oil lubricants do not play a significant role since maximum operational temperatures of the bearings do not exceed those of the lubricants [Ara88]. Comparison of the performances of hybrid to all-metal bearings yields a tenfold increase in wear resistance and a three to fivefold increase in fatigue life [Han88,Sil90].

All-ceramic bearing systems made exclusively of silicon nitride rolling elements and raceways further broaden bearing applications which are limited for hybrid bearings by steel components. Ceramic bearings offer advantages such as high temperature limits greater than 1000°C, high speed capabilities, increased lifetime and wear resistance, minimal lubrication requirements, and resistance to stress rupture, creep, fatigue, and corrosion [Han88,Lin94,Par75,Sil90]. Avenues other than oil lubricants must be pursued for application under the extended temperature ranges available with these bearings. Ceramic bearings yield 10-50 times greater fatigue life than steel bearings; however, ceramic bearings do exhibit three times more torque than hybrid bearings, increasing slip and sliding behavior [Sil90]. Further disadvantages include processing costs and mounting difficulties [Han88,Ste90].

Analysis of bearing components before installation is vital in eliminating defective parts from service [Bra49,Gee94,God95]. Inclusions created by contaminants during heat treatment and surface asperities generated during finishing must be detected. Damage to components resulting from handling, both before and after finishing, can also lead to premature failure. Commonly used techniques for detection of these types of defects in both silicon nitride and M-50 steel components include x-ray radiography, high frequency ultrasonic testing, acoustic microscopy, thermal imaging, fluorescent die penetrant testing, and light microscopy [Galb92]. These nondestructive types of evaluation are used on-line to analyze all parts being processed.

2.6. Failure Behavior

The failure behavior of bearing systems can be dramatically altered by material selection, environment, and lubricant specification. In aerospace applications, bearing systems are introduced to high temperatures generated by engine performance, high stresses from centripetal forces and gyroscopic moments, and highly corrosive environments consisting of combustion products, oxidants, and unburned fuels[Bro90,Dan91,Par75]. Physical and chemical characteristics of each component in a given system affect performance and failure. Determining the role each of these factors have on the failure behavior of bearing systems is vital for improving system performance and lifetime.

Typical failure in metal bearings under rolling contact is induced by classical fatigue failure [Ara88,God95,Wed87]. As previously mentioned, stresses generated by high centrifugal forces create subsurface cracks in the rolling element and outer raceway. These cracks propagate and result in the removal of large portions of material, referred to as spalls. When failure in metal bearings initiates, the EHL film breaks down and allows the ball and raceway to come into contact, causing friction and increasing temperature at the contact. Besides increasing temperature, wear, and vibrations, spalling can also result in welding at the contact, causing catastrophic failure in the bearing.

For hybrid bearing systems, failure rarely occurs as a result of classical fatigue, but rather due to surface flaw induced failure [Braz89,Gee94,God95,Sil90]. Surface imperfections, such as dimensional discrepancies (flaws, pores, impurities), overrolling due to contamination in the lubricant, and corrosion pitting, act to form stress raisers which initiate the fatigue oriented failure. Fatigue failure in ceramic silicon nitride bearings is even more unlikely due to the fact that the previously mentioned nongalling behavior and higher surface finish characteristics promote proper EHL behavior [Sil90]. However, sliding behavior of contacts in ceramic bearings is of more critical concern than with hybrid bearings. Sliding generates tensile stresses in the plane of the sliding surfaces, initiating cracks at the grain boundaries [Sli94]. Grains debond in the form of microfracture wear debris.

As previously mentioned, under current applications where bulk operating temperatures range between 75-150°C, boundary and elastohydrodynamic contact temperatures can reach 250-350°C due to frictional heating [Kla85,Kla91]. Chemical reactions, which normally are nonexistent or of low reaction rate, can be accelerated under these temperature conditions [Gee94]. When operating for extended time at temperatures over 200°C, most commercial ester-based lubricants oxidize, polymerize, or evaporate [Aja92]. The most common mechanisms for the degradation of these hydrocarbon lubricants are oxidative and thermal degradation mechanisms [Hsu86]. Both degradation processes consist of a free radical chain mechanism [Bak92,Hsu86,Hun93a,Jon85a, Jon85b,Kau95a,Kla85]. In these processes, free radicals are generated through either a carbon-carbon scission mechanism [2.3], a hydroperoxide radical mechanism [2.4 and 2.5], or through direct reaction with oxygen [2.6]. Free radical molecules (XH) then act to polymerize other lubricant constituents by starting reaction chains via abstraction of hydrogen atoms from parent hydrocarbons. Antioxidant species act to satisfy these free radicals by donating a hydrogen [2.7].

$$R\text{-}CH_2\text{-}CH_3 \rightarrow R\cdot + R\text{-}CH_2\text{-}CH_2\cdot \qquad [2.3]$$

$$R\cdot + O_2 \rightarrow RO_2\cdot \qquad [2.4]$$

$$RO_2\cdot + RH \rightarrow RO_2H + R\cdot \qquad [2.5]$$

$$RH + O_2 \rightarrow R\cdot + HO_2\cdot \qquad [2.6]$$

$$RO_2\cdot + XH \rightarrow RO_2H + X\cdot \qquad [2.7]$$

Primary ester byproducts include hydroxyl groups (-OH), carbonyl groups (C=O), alkenes (C=C), and conjugated dienes (C=C-C=O).[Bak92,Jon85a] Previously mentioned antioxidant additives act to eliminate this free radical chain propagation mechanism by donating a proton to the free radicals, therefore rendering them inactive. The antioxidant molecule then becomes a free radical, but stabilizes itself by resonance [Hun93a]. In this method, antioxidants delay thermal and oxidation degradation mechanisms until all antioxidants are depleted.

Typical ester degradation products include the formation of carboxylic acids, ketones, aldehydes, alcohol, water, gases, and the formation of new ester species [Bak92,Jon85a]. Both alcohol and water can form when alkyl hydroperoxides thermally degrade and form alkoxy and hydroxy radicals [2.8], which then react with the parent hydrocarbon [2.9 and 2.10] [Jon85a]. The formation of carboxylic acid, aldehyde, and ketone species involves the oxidative degradation of the base ester in the presence of a free radical [2.11] [Bak92]. Transesterification, which can result in the formation of either higher or lower molecular weight molecules, occurs by reaction with an alcohol and is typically catalized by a weak acid [2.12] [Fie50]. The formation of high molecular weight degradation products can occur by condensation reactions between oxidaized ester products [2.13] and is accompanied by the generation of water [Bak92].

$$\mathrm{RH + O_2 \rightarrow RO\cdot + \cdot OH} \qquad [2.8]$$

$$\mathrm{RO\cdot + RH \rightarrow ROH + R\cdot} \qquad [2.9]$$

$$\mathrm{\cdot OH + RH \rightarrow HOH + R\cdot} \qquad [2.10]$$

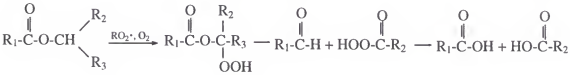

$$\mathrm{R_1\text{-}\overset{O}{\overset{\|}{C}}\text{-}O\text{-}CH\begin{matrix}R_2\\R_3\end{matrix} \xrightarrow{RO_2\cdot,\,O_2} R_1\text{-}\overset{O}{\overset{\|}{C}}\text{-}O\text{-}\underset{OOH}{\overset{R_2}{C}}\text{-}R_3 — R_1\text{-}\overset{O}{\overset{\|}{C}}\text{-}H + HOO\text{-}\overset{O}{\overset{\|}{C}}\text{-}R_2 — R_1\text{-}\overset{O}{\overset{\|}{C}}\text{-}OH + HO\text{-}\overset{O}{\overset{\|}{C}}\text{-}R_2}$$

[2.11]

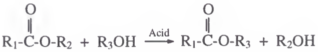

$$\mathrm{R_1\text{-}\overset{O}{\overset{\|}{C}}\text{-}O\text{-}R_2 + R_3OH \xrightarrow{Acid} R_1\text{-}\overset{O}{\overset{\|}{C}}\text{-}O\text{-}R_3 + R_2OH}$$

[2.12]

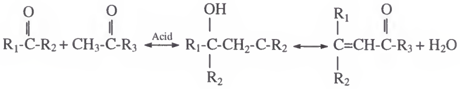

$$\mathrm{R_1\text{-}\overset{O}{\overset{\|}{C}}\text{-}R_2 + CH_3\text{-}\overset{O}{\overset{\|}{C}}\text{-}R_3 \xleftrightarrow{Acid} R_1\text{-}\underset{R_2}{\overset{OH}{C}}\text{-}CH_2\text{-}C\text{-}R_2 \longleftrightarrow \underset{R_2}{\overset{R_1}{C}}{=}CH\text{-}\overset{O}{\overset{\|}{C}}\text{-}R_3 + H_2O}$$

[2.13]

Metallic surfaces and debris have been shown to play an increasing role in ester based lubricant breakdown above 180°C by increasing the rate of degradation [Gat91,Hsu86,Jon85a,Kau85,Kla85,Kla91]. These metallic surfaces can act as catalysts, either inhibiting or promoting oil degradation. Organometallics, oxides, and inorganic compounds all form upon reaction between metal surfaces, oil constituents, and contaminants, acting in the same manner as catalysts [Jon85a,Kla85]. Reactions with metallic debris can be more serious than those with metal surfaces due to higher reactivity of the debris [Kau85]. Ceramic surfaces are less active and have been shown to form passivation layers as previously mentioned [Gat91]. These passivation layers are generated by reaction with water absorbed in the oil and water vapor generated as a combustion product [Dan91,Jon85a]. For ceramics, reactions with oil constituents are limited by the passivation films unless the rate of wear is faster than the reactions. In this manner, the formation of oxide and oxynitride films on silicon nitride can produce lower coefficients of friction and wear rates in hybrid and ceramic bearings [Cra88,Gee94,Kat90,Par75]. However, oxide films formed on metal surfaces result in junction growth [Kat90]. Oxide debris collect around the contact regions and do not lower the coefficient of friction.

2.7. Oil Analysis

Conventional techniques for oil characterization has been well documented [Bel86,Coa86,God95,Hos91,Kau85,Lin94,Loc92,Pac89,Pow93]. Due to the complexity of additive packages used in synthetic oils, analytical techniques must be able to monitor for additive levels, degradation products, and contaminants. Infrared spectroscopy is presently implemented for such analysis due to equipment sensitivity and flexibility [Coa86,Dan91]. Spectrometric techniques, such as atomic absorption (AA), atomic emission spectroscopy (AES), inductively coupled plasma emission spectroscopy

(ICPES), and X-ray fluorescence (XRF), are used for elemental analysis of wear metal concentrations, but are limited by the inability to discern chemical states of elements detected [Hos91,Kau85,Pac89]. Differential scanning calorimetry (DSC) is used to determine thermooxidative stability of the oils [Pac89]. Chromatographic methods, including gas chromatography (GC) and gel permeation chromatography (GPC), are used to discern additive concentrations which are unavailable for proprietary reasons and to determine degradation patterns and products [Jon85a,Pac89]. Ferrography and spectrometry are limited in usefulness, since both techniques require periodic sampling [God95]. Ferrography, along with most other debris collection and sensing devices are also limited to the analysis of magnetic debris only, limiting usefulness as techniques for hybrid and all-ceramic bearing systems [Bel86,Lin94,Sei72].

2.8. Summary

Demands for increasing performance and longer lifetimes of gas turbine engines have resulted in numerous research endeavors into understanding the failure behavior of hybrid bearing systems. Also critical is the identification of a technique to monitor an engine's behavior *in-situ*, therefore predicting and preventing system failure. The most promising approach for analysis of engine performance is monitoring the lubricating system.

The purpose of research performed in this thesis is to gain an understanding of how these lubricating systems fail, and how such failure influences the performance characteristics of the bearing systems. Specific aspects include the thermal degradation of lubricants meeting military specifications MIL-L-23699, and the use of degraded samples in friction and wear tests. Results from kinetic studies designed to analyze the individual effects of various parameters on oil degradation are also presented. Finally, a novel technique for monitoring lubricating systems is presented as a possible method for *in-situ* analysis.

CHAPTER 3

EFFECTS OF OIL DEGRADATION ON THE FRICTION AND WEAR PROPERTIES OF SILICON NITRIDE/M-50 STEEL SLIDING COUPLES

3.1. Introduction

The effect of oil degradation on the wear behavior of the silicon nitride/M50 steel system has been studied. Degraded oil samples were generated by heating a conventional gas turbine lubricant (MIL-L-23699) to temperatures between 200-300°C for various time durations. Sample characterization was performed using total acid number, antioxidant concentration, rheometry, water content, surface tension, spectroscopy, and size exclusion chromatography. Coefficient of friction and rate of wear were measured on the oil samples using a pin-on-disk test apparatus under a Hertzian contact stress of 1.6 GPa at 25±1°C.

3.2. Background

Current understanding of the effects of oil degradation on the wear behavior of the silicon nitride/M-50 system is limited. Lubricants are composed of complex additive packages blended with multiple base stocks. Formulations vary between both vendor and grade. Friction and wear studies performed are usually simplified by testing individual additives and base stocks, allowing easy determination of system interactions and behavior. These simplifications are limited in relation to real-life systems: Interactions between the numerous oil constituents are not observed. Further hindering understanding of these oil systems are degradation tests which are also simplified and do not allow for analysis of competing degradation mechanisms.

3.2.1 Bearing Design

All-metal ball bearings are designed to allow the ball elements to roll along the inside of the bearing raceway, generating subsurface tensile stresses which ultimately should lead to spalling along either component as the source of failure [Jac91]. Conventional design incorporates materials with high elastic moduli, such as metals and ceramics, and the use of liquid lubricants which reflect Newtonian behavior to generate a contact area which are consistent with elastohydrodynamic lubrication (EHL) [Den95,Ham85,Jac91,Wak74]. With ideal rolling contact and EHL behavior, the ball and outer raceway elastically deform under high pressures within the contact region, generating a larger contact area. Oil is drawn into the contact region under hydrodynamic lubrication. The high pressure increases the lubricant viscosity, creating a film which separates the ball and raceway, allowing the ball to roll with only a small degree of sliding [Jac91,Wak74]. The higher the viscosity, the thicker the film and, therefore, the better protection against wear (assuming adequate flow) [Lin94]. However, non-ideal behavior does exist within rolling bearing systems [Jac91]. Larger amounts of slip and spin result as centripetal forces and gyroscopic moments separate the contact angle between raceways, increasing torque and breaking down the EHL layer [Den95,Gen94,Jac91,Sli94]. Surfaces come into contact, generating high wear rates and increased temperatures. The combination of these non-ideal behaviors result in the generation of other modes of lubrication, namely those characteristic of dry lubrication and boundary lubrication, in which surface wear and tribochemical reactions occur to a much greater extent [Wak74].

3.2.2. Wear of Bearing Components

The behavior of wear falls into two general categories, namely mechanical wear and tribochemical wear [Aka90,Kat90,Wak74]. Mechanical wear can include different mechanisms, namely adhesion, abrasion, and fatigue. Tribochemical wear mechanisms include oxidation and corrosion, where contaminants and degradation products react with sliding surfaces to either promote or hinder the rate of material removal. The effectiveness of a given material in preventing the generation of wear is dependent on material properties and surface condition. High yield strength, fracture strength, hardness, toughness, corrosion resistance, and low thermal conductivity at both low and high operating temperatures help to minimize the generation of debris and organometallic products [Kat90,Luc92,Wak74].

3.2.3. Behavior of Lubricants

Under proper EHL conditions, the lubricant offers further advantages by cooling the bearing and removing debris from the contact area. However, under non-idea behavior such as boundary lubrication conditions, the lubricant serves a second purpose by lowering the coefficient of friction and thus minimizing wear. The chemical properties of the lubricant dictate the effectiveness in reducing friction by either forming protective oxide films (typical of silicon nitride reacting with water and M-50 steel reacting with tricresylphosphate) or the formation of organic compounds typically catalyzed by metallic surfaces [Gat91,Kla91]. Additive compounds containing phosphor and sulfur have been shown to lower friction and the rate of wear, whereas chlorine containing compounds have been shown to have the opposite effect [Gat91].

3.2.4. Oil Monitoring

Current oil monitoring techniques fall into three main categories. These categories include study of basic fluid parameters such as viscosity and total acid number, analytical techniques used to determine chemical changes in additive concentrations and base stock, and off-line techniques which have been developed to give quick information on oil condition.

Basic Fluid Parameters

As a first look at the extent of degradation in used oil samples, two basic techniques are used. The extent to which degradation has affected the physical condition of the oil, viscosity testing is employed. To determine the extent to which the oil has chemically degraded, total acid number[1] is determined. Total acid number (TAN) is a technique in which a small amount of the oil sample is dissolved in solvents and titrated using 0.1N alcoholic KOH. As a result, the amount of KOH solution needed to titrate the oil sample to a specific pH represents the concentration of base neutralized acidic sites on the various oil constituents and degradation products.

---

[1] ASTM 664-89.

Analytical Techniques

Due to the complexity of additive packages used in synthetic oils, analytical techniques must be utilized to monitor for additive levels, degradation products, and contaminants. Infrared spectroscopy is presently implemented for such analysis due to equipment sensitivity and flexibility [Coa86,Dan91]. Spectrometric techniques, such as atomic absorption (AA), atomic emission spectroscopy (AES), inductively coupled plasma emission spectroscopy (ICPES), and X-ray fluorescence (XRF), are used for elemental analysis of wear metal concentrations, but are limited by the inability to discern chemical states of elements detected [Hos91,Kau85,Pac89]. Differential scanning calorimetry (DSC) is used to determine thermooxidative stability of the oils [Pac89]. Chromatographic methods, including gas chromatography (GC) and gel permeation chromatography (GPC), are used to discern additive concentrations as well as degradation patterns and products [Jon85a,Pac89].

Off-line Techniques

Over the past decade, a number of techniques have been developed to determine the condition of degraded oil samples. Through the investigations of Kauffman et al, one particular technique has earned most notable recognition: the remaining useful lubricant life evaluation rig[2] (RULLER) [Kau89,Kau95a,Kau95b]. A small sample of degraded oil is dissolved into a solvent and tested using a voltametric method to determine the antioxidant concentration is the oil sample. Taking into account that the lubricant begins to degrade before the antioxidant content is completely depleted, the percent of antioxidant remaining is related to the remaining useful life of the used oil, thus determining when an engine's oil must be changed.

3.2.5. Oil Degradation Mechanisms

The most common mechanisms for the degradation of these polyester lubricants are oxidative and thermal degradation mechanisms [Hsu86]. Both degradation processes consist of a free radical chain mechanism, in which free radicals are generated through either a carbon-carbon scission mechanism [3.1], a hydroperoxide radical mechanism [3.2 and 3.3], or through direct reaction with oxygen [3.4] [Bak92,Hsu86,Hun93a,Jon85a, Jon85b,Kau95a,Kla85]. Free radical molecules (XH) then act to polymerize other lubricant constituents by starting reaction chains via abstraction of hydrogen atoms from parent hydrocarbons. Antioxidant species act to satisfy these free radicals (e.g. R· and $RO_2\cdot$) by donating a hydrogen [3.5].

$$R\text{-}CH_2\text{-}CH_3 \rightarrow R\cdot + R\text{-}CH_2\text{-}CH_2\cdot \qquad [3.1]$$

$$R\cdot + O_2 \rightarrow RO_2\cdot \qquad [3.2]$$

$$RO_2\cdot + RH \rightarrow RO_2H + R\cdot \qquad [3.3]$$

$$RH + O_2 \rightarrow R\cdot + HO_2\cdot \qquad [3.4]$$

$$RO_2\cdot + XH \rightarrow RO_2H + X\cdot \qquad [3.5]$$

Primary ester byproducts include hydroxyl groups (-OH), carbonyl groups (C=O), alkenes (C=C), and conjugated dienes (C=C-C=O) [Bak92,Jon85a]. Previously mentioned antioxidant additives act to eliminate this free radical chain propagation mechanism by

---

[2] University of Dayton Research Institute, Dayton, OH 45469.

donating a proton to the free radicals, therefore rendering them inactive. The antioxidant molecule then becomes a free radical, but stabilizes itself by resonance [Hun93a]. In this method, antioxidants delay thermal and oxidation degradation mechanisms until all antioxidants are depleted.

Typical ester degradation products include the formation of carboxylic acids, ketones, aldehydes, alcohol, water, and the formation of new ester species [Bak92,Jon85a]. Both alcohol and water can form when alkyl hydroperoxides thermally degrade and form alkoxy and hydroxy radicals [3.6], which then react with the parent hydrocarbon [3.7 and 3.8] [Jon85a]. The formation of carboxylic acid, aldehyde, and ketone species involves the oxidative degradation of the base ester in the presence of a free radical [3.9] [Bak92]. Transesterification, which can result in the formation of either higher or lower molecular weight molecules, occurs by reaction with an alcohol and is typically catalyzed by a weak acid [3.10] [Fie50]. The formation of high molecular weight degradation products can occur by condensation reactions between oxidaized ester products [3.11] and is accompanied by the generation of water [Bak92].

$$RH + O_2 \rightarrow RO\cdot + \cdot OH \qquad [3.6]$$

$$RO\cdot + RH \rightarrow ROH + R\cdot \qquad [3.7]$$

$$\cdot OH + RH \rightarrow HOH + R\cdot \qquad [3.8]$$

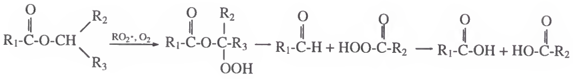

$$R_1\text{-}\overset{\overset{O}{\|}}{C}\text{-}O\text{-}CH\begin{matrix} \diagup R_2 \\ \diagdown R_3 \end{matrix} \xrightarrow{RO_2\cdot,\, O_2} R_1\text{-}\overset{\overset{O}{\|}}{C}\text{-}O\text{-}\overset{\overset{R_2}{|}}{\underset{\underset{OOH}{|}}{C}}\text{-}R_3 \longrightarrow R_1\text{-}\overset{\overset{O}{\|}}{C}\text{-}H + HOO\text{-}\overset{\overset{O}{\|}}{C}\text{-}R_2 \longrightarrow R_1\text{-}\overset{\overset{O}{\|}}{C}\text{-}OH + HO\text{-}\overset{\overset{O}{\|}}{C}\text{-}R_2$$

[3.9]

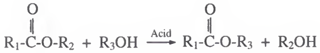

$$R_1\text{-}\overset{\overset{O}{\|}}{C}\text{-}O\text{-}R_2 + R_3OH \xrightarrow{Acid} R_1\text{-}\overset{\overset{O}{\|}}{C}\text{-}O\text{-}R_3 + R_2OH$$

[3.10]

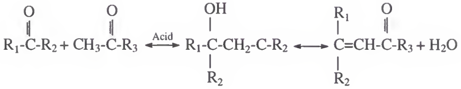

$$R_1\text{-}\overset{\overset{O}{\|}}{C}\text{-}R_2 + CH_3\text{-}\overset{\overset{O}{\|}}{C}\text{-}R_3 \xleftrightarrow{Acid} R_1\text{-}\underset{\underset{R_2}{|}}{\overset{\overset{OH}{|}}{C}}\text{-}CH_2\text{-}C\text{-}R_2 \longleftrightarrow \underset{\underset{R_2}{|}}{\overset{\overset{R_1}{|}}{C}}{=}CH\text{-}\overset{\overset{O}{\|}}{C}\text{-}R_3 + H_2O$$

[3.11]

3.2.6. Objective

The objective of this Chapter is to investigate the effects of oil degradation on friction and wear of the silicon nitride/M-50 steel system using a conventional synthetic oil. Oil samples have been thermally degraded and characterized to determine oil condition before performing friction and wear tests at 25±1°C.

3.3. Materials and Methods

Samples of as-received Exxon synthetic oil ETO 2380[3] (MIL-L-23699) were tested for various times according to the three heating schedules shown in Figure 3-1. A total of twelve samples were tested, four per schedule, at total test times of 3, 5, 7 and 9 hours for each heating schedule. The test apparatus (shown in Figure 3-2) consisted of 500 ml of as-received oil placed in a 1000 ml Pyrex beaker on a manually controlled heating plate with a K-type thermocouple inserted into the oil. Humidity was not

---

[3] Exxon Company USA, A Division of of the Exxon Corporation, Houston, TX 77252.

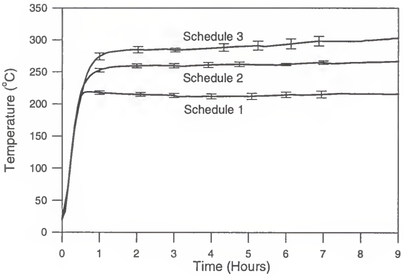

Figure 3-1. Heating schedules for oil degradation experiments. Error bars reflect standard deviation.

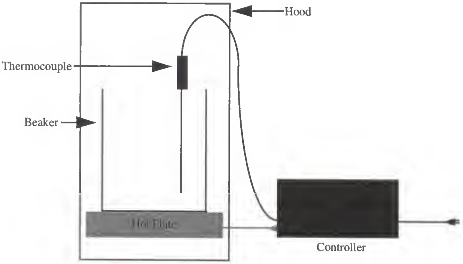

Figure 3-2. Assembly for degradation experiments.

controlled during these tests. Error bars in Figure 3-1 reflect standard deviation values for temperatures at given times.

Characterization of the degraded oil samples was performed using various analytical techniques yielding insight to the physical and chemical changes generated in the oil samples. Viscosity measurements on the samples were performed using a variable speed viscometer[4] with a 0.8° cone angle. Temperature was held at 40±0.1°C as per military specifications using a constant temperature water bath. Shear stress and viscosity measurements were made at shear rates between 0.75 and 450 s^{-1}. Surface tension measurements were made for the oil samples using the maximum bubble pressure method.[5] This test method uses submerged capillary tubes, thus eliminating possible sources of error from surface contaminants and surface foam. Coulometric Karl Fisher titration[6] measurements were also performed for each sample, thus determining changes in water content.

Optical absorption characteristics for the oil samples versus test time for each temperature regime were determined using a variable wavelength spectrometer[7] with ±0.1% accuracy, covering the ultraviolet and visible regions of the electromagnetic spectrum between 200 and 900 nm. Values for the total loss edge were determined by extrapolating the tangent for each data curve to the 0 transmittance intercept of the wavelength axis. Further spectrometry analysis was carried out in the infrared region of the electromagnetic spectrum using transmission FTIR[8] and nitrogen purge gas, analyzing chemical changes in the oil samples through analysis of the absorption peaks characteristic to the oil.

---

[4] Brookfield RVDV-III, Brookfield Engineering Laboratories, Inc., Stoughton, MA 02072.

[5] SensaDyne PC9000 Surface Tensiometer, Chem-Dyne Research Corporation, Mesa, AZ 85275.

[6] Accumet 150 Controller with 110 KF Titration Module, Fisher Scientific, Pittsburgh, PA 15219.

Size exclusion chromatography, or gel-permeation chromatography (GPC),[9] was performed using a UV/VIS detector with a pre-filter and 50-1000, 500-10,000, and 20,000-300,000 molecular weight range columns[10] to determine the molecular weight distribution of the samples with tetrahydrofuran as the solvent carrier. The columns were calibrated using polystyrene molecular weight standards and toluene. Approximately 20-30 mg of each sample was mixed with 10 ml of tetrahydrofuran and filtered three times through a 0.22 μm Teflon filter before injection. Flow rate was set to 0.4 ml/min, and the injection volume was 20 μl. Data for the oil samples was collected at a constant wavelength of 216 nm and calibrated against the standards to generate molecular weight distributions from the measured time distributions. In order to accurately compare results from each run, the area under each data curve was normalized.

Two common techniques for oil analysis were also employed, namely a remaining useful lubricant life evaluation rig[11] (RULLER) and total acid number.[12] These techniques are used to predict when an oil is likely to degrade and the extent to which

---

[7] Ultrospec III, Pharmacia LKB Biochrom LTD, Cambridge, England.

[8] 20SXB and Omnic™ software, Nicolet Instrument Corporation, Madison, WI 53711.

[9] 600E System Controller, 610 Fluid Unit, 717 Auto Sampler, and 996 Photodiode Array Detector, Waters™ Chromatography Division, Millipore Corporation, Milford, MA 01757.

[10] Phenogel 4.6×300 mm columns, with 5 μm particles and 100, 500, 10^4 and 10^5 Å pore sizes, Phenomenex, Torrence, CA 90501.

[11] University of Dayton Research Institute, Dayton, OH 45469.

[12] ASTM 664-89.

degradation has occurred, respectively. In combination, they are use to determine oil condition.

Effects of oil degradation on the friction and wear behavior of the silicon nitride/M-50 steel system were measured by tribological experiments using the previously degraded oil samples. The test apparatus was a pin-on-disk machine,[13] designed to reflect boundary lubrication conditions when being used in a liquid environment. Commercial yttria/alumina doped silicon nitride 3.2 mm diameter bearing grade (surface finish = 0.2 µm) rolling elements were used as pin materials. M-50 steel 41.3 mm diameter rolling elements supplied by MRC Bearings, Inc.[14] were cut into 6.35 mm thick disks using a precision wire electrical discharge machine,[15] ground and lapped to a 0.2 µm surface finish,[16] heat treated to attain high hardness (R_c>52), and used as disk materials. Parameters for all experiments included a 2000g (19.61N) load, 8.5 cm/s linear speed, 50% relative humidity atmosphere, and 25±1°C. The corresponding Hertzian contact stress was 1.6 GPa and the theoretically predicted initial contact diameter was 111.69 µm. Wear track radii on the disk materials were varied between 10.0, 12.5, and 15.0 mm, allowing for multiple tests on each disk sample.

Friction data determined by lateral displacement at constant load was recorded as a function of sliding distance for the duration of testing. Coefficient of friction values for each experiment were taken at sliding distances of 2500 meters, allowing for adequate run-in time. Analysis of wear tracks for both surfaces was performed using a scanning electron microscope.[17] Wear data for disk materials is reported as wear track thickness/sliding distance (µm/1000m), and wear data for pin materials is reported in terms of the specific wear rate (weight loss/sliding distance).

---

[13] ISC-200PC Tribometer, Implant Sciences Corporation, Wakefield, MA 01880.
[14] MCR Bearing Division of SKF Aerospace Bearings, USA, Inc., Jamestown, NY 14702.
[15] HS-100, Raycon Corporation, Ann Arbor, MI 48104.

3.4. Results and Discussion

Results of the techniques used to characterize the oil samples are shown in Table 3-1. The results show the same general trends for each test method as a function of test time. As viscosity increased, total loss edge increased, total acid number and corresponding molal values increased, antioxidant content decreased, and surface tension remained relatively constant at 0.04 N/m. Antioxidant concentration fell below the 50% level for the most extreme test samples, suggesting a high degree of degradation. However, TAN results only showed moderate increases to 1.48 mg KOH/g.

3.4.1. Rheological Analysis

Results for viscosity testing performed at 40±0.1°C showed all samples to exhibit Newtonian behavior without Bingham yield points. Values for each sample are given in Table 3-1, where a general trend of increasing viscosity as test time proceeds is observed for the three schedules. Values for samples from schedule 1 fluctuated about the 23.2 cP value of the as-received oil sample, whereas results for schedules 2 and 3 yielded significant viscosity increases up to 50%. The observance of an initial negative change in

---

[16] Superfinishers, Inc., Macedonia, OH 44056.

[17] 6400 Scanning Electron Microscope, Joel USA, Inc., Peabody, MA 01961.

viscosity of -2.3% for the schedule 1, 3 hour sample is not significant, as this is a common occurrence for lubricants in turbine environments.

Table 3-1. Physical data determined for samples from three heating schedules. "Sch" refers to schedule number and "hrs" refers to hours tested.

Sample ID	Viscosity (cP)	Total Loss Edge (nm)	TAN (mg KOH/g)	Molal (10^{-3})	Antioxidant Content (%)	Surface Tension (N/m)	Water (ppm)
As-received	23.23	390	0.37	3.5	NA	0.0364	566
Sch 1, 3 hrs	22.69	525	0.58	3.5	96	0.0385	465
Sch 1, 5 hrs	24.11	570	0.75	4.5	91	0.0386	322
Sch 1, 7 hrs	23.81	567	0.69	4.5	90	0.0368	309
Sch 1, 9 hrs	24.36	616	1.19	10.5	80	0.0386	456
Sch 2, 3 hrs	25.42	565	1.00	4.0	85	0.0391	312
Sch 2, 5 hrs	26.78	620	1.19	6.5	--	0.0393	286
Sch 2, 7 hrs	28.65	678	1.67	9.0	73	0.0397	405
Sch 2, 9 hrs	30.03	712	1.87	11.5	54	0.0404	312
Sch 3, 3 hrs	26.13	595	0.97	4.5	70	0.0394	463
Sch 3, 5 hrs	28.00	675	0.91	6.0	58	0.0380	360
Sch 3, 7 hrs	32.99	785	1.42	8.0	49	0.0382	309
Sch 3, 9 hrs	34.69	810	1.48	9.0	48	0.0388	360

3.4.2. Water Content Analysis

Results from coulometric Karl Fisher titration of the oil samples showed the as-received oil to have a water content of 566 ppm. For all three test schedules, water content fell to values below 475 ppm and fluctuated with test time, yielding no general correlations. However, due to the fact that water content did not fall below 286 ppm and become completely removed from the oil samples, the result suggest that water is indeed a product of the oil degradation.

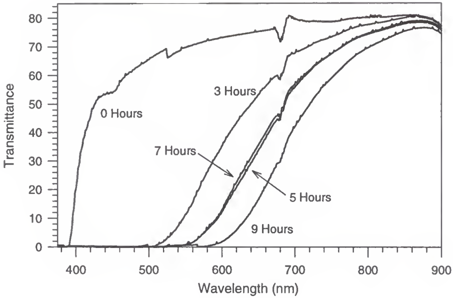

Figure 3-3. UV/VIS spectrometry data for samples run according to heating schedule 1.

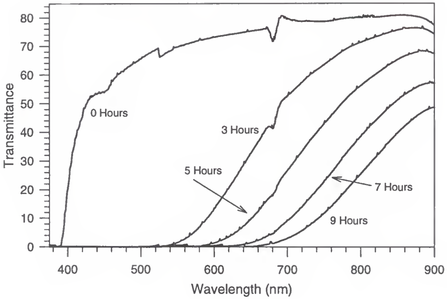

Figure 3-4. UV/VIS spectrometry data for samples run according to heating schedule 2.

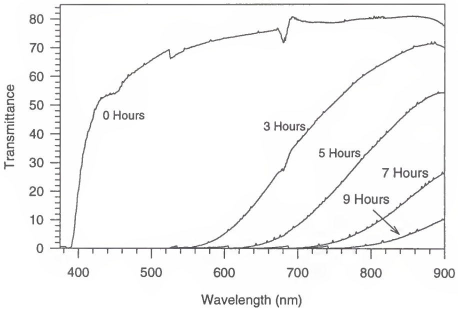

Figure 3-5. UV/VIS spectrometry data for samples run according to heating schedule 3.

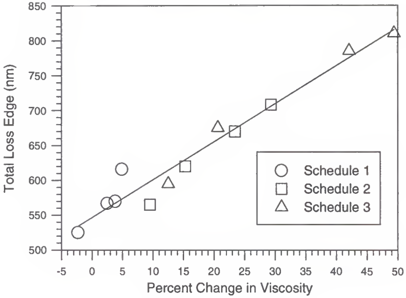

Figure 3-6. Total loss edge versus change in viscosity, showing a linear relationship with the correlation coefficient r^2=0.96.

3.4.3. Spectroscopic Analysis

Results of ultraviolet and visible spectrometry experiments performed on samples from the three heating schedules are shown in Figures 3-3 through 3-5. All samples yielded negligible transmission results in the ultraviolet region, with the majority of relative data existing above 375 nm. Inflections observed at approximately 525 and 675 nm are equipment anomalies, and therefore do not represent spectral characteristics of the samples. Characteristic to the data presented was a trend of decreasing transmission as a function of test time. The only exception to this trend was the transmission data for the 3 and 5 hour samples from schedule 1 (Figure 3-3). Variations from the general behavior for these samples is attributed to modest fluctuations in the heating schedules. Also characteristic to these samples was an increase in the total loss edge as a function of test time (375 nm for the as-received and 810 nm for the schedule 3, 9 hours sample), as shown for each schedule in Table 3-1.

Comparison of total loss edge data and viscosity results are shown in Figure 3-6, where viscosity is plotted in percent change and a master line generated by linear regression analysis. The regression coefficient (r^2) for this line was found to be 0.96, and the slope was 5.44. This correlation suggests that the optical behavior of the oil samples and the viscosity changes are related, possibly by a factor which generates both results. However, the as-received oil sample was found to have a total loss edge value of 390 nm, which does not correlate with the results for the degraded oil samples. The issue of this relationship between total loss edge values and viscosity changes will be studied in greater detail in Chapter 5.

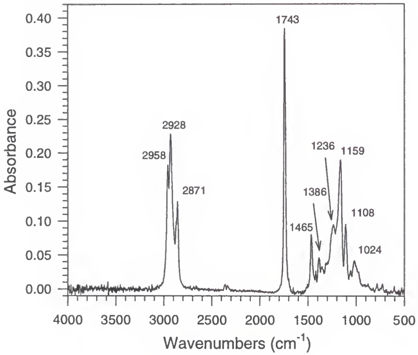

Figure 3-7. Infrared spectra for the as-received sample of ETO 2380 (MIL-L-23699).

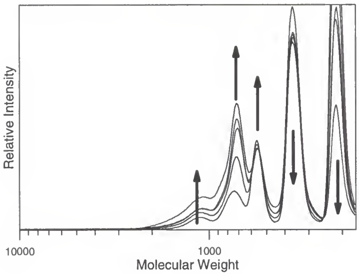

Figure 3-8. GPC data for schedule 1. Arrows indicate direction of changes with test time.

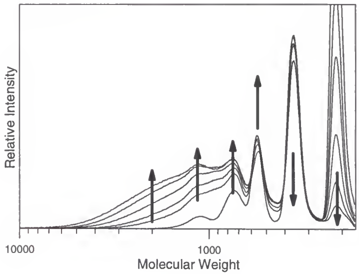

Figure 3-9. GPC data for schedule 2. Arrows indicate direction of changes with test time.

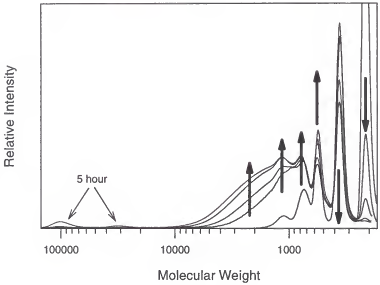

Figure 3-10. GPC data for Schedule 3. Arrows indicate direction of changes with test time. (note: Molecular weight range differs from previous figures).

Results from infrared analysis yielded peaks for the as-received sample as shown in Figure 3-7. The strong absorption peaks between 2850-3000 cm^{-1} and the weak peak at 1465 cm^{-1} reflect an alkane structure. The strong peak at 1743 cm^{-1} for the as received oil reflects one or more carbonyl peaks for ester structures within the base oil. The variety of lower intensity peaks between 1000-1465 cm^{-1}, which include the C-C(=O)-O (lactone) and the O-C-C peaks, are not distinguishable.[Sil81] For the degraded oil samples, peak broadening as a function of test time was observed for the carbonyl peak. This is the result of the generation of new carbonyl peaks, however the structure(s) associated with the new species is not discernible. Transesterification, the formation of ketones, and the formation of carboxylic acids are all possible sources for the new carbonyl species.

3.4.4. Molecular Weight Analysis

Results from GPC testing are shown in Figures 3-8 through 3-10. The as-received oil sample showed peaks at 215, 360, 565, 775, and 1125 MW. As a function of test time, samples from all three heating schedules yielded decreasing intensities for the 216 and 360 MW peaks, and increasing intensities for the 565, 775, and 1125 MW peaks. Samples for Schedules 2 and 3 (Figures 3-9 and 3-10 respectively) showed the generation of a higher molecular weight species in the form of a broad peak between 1500-3000 MW. The decrease in intensity for the low molecular weight species can be attributed in part to evaporation. Increases in the intensity of the higher molecular weight species and the generation of the 1500-3000 MW peak suggests reaction between the species with decreasing intensities.

Further information is gained from data for the 5 hour test sample from Schedule 3, which shows the generation of two low intensity peaks at approximately 31,500 and 101,000 MW. For the 7 hour sample, the 31,500 MW peak is not observed and the 101,000 MW peak is of lower intensity. For the 9 hour sample, neither peaks are present. These results suggest the generation of higher molecular weight species which are subsequently removed, a process commonly referred to as coking. Comparing these results with infrared data, a general description of the coking process can be drawn. The base ester undergoes a reaction to form new ester, ketone, or carboxylic acid species which generates higher molecular weight ester species, which subsequently deposit into a carbon residue.

Table 3-2. Tribological data generated for the oil samples using a pin-on-disk apparatus. "Sch" refers to schedule number and "hrs" refers to hours tested.

Sample	Coefficient of Friction (μ)	Specific Wear Rate: Pin Surface (pg/m)	Wear Rate: Disk Surface (μm/1000m)	Molal Concentration Eq. (3.2)
As-received	0.08	14.2	9.1	0.30
Sch 1, 3 hrs	0.10	53.3	16.3	0.30
Sch 1, 5 hrs	0.10	43.1	18.8	0.39
Sch 1, 7 hrs	0.09	35.5	15.7	0.39
Sch 1, 9 hrs	0.10	25.6	12.9	0.90
Sch 2, 3 hrs	0.10	26.0	9.7	0.35
Sch 2, 5 hrs	0.10	15.3	5.7	0.56
Sch 2, 7 hrs	0.10	17.0	7.4	0.78
Sch 2, 9 hrs	0.12	47.4	13.7	1.00
Sch 3, 3 hrs	0.09	23.9	9.1	0.39
Sch 3, 5 hrs	0.09	26.0	12.3	0.52
Sch 3, 7 hrs	0.10	25.3	15.2	0.71
Sch 3, 9 hrs	0.10	30.6	13.8	0.80

3.4.5. Tribological Analysis

Results for coefficient of friction and rate of wear data are shown in Table 3-2. For the as-received oil sample, the coefficient of friction (μ) was found to be 0.08, specific wear rate for the pin was 14.2 pg/m (picograms/meter), and wear rate for the disk in terms of track width versus sliding distance was 9.1 μm/1000m.

In order to compare the effects of oil degradation on the friction and wear behavior of the silicon nitride/M-50 steel system, a method to quantify the extent of degradation for samples from each heat schedule must be determined. Since oil degradation is reflected by both physical and chemical changes, and since these changes are reflected in viscosity and total acid number measurements, a correlation between these experimental values and the oil condition for each sample must be made. Assuming that changes in viscosity are the result of the formation of high molecular weight degradation products which act as particulate species, the Einstein equation for changes in viscosity as a function of particle volume for Newtonian fluids may be used (Eq. (3.1)).

$$\eta^* = \eta o \cdot (1 + \frac{5}{2} \cdot \phi) \tag{3.1}$$

The η^* refers to the experimental viscosity, η_o refers to the as-received viscosity, and ϕ refers to the percent particle volume of the system [Ein56]. From this relation, the molal concentration of particulate species may be determined assuming a set density for the particulate species (for this study the density was assumed to be 2.0 g/cc). From the TAN values, molal values which reflect the number of base neutralized acidic sites may alos be calculated. A combination of the two molal values can be used to generate an overall molal concentration value for the oil samples (Eq. (3.2)).

$$MC = \frac{m_{TAN} + m_{\phi}}{m_{TAN}^{*} + m_{\phi}^{*}} \tag{3.2}$$

MC refers to the molal concentration, m $_{TAN}$ refers to the molal value calculated from TAN values, m_{ϕ} refers to the molal value determined from the particle volume, m^*_{TAN} and m^*_{ϕ} refer to the molal values determined for the most degraded oil sample in this study (Sch 2, 9 hrs). The results for molal concentration values are shown in Table 3-2.

Results for coefficient of friction measurements are shown in Table 3-2 and plotted versus the aforementioned molal concentration as shown in Figure 3-11. Friction values range from 0.08 and 0.12. From the regression curve drawn for all data points, a general increase in friction is observed as the degree of degradation increases.

Rate of wear data (Table 3-2) is presented for pin and disk sliding surfaces in Figures 3-12 and 3-13 respectively. Values for the specific wear rate of the pin surfaces range between 14.2 and 47.4 pg/m. Rate of wear values for the disk surfaces range between 9.1 and 18.8 μm/1000m. For both plots, no correlations are shown for the rate of wear versus the overall molal concentration.

3.5. Conclusions

Characterization was performed on the oil samples presented in Table 3-1. Rheology showed viscosity changes between -2.3% and 49.4% relative to the as-received oil. Results of molecular weight analysis of the samples for the most extreme testing conditions showed the formation of high molecular weight species, which subsequently removed as test time proceeded, suggesting coking behavior. In correlation with infrared

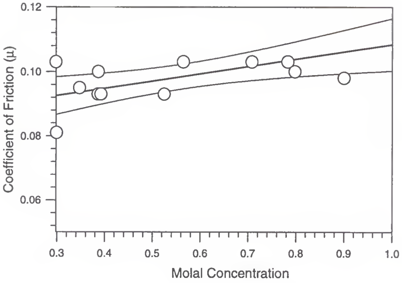

Figure 3-11. Coefficient of friction data for oil samples plotted versus molal concentration of the degradation product (Eq. (3-2)). Lines refer to a linear regression fit with m= 0.023 and corresponding 95% confidence intervals.

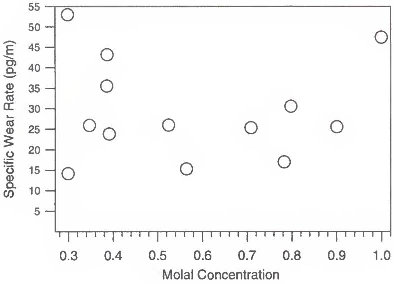

Figure 3-12. Rate of wear data for pin surfaces given in weight loss versus sliding distance (picograms/meters) plotted against molal concentration of the degradation product for oil the samples (Eq. (3-2)).

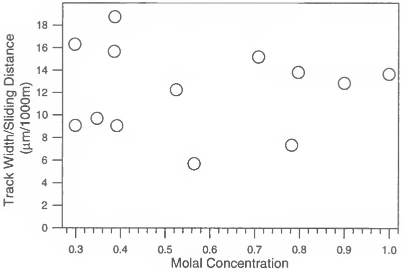

Figure 3-13. Rate of wear data for disk surfaces given in increasing track width versus sliding distance (microns/meters) plotted against molal concentration of the degradation product for oil the samples (Eq. (3-2)).

spectrometry results which showed peak broadening effects, the degradation mechanism for the system at hand could not be determined, as the formation of carboxylic acids, ketones, and esters (via transesterification) are all possible reaction products. The fact that oil samples retain Newtonian behavior throughout testing does suggests the formation of secondary ester products as the primary degradation reaction.

A linear relationship was found to exist between total loss edge values and changes in viscosity. This observation suggests that the changes in optical behavior of the oil is dependent on physical changes which result during degradation. Results from an investigation into the use of this technique for oil analysis and monitoring will be discussed in Chapter 5.

Friction and wear testing of the previously degraded oil samples was performed in order to determine effects of oil degradation on the tribological properties of the silicon nitride/M50 steel system using a conventional synthetic lubricant. Results from testing under boundary lubrication conditions show the coefficient of friction to increase with respect to oil condition. Results for wear measurements showed the rate of wear for both the silicon nitride and M-50 surfaces to be independent of oil condition with no correlations to any of the characterization techniques used for this report. The lack of wear rate information suggests that information attained from pin-on-disk testing must be supported with wear testing performed using test machines which more accurately reflect bearing failure behavior (e.g. rolling contact fatigue testing).

CHAPTER 4

A KINETIC STUDY ON THE DEGRADATION EFFECTS OF VARIOUS ENVIRONMENTAL PARAMETERS

4.1. Introduction

Individual effects of thermal, oxidative, and tribochemical degradation mechanisms on a conventional synthetic lubricant (MIL-L-23699) have been studied. Degraded oil samples were generated under experimental conditions performed in the presence of oxidative and non-oxidative environments, high and low humidities, and the presence of or lack of M-50 steel as a catalyst material. All experiments were performed at 250°C and samples were collected as a function of time. Samples were characterized for total acid number, antioxidant content, water content, viscosity, spectrometry, and molecular weight. Molecular weight peak analysis was performed assuming Gaussian distributions. Results were compared to determine influences of the aforementioned variables on the rate of formation of higher molecular weight species in the synthetic oil. From these results, and from experiments performed on condensed vapors collected during the degradation runs, influences of each variable on the depletion of antioxidant and generation of high molecular weight species are shown.

4.2. Background

Current understanding of the degradation behavior of the lubrication systems used for gas turbine engines is limited. The individual effects of each variable encountered during engine operation has not been completely investigated. Of the kinetic studies which have been reported, test systems have been simplified by limiting studies to one additive mixed into one base stock. For conventional lubricants which are blends of multiple additives and base stocks, results from simplified tests may not be representative: The effects of competing degradation mechanisms are not taken into account. Interest in oil degradation behavior stems from the effects of thermal, oxidative, and tribochemical degradation mechanisms, as well as the influences of high humidity environments.

4.2.1. Current Understanding of Degradation Mechanisms

Under current bearing applications where bulk lubricant operating temperatures range between 75-150 °C, boundary and elastohydrodynamic contact temperatures can reach 250-350 °C due to frictional heating [Kla85,Kla91]. Chemical reactions, which normally are nonexistent or of low reaction rate, can be accelerated under these temperature conditions [Gee94]. When operating for extended time at temperatures over 200°C, most commercial ester-based lubricants oxidize, polymerize, or evaporate [Aja92]. The most common mechanisms for the degradation of these hydrocarbon lubricants are thermal and oxidative degradation mechanisms, as well as tribochemical degradation mechanisms [Hsu86].

Thermal and Oxidative Degradation

Both thermal and oxidative degradation processes consist of a free radical chain mechanism [Bak92,Hun93a,Kau95a,Kla85]. In these processes, free radicals are generated through either a hydroperoxide radical mechanism, a carbon-carbon scission mechanism, or both. These free radicals then act to polymerize other lubricant constituents by starting reaction chains via abstraction of hydrogen atoms from parent hydrocarbons [Jon85b]. Free radical chain propagation is the most detrimental oil degradation mechanism. This type of degradation is in part controlled by the addition of antioxidant additives.

Antioxidant Behavior

Oxidation degradation is minimized in synthetic lubricants by the addition of oxidation inhibitors referred to as antioxidants. Antioxidant additives act to eliminate this free radical chain propagation mechanism by donating a proton to the free radicals, therefore rendering them inactive. The antioxidant molecule then becomes a free radical which is self stabilized through resonance [Hun93a]. In this method, antioxidants delay thermal and oxidative degradation mechanisms until all antioxidants are depleted.

Tribochemical Degradation Mechanisms

Metallic surfaces and debris have been shown to play an increasing role in ester based lubricant breakdown above 180°C by increasing the rate of degradation [Gat91,Hsu86, Jon85a,Kau85,Kla85,Kla91]. These metallic surfaces can act as catalysts, either inhibiting or promoting oil degradation. Organometallics, oxides, and inorganic compounds all form upon reaction between metal surfaces, oil constituents, and contaminants, acting in the same manner as catalysts [Jon85a,Kla85]. Reactions with metallic debris can be more serious than those with metal surfaces due to higher activity of the debris [Kau85]. Ceramic surfaces are less active and have been shown to form passivation layers [Gat91]. These passivation layers are generated by reaction with water absorbed in the oil and water vapor generated as a combustion product [Dan91]. For ceramics, reactions with oil constituents are limited by the passivation films unless the rate of wear is faster than the rate of reaction. In this manner, the formation of oxide and oxynitride films on silicon nitride can produce lower coefficients of friction and wear rates in hybrid and ceramic bearings [Cra88,Gee94,Kat90,Par75]. However, oxide films formed on metal surfaces result in junction growth [Kat90]. Oxide debris collect around the contact regions and do not lower the coefficient of friction.

4.2.2. Current Oil Monitoring Techniques

Current oil monitoring techniques fall into three main categories. These categories include study of basic fluid parameters such as viscosity and total acid number, analytical techniques used to determine chemical changes in additive concentrations and base stock, and off-line techniques which have been developed to give quick information on oil condition.

Basic Fluid Parameters

As a first look at the extent of degradation in used oil samples, two basic techniques are used. To determine the extent to which degradation has effected the physical condition of the oil, viscosity testing is employed. To determine the extent to which the oil has chemically degraded, total acid number[1] is determined. Total acid number (TAN) is a technique in which a small amount of the oil sample is dissolved in solvents and titrated using 0.1N alcoholic KOH. As a result, the amount of KOH solution needed to titrate the oil sample to a specific pH represents the concentration of base neutralized acidic sites on the various oil constituents and degradation products.

Analytical Techniques

Analytical techniques for oil characterization has been well documented [Bel86,Coa86,God95,Hos91,Kau85,Lin94,Loc92,Pac89,Pow93]. Due to the complexity of additive packages used in synthetic oils, analytical techniques must be able to monitor for additive levels, degradation products, and contaminants. Infrared spectroscopy is presently implemented for such analysis due to equipment sensitivity and flexibility [Coa86,Dan91]. Spectrometric techniques, such as atomic absorption (AA), atomic emission spectroscopy (AES), inductively coupled plasma emission spectroscopy (ICPES), and X-ray fluorescence (XRF), are used for elemental analysis of wear metal concentrations, but are limited by the inability to discern chemical states of elements detected [Hos91,Kau85,Pac89]. Differential scanning calorimetry (DSC) is used to determine thermooxidative stability of the oils [Pac89]. Chromatographic methods, including gas chromatography (GC) and gel permeation chromatography (GPC), are used to discern additive concentrations which are unavailable for proprietary reasons and to determine degradation patterns and products [Jon85a,Pac89]. Ferrography and spectrometry are limited in usefulness, since both techniques require periodic sampling [God95]. Ferrography, along with most other debris collection and sensing devices are also limited to the analysis of magnetic debris only, limiting usefulness as techniques for hybrid and all-ceramic bearing systems [Bel86,Lin94,Sei72].

---

[1] ASTM 664-89.

Off-line Techniques

Over the past decade, a number of techniques have been developed to determine the condition of degraded oil samples. Through the investigations of Kauffman et al., one particular technique has earned notable recognition. This techniques is referred to as the remaining useful lubricant life evaluation rig[2] (RULLER) [Kau89,Kau95a,Kau95b]. A small sample of degraded oil is dissolved into a solvent and tested using a voltametric method to determine the antioxidant concentration is the oil sample. Taking into account that the lubricant begins to degrade before the antioxidant content is completely depleted, the percent of antioxidant remaining is related to the remaining useful life of the used oil sample.

A second notable off-line technique is the complete oil breakdown rate analyzer[3] (COBRA). With this technique, changes in the electrochemical properties of oil samples are evaluated. Analysis is simple and quick, and results have been shown to correlate well with results from TAN analysis. Due to this correlation with TAN and to faster analysis times, COBRA has been implemented as a technique to predict TAN results.

4.2.3. Previous Kinetic Studies

Although many kinetic studies have been reported for the determination of individual effects on specific lubricant additives, one report is of particular note. A pressurized Penn State microoxidation tester was used by Hunter et al. to determine the kinetic behavior and optimal concentration of an antioxidant additive [Hun93a]. Experiments were performed using various mixing ratios of the antioxidant phenyl alpha naphthylamine in the polyol ester trimethylolpropane triheptanoate. The microoxidation test consisted of placing a thin film of oil onto a metal catalyst surface in a pressure controlled environment with flowing gas at temperatures below 200°C. Tested samples were studied for molecular weight changes using gel permeation chromatography (GPC). Results showed that removal of the lower molecular weight peak which represented the PAN did coincide with slight increases in the generation of higher molecular weight species. Furthermore, the rate of generation for the higher molecular weight species increased significantly after complete removal of the PAN. These results are of particular interest due to the fact that antioxidant concentration was monitored and related to the direct formation of higher molecular weight species.

---

[2] University of Dayton Research Institute, Dayton, OH 45469.

[3] COBRA Program, WPAFB, OH 45433.

Hunter et al. have taken the first step in determining how the depletion of antioxidant directly affects oil degradation. However, results were presented for one environment without changing test variables and are therefore limited in determining how a particular additive or oil base stock could be improved. If the individual degradation effects of each variable faced in an operating turbine engine could be determined, both oils and additives could be engineered for improved performance with respect to a specific degradation mechanism, rather than with respect to competing mechanisms.

4.2.4. Objective

The most significant limitation in determining ways for improving lubricant performance is the lack of understanding in the individual effects of variables encountered during engine operation. The object of this chapter is to determine how thermal degradation, oxidative degradation, high humidity, and the presence of the M-50 steel catalyst effect oil degradation. Of particular emphasis will be antioxidant depletion and the formation of high molecular weight species.

4.3. Materials and Methods

In order to determine the individual effects of thermal, oxidative, and tribochemical degradation mechanisms, a series of experiments was designed and performed under varying environments. As shown in Table 4-1, a total of eight experiments were performed while varying atmosphere, humidity, and the presence of M-50 steel surfaces. For each test, 750 ml of as-received ETO 2380 synthetic oil (MIL-L-23699) was placed in a Pyrex beaker on a hot plate (see Figure 4-1). The hot plate was connected to a constant temperature controller. The thermocouple from the controller was covered with a glass capillary tube, sealed at the end with a H_2/O_2 torch, before being placed into the oil bath. Gas flow was supplied to the oil bath using a flow meter set to 0.83 L/min and a glass dispersion tube placed into the bath. Finally, the beaker was wrapped in fiberglass insulation to aid in temperature control. In this manner, the oil was completely isolated from metallic surfaces which might act as catalysts. The hot plate was set to the highest setting and the temperature controller was set to 250°C, resulting in a heating rate of approximately 225°C/hour.

In accordance with Table 4-1, gas flow supplied to each experiment was either compressed argon, resulting in a mildly reducing (non-oxidative) atmosphere which would promote thermal degradation without oxidative degradation, or compressed air which would promote both thermal and oxidative degradation. Samples of M-50 steel were supplied as catalyst surfaces for the designated tests in the form of 1/4" diameter bearing balls placed in the oil bath at the beginning of each of the experiments. The resulting ratio of available surface area to oil was 3.6 mm^3/ml, which was kept constant for each of the appropriate tests. For tests performed under low humidities, gas flow for both compressed argon and air was determined with an on-line sensor[4] as ≤12%. For the tests performed under high humidity, a liquid bubbler filled with distiller water was placed between the flow meter and the oil bath. The resulting relative humidities for the gas flow entering the bath were 85% for argon and 92% for air.

Table 4-1. List of degradation experiments for the kinetic study.

Test ID	Temperature	Atmosphere	Humidity	Catalyst
IN12NC	250°C	inert	<12 %	None
IN12C	250°C	inert	<12 %	M-50
IN85NC	250°C	inert	~85 %	None
IN85C	250°C	inert	~85 %	M-50
OX12NC	250°C	oxidative	<12 %	None
OX12C	250°C	oxidative	<12 %	M-50
OX92NC	250°C	oxidative	~92 %	None
OX92C	250°C	oxidative	~92 %	M-50

---

[4] Implant Sciences Corporation, Wakefield, MA 01880.

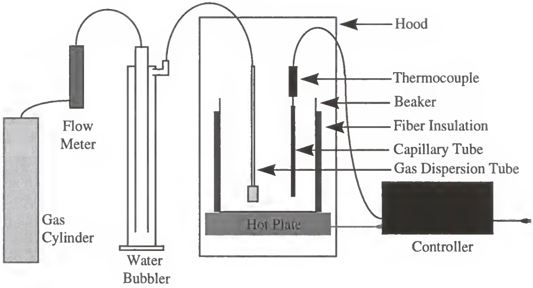

Figure 4-1. Assembly for degradation experiments. Water bubbler, presence of M-50 bearing balls placed in the beaker, and gas type dependent on individual test description.

In order to analyze the kinetic aspects of the degradation processes, 50 ml samples were taken during each experiment using a glass pipette. Sample times recorded from initial heatup were 3, 5, 7, 9, and 13 hours. Each sample was stored in a glass bottle with a Teflon lined lid to protect the oil samples from the environment and to prevent absorption of water, which might lead to further degradation.

Analysis of the oil constituents and degradation byproducts which evaporated during these tests was performed by collecting the vapors at various times during test OX12NC. Collection was performed using a vacuum pump which pulled vapors from the beaker through Teflon tubing and into a condenser tube cooled by liquid nitrogen. After vapors were collected, the condenser tube was removed from the liquid nitrogen and sealed to prevent condensation not associated with the test.

In order to determine the effects of degradation on the physical behavior of the oil samples, viscosity tests were performed using a variable speed rheometer[5] with a 0.8° cone angle between shear rates of 0.75 and 450 s^{-1}. Experiments were performed at 40±0.1°C using a constant temperature water bath, therefore producing results which can be directly compared with military specifications. Furthermore, water content of the oil samples was determined using coulometric Karl Fisher titration.[6]

The extent to which oil degradation had occurred for each sample was determined using a number of analytical techniques. Antioxidant concentration for each sample was determined using a remaining useful lubricant life evaluation rig (RULLER), electrochemical characteristics were determined using the complete oil breakdown rate analyzer (COBRA), and the extent to which degradation had occurred was determined from the total acid number (TAN). For TAN experiments, exceptions from the ASTM designation were the use of aqueous based standards and titration to pH 11. These techniques are used in combination to predict when an oil is likely to degrade and the extent to which degradation has occurred.

---

[5] Brookfield RVDV III, Brookfield Engineering Laboratories, Inc., Stoughton, MA 02072.

[6] Accumet 150 Controller and 110KF Titration Module, Fisher Scientific, Pittsburgh, PA 15219.

Chemical analysis of the tested samples and condensed vapors was performed spectroscopically using transmission FTIR[7] with KRS-5 salt crystals for sample mounting and a circular fluid cell for dilute samples, with nitrogen as the purge gas. This technique allowed for the partial analysis of chemical changes in the oil samples through observation of changes in the characteristic absorption peaks.

In order to determine the differences in rates of degradation resulting from thermal and oxidative degradation mechanisms, as well as the influences of catalytic surfaces and high humidity environments, molecular weight analysis was performed on the oil samples and the collected vapors. Size exclusion chromatography, also known as gel-permeation chromatography (GPC), was performed using an ultraviolet/visible (UV/VIS) wavelength detector.[8] A pre-filter and 50-1K, 5K-10K, 20K-300K and 100K-1000K molecular weight range columns[9] were used to determine the molecular weight distribution of each sample, with tetrahydrofuran as the solvent carrier. The columns were calibrated between

---

[7] 20SXB with Omnic™ Software, Nicolet Instrument Company, Madison, WI 53711.

[8] 600E System Controller, 610 Fluid Unit, 717 Auto Sampler, and 996 Photodiode Array Detector, Waters™ Chromatography Division, Millipore Corporation, Milford, MA 01757.

[9] Phenogel 4.6×300 mm columns, with 5 μm particles and 100, 500, 10^4 and 10^5 Å pore sizes, Phenomenex, Torrence, CA 90501.

92 and 870,000 MW using polystyrene molecular weight standards and toluene. Approximately 20-30 mg of each sample was mixed with 10 ml of tetrahydrofuran and filtered three times through a 0.22 μm Teflon filter before injection. The flow rate was set to 0.4 ml/min, and the injection volume was 20 μl. UV/VIS data for the oil samples was processed at a constant wavelength of 216 nm. Data was calibrated against the polystyrene standards to generate molecular weight distributions from the measured elution times. In order to accurately compare results from each run, all data was corrected by normalizing the areas under each data curve. Evaluation of changes in peak intensities and locations was performed using peak separation and analysis software[10] assuming a Gaussian distribution.

4.4. Results and Discussion

Results of characterization testing performed on the experiments described in Table 4-1 are separated according to rheological analysis, chemical analysis, molecular weight analyses, and peak analysis of the molecular weight distributions. Analysis of condensed volatile was performed in order to determine the low molecular weight degradation products. Results for rates of degradation and the formation of particulates are presented for each test series. Results for total loss edge data and interpretation will be presented in Chapter 5.

---

[10] Peakfit™ V 4.0, Jandel Scientific Software, San Rafael, CA 94901.

4.4.1. Rheological Analysis

As a first step in determining the extent to which degradation in the oil samples had occurred, viscosity data was plotted versus test time for each series of experiments (Figure 4-2). All results yielded Newtonian behavior without a Bingham yield point, thus the data reflects average viscosity changes for the tested shear rates. Viscosity changes for the tests performed in an inert (non-oxidative) environments gradually increased to 23-30% change for the 13 hour test samples. Results for tests performed in oxidative environments showed higher rates of viscosity change, with the final 13 hours test samples reflecting viscosity changes above 100%. Of the tests performed in oxidative environments, the tests which included the M-50 steel catalyst showed greater changes than those without catalyst. Furthermore, high humidity environments resulted in lower changes in viscosity. Effects of catalyst (M-50 steel) and high humidities were not shown to affect viscosity changes for the tests performed in non-oxidative environments.

4.4.2. Chemical Analysis

Determination of the extent to which degradation has occurred in the test samples began with analysis of the antioxidant content. Results from RULLER experiments are shown in Figure 4-3, plotted as antioxidant concentration versus test time. Antioxidant levels for samples tested in inert (non-oxidative) atmospheres gradually decreased at approximately identical rates to concentrations between 54-57% for the 13 hour test samples. Results for experiments run in oxidative environments indicate that humidity and the presence of a catalyst affected the depletion of antioxidant in much the same way as with increasing viscosity changes shown in Figure 4-2. Degradation experiments

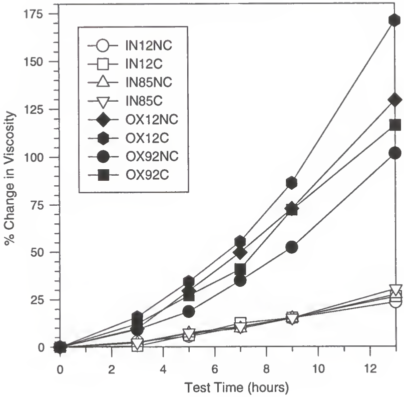

Figure 4-2. Changes in viscosity as a function of test time for all test series.

performed with catalyst material showed increased rates of antioxidant removal, whereas experiments performed in high humidity environments showed decreasing rates of antioxidant removal. For the tests performed in oxidative environments, the antioxidant concentrations leveled out between 35-40% for the 9 hours test samples. The observation of antioxidant content leveling out is characteristic of complex oils due to the formation of degradation products which are interpreted by the RULLER to be antioxidant species. Results therefore show that significant degradation occurs before the 40% antioxidant concentration is met.

Further analysis of the condition of the samples was determined using total acid number (TAN). Figure 4-4 shows TAN results plotted versus time. Molality values are also presented, showing the concentration of base neutralized acid sites. Results showed that the extent to which degradation had occurred in the various tests followed the same trends as with viscosity and antioxidant changes. Results for tests performed in non-oxidative environments showed TAN values increased to approximately 0.45 (0.008 m). Since TAN values are not considered significant until above 1.0, these results show low amounts of degradation for those experiments performed in non-oxidative environments, with no evident catalyst or humidity effects. For the samples performed in oxidative environments, TAN values grew above 2.9 for the 13 hour test samples. Greater amounts of degradation were shown for experiments performed with M-50 steel catalyst, and the experiments performed in high humidity environments exhibited lower amounts of degradation.

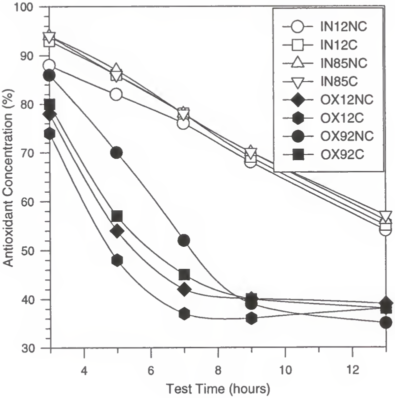

Figure 4-3. Changes in antioxidant content as a function of test time for all test series.

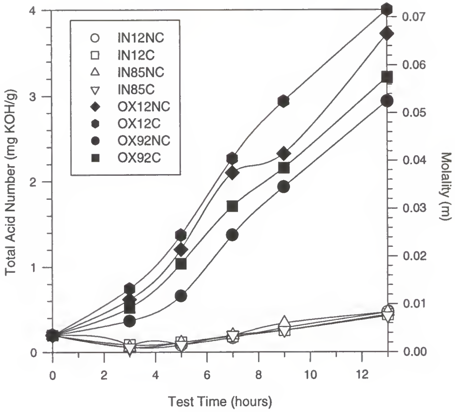

Figure 4-4. Changes in total acid number as a function of test time.

FTIR analysis of the as-received sample for the ETO 2380 was reviewed in Chapter 3. As seen in Figures 3-7 and 4-5, strong absorption peaks between 2850-3000 cm^{-1} as well as the 1465 cm^{-1} peak reflect an alkane structure. The strong peak at 1743 cm^{-1} for the as received oil reflect one or more carbonyl peaks for ester structures within the base oil. The variety of lower intensity peaks between 1000-1465 cm^{-1}, which include the C-C(=O)-O (lactone) and the O-C-C peaks, are not distinguishable.[Sil81] As for changes in the spectra of the oil samples as a function of test time, results showed broadening of the carbonyl peak (1743 cm^{-1}) which could not be attributed to any one mechanism. Possibilities included transesterification, the formation of ketones, and the formation of carboxylic acids. With increasing test time, changes in peak ratios occurred between the alkane and carbonyl vibration peaks, as well as the peaks in the fingerprint region of the spectrum. For the results of high test time samples from oxidative environments, a hydroxyl peak appeared in the range 3300-3700 cm^{-1}, suggesting the formation of either carboxylic acids, alcohols, or water (see Figure 4-5).

4.4.3. Molecular Weight Analysis

Although results from viscosity, antioxidant, and TAN testing suggest trends in the degradation behavior of the oil system under various test conditions, these results only reflect chemical and physical responses to degradation. The results do not describe or explain the kinetics of the individual degradation mechanisms. In order to better understand the influences of the individual mechanisms on the rate of degradation, molecular weight analysis was performed.

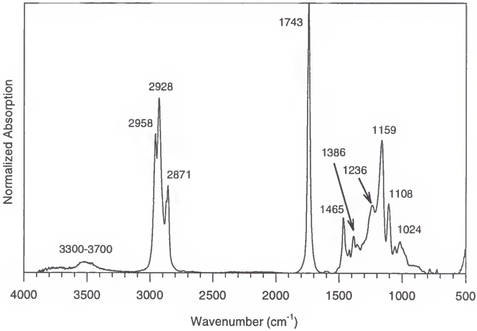

Figure 4-5. FTIR spectra for the 13 hours sample from test OX12NC.

Size exclusion chromatography results are presented for the IN12NC 3 hour test sample in Figure 4-6. A total of six peaks are shown for the as-received oil sample, with molecular weights of 215, 267, 432, 662, 863, and 1292. In order to determine how the molecular weight distributions change as a function of test time, peak separation and analysis ($r^2 \geq 0.996$) was performed using Gaussian curve fitting for each of the tests. Figure 4-6(a) shows the as-received molecular weight distribution and the fitted plot with a correlation coefficient of $r^2=0.999$. As seen in Figure 4-6(b), the corresponding peaks are numbered 1 through 6 for future reference. Changes in the molecular weight distributions varied for each test series: Figures 4-7(a) and (b) compare the changes for tests IN12NC and OX12NC, respectively. For both test series, decreases in intensities were observed for peaks 3, 4, 5, and 6. Increases in intensities were observed for the peaks 1 and 2. The increasing intensity for peak 1 in test OX12NC is accompanied by an increase in molecular weight.

Comparing changes for the inert (non-oxidative) and oxidative test series, the peaks which undergo the greatest changes are peak 1 (1292 MW) and peak 5 (267 MW). To further compare the differences in peak changes for the two test series, Figure 4-8 shows the fitted Gaussian curves and corresponding changes in percent area (at 216 nm) with time for tests IN12NC and OX12NC. As seen for peak 1, Figures 4-8 (a) and (c), greater increases in area occur for the test performed in an oxidative environment. Furthermore, the increase in area for OX12NC is accompanied by an increase in the mean molecular weight value for the peak. For peak 5, Figures 4-8 (b) and (d), more significant decreases in area are shown as a function of test time for the test performed in

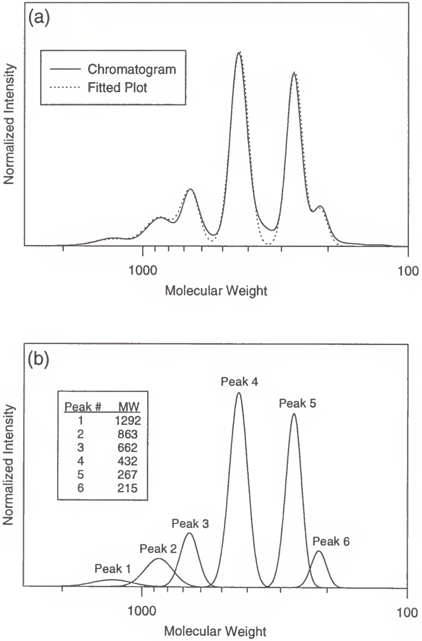

Figure 4-6. Comparison of molecular weight chromatogram and fitted data for the IN12NC 3 hour sample (r^2= 0.999) (a) and peak fit curves generated for the as-received sample (b).

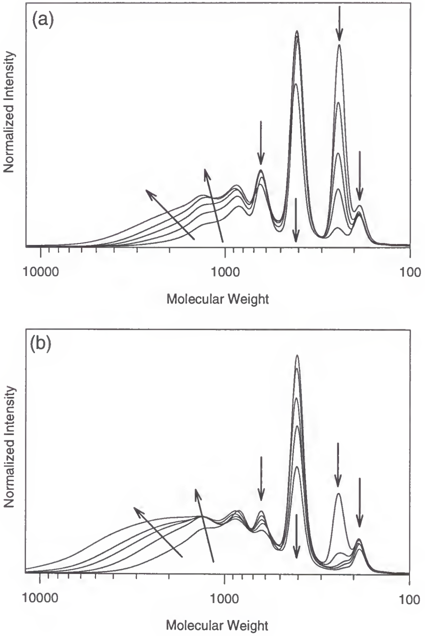

Figure 4-7. Comparison of molecular weight chromatogram curves for tests IN12NC (a) and OX12NC (b).

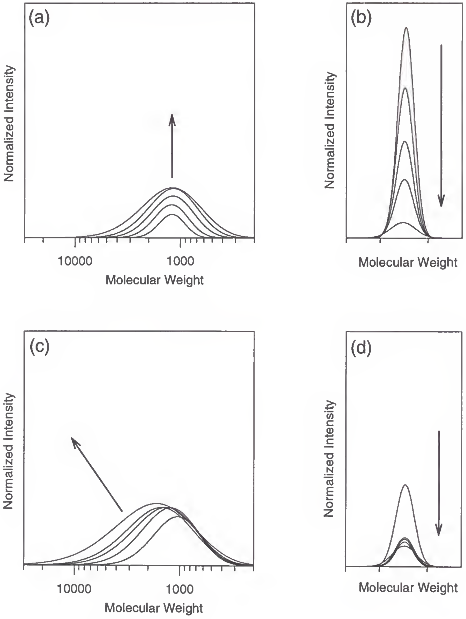

Figure 4-8. Comparison of 1292 and 225 molecular weight curves for tests IN12NC, (a) and (b), and for OX12NC, (c) and (d).

the oxidative environment. However, it should be noted that for peak 5 of OX12NC, the peak location appears to decrease in molecular weight (see Figure 4-7(b)). This decrease could be the result of a peak shift, but is more likely of the observance of a second species which was initially hidden by peak 5 (the known antiwear additive tricresylphosphate has a molecular weight of 360). This suggests that peak 5 might not be accurately represented by including the information from the new peak. Therefore, analysis of results for peak 5 will be performed for peak height, not peak area.

4.4.4. Peak Analysis

The significance of the changes for peaks 1 (1292 MW) and 5 (267 MW) can be understood from the observation of a number of correlations. Figure 4-9 shows viscosity changes versus the formation of high molecular weight species reflected by increasing area in peak 1. Two fitted curves are presented, one for the data points from tests performed in non-oxidative environments and the other for data points representing oxidative testing. The two curves deviate at approximately 25% viscosity change and 55% peak area, showing dramatic increases in peak area for the test performed in oxidative environments. Further comparisons were made for TAN results plotted against peak 1 area, as shown in Figure 4-10. Again two fitted curves are presented, one for each test environment. Changes in peak area increased dramatically for the oxidative environment data at TAN values above 0.8 and 55% peak area. The increases in peak area as a function of both viscosity and TAN values initially began at the same approximate peak area of 55%. This suggests that the viscosity changes are a direct result of the oil degradation as indicated by the TAN results. Fitted curves for data from the experiments performed in oxidative environments are represented by $y = 5.11 \cdot 10^{-6} \cdot x^{3.95}$ and $y = 5.43 \cdot 10^{-7} \cdot x^{3.66}$ for viscosity changes and TAN values respectively.

Similar correlations were made with changes in intensities for peak 5 (267 MW). As shown in Figure 4-11, decreases in peak height directly correlate with decreasing antioxidant content along the curve $y = 33.04 \cdot x^{0.23}$. Since the minimum molecular weights for the base stock esters pentaerythritol and 1,1,1-trimethylolpropane (Figure 2.3) are 374 amd 302 respectively, peak 5 can be attributed directly to the antioxidant.

A second correlation for peak 5 is shown in Figure 4-12, where peak height is plotted versus changes in viscosity. These results show that viscosity increased at a constant rate to 25% change, reflected by a 10% height in peak 5, before increasing significantly. This shows that increasing viscosity was not dependent on the removal of a low molecular weight species (as is one possibility), but rather completely dependent on the depletion of the antioxidant. Furthermore, Figure 4-12 shows that the effectiveness of the antioxidant is lost when peak 5 height has dropped to approximately 10%, thus correlating with Figure 4-11 to an antioxidant concentration between 55-60% as determined by the RULLER technique.

To establish if the removal of the antioxidant is dependent on the individual variables presented in this chapter's series of experiments, peak 5 heights for all 8 test series were plotted versus test time (Figure 4-13). Results were compared for experiments performed in non-oxidative environments with catalyst and/or high humidities to results for the RED12NC test. Peak heights decreased at a constant rate

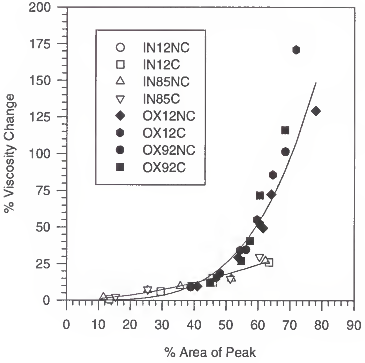

Figure 4-9. Viscosity changes versus changes in percent area of peak 1. Plotted lines correspond to oxidative environments ($y = 5.11 \cdot 10^{-6} \cdot x^{3.95}$) with r^2=0.82 and non-oxidative environments ($y = 0.019 \cdot x - 1.75$) with r^2=0.94.

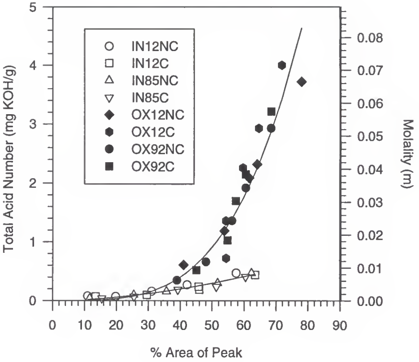

Figure 4-10. Changes in total acid number versus changes in percent area for peak 1. Plotted lines correspond to oxidative environments ($y = 5.43 \cdot 10^{-7} \cdot x^{3.66}$) with r^2=0.75 and non-oxidative environments ($y = 2.95 \cdot 10^{-4} \cdot x^{1.77}$) with r^2=0.92.

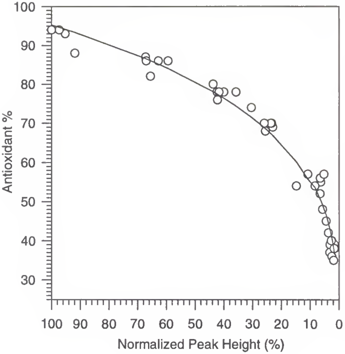

Figure 4-11. Changes in antioxidant content versus normalized height for peak 5. Fitted line reflects $y = 33.04 \cdot x^{0.23}$ with r^2=0.98.

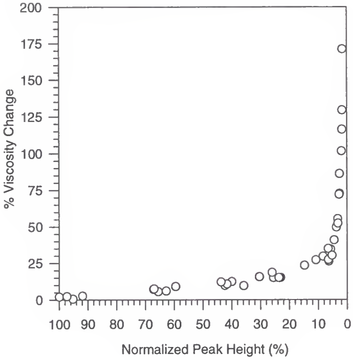

Figure 4-12. Changes in viscosity versus normalized height for peak 5.

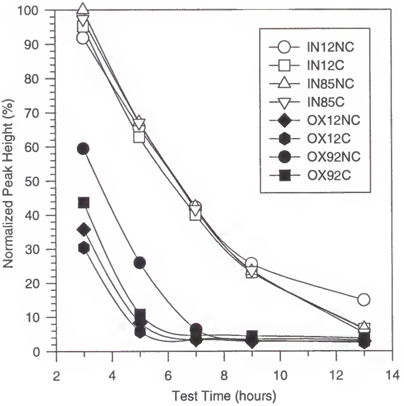

Figure 4-13. Changes in normalized height of peak 5 versus test time for all test series.

until the 9 hour sample time (~25% peak height), at which time the rate of change for the peak 5 height decreased, particularly for the IN12NC test. This suggests that the depletion of antioxidant as a result of the thermal degradation mechanisms is increased slightly by both the presence of catalyst surfaces and high humidities.

Results for the test series performed in oxidative atmospheres yielded dissimilar results. Initial rates of decreasing peak 5 height are not the same, as high humidity environments decreased the rate in which peak 5 changed, while the presence of the catalyst material increased the rate at which peak 5 was removed. This information supports the results shown in Figures 4-2 through 4-4, where viscosity, TAN, and antioxidant concentration data showed identical trends with respect to catalyst and humidity. The depletion of antioxidant, increase in TAN values, and the increase in viscosity were accelerated by the presence of catalyst, and hindered by high humidity for the experiments performed in oxidative environments.

4.4.5. Analysis of the Volatiles

Analysis of the condensed vapors from the OX12NC test showed the evaporation of at least two distinct chemical species which spontaneously phase separated, with the denser phase incorporating more than 75% of the liquid volume. Analysis of the first species was performed using FTIR with a circular fluid stage and results compared to those for deionized water. As seen in Figure 4-14 (a), the hydroxyl peaks located between 3000-3500 and at 1635 cm^{-1} are identical for both spectra. Minor peaks are located between 2800-3000 cm-1, representing vibrational characteristics of alkane species.[Sil81] This suggests that the sample might contain small amounts of alcohol.

Since special care was taken to ensure that no condensation would occur between sampling and cooling of the condenser tube, these results show that water is a major degradation product for the synthetic oil.

Transmission FTIR showed the second species to be either an ester, ketone, or carboxylic acid (see Figure 4-14(b)). As with the previously mentioned results for the oil samples, the only peaks which could be identified were those representing alkane and carbonyl vibrations. For vapor samples which were collected as a function of test time, spectra for this species did show changes in peak ratios. However, the significance of these changes could not be determined due to the fact that identification of this compound has not been confirmed.

Molecular weight tests performed on a mixture of both species show changes in peak heights and locations. As seen in Figure 4-15, the 3 hour sample consisted of species with similar molecular weights to those of the as-received oil sample. For the 7 hour test sample, the lower molecular weight peaks shift. These results show original species of the oil are evaporating at the 250°C test conditions. Furthermore, volatile degradation products are generated and not detected in the oil samples. These molecular weight results also suggest that the antioxidant (or a degradation product of the antioxidant) is one of the volatiles.

In order to confirm the formation of water as a volatile degradation product, coulometric Karl Fisher was performed. The as-received oil sample had a water content of 566 ppm. Water content initially fell during the first hours of oil testing, but leveled off or increased for higher test times. This confirms the FTIR results which showed water

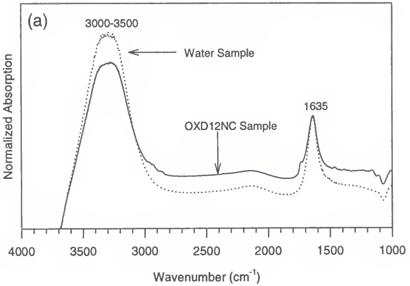

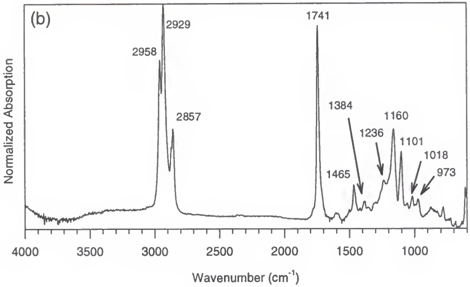

Figure 4-14. FTIR spectrums for volatile phases condensed from test OX12NC. The denser phase (a) consists of a water solution, and the less denser phase (b) consists of an ester.

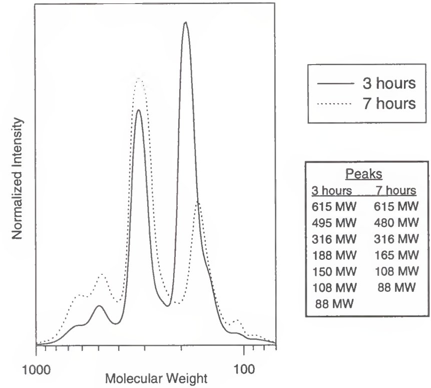

Figure 4-15. Molecular weight distibution for condensed volatiles from test OX12NC at 3 and 7 hour test times.

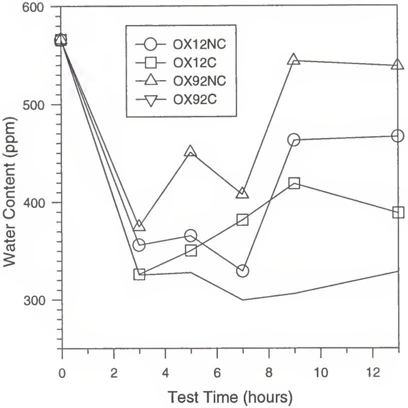

Figure 4-16. Water content for tests performed in oxidative environments.

to be a degradation product. Results for the tests performed in non-oxidative environments showed no obvious correlations between test conditions and times, as water content fluctuated between 325-575 ppm. Results for samples from the oxidative test environments are shown in Figure 4-16, where water content is shown to initially fall below 400 ppm, before gradually increasing at rates which were increased by the presence of high humidities and catalyst materials. Final water content values for the oxidative test environments ranged between 327 ppm for the OX12NC test and 538 ppm for the OX92C test. Although both catalyst and high humidity increased water content and therefore seem to increase water generation, the humidity variable is not actually behaving in this manner. Results for viscosity, total acid number, and antioxidant content testing presented in Figures 4-2 through 4-4 show that the high humidity environments slow the degradation process. Therefore, the results of increasing water content in high humidity environments is attributed to the absorption of water vapor by the oil.

A mechanism for the lower degradation rate for oil samples tested under high humidity environments can now be proposed. Water vapor which is absorbed by the oil acts to hinder the formation of the high molecular weight degradation products by slowing the reaction which depleted the antioxidant, thus delaying the chemical and physical changes associated with extreme oil degradation.

4.4.6. Rate of Degradation

The effects humidity and catalyst presence have on the actual rate of degradation can be determined. The degree of degradation was generated for peak 1 results using the following:

$$\text{Growth Factor} = \text{Mean Molecular Weight} \times \text{Peak Area Fraction} \qquad (4\text{-}1)$$

Rate of degradation was then determined by plotting growth factor versus test time for each test series performed in an oxidative environment (Figure 4-17(a)). Since the growth factor is a representation of the concentration of high molecular weight degradation product, the linear relationship for each test with time indicates that the 1292 MW peak is represented by multilple species and that the formation of the degradation products follows a high order kinetic reaction (2nd or higher) [Ste89]. Table 4-2 lists linear correlation coefficients ($r^2 \geq 0.985$) and slopes for each test series. With high order kinetic reactions, the slope *m* of the concentration is related to the rate constant by the following equation:

$$m = 2 \cdot k \qquad [4\text{-}2]$$

The rate constant *k* is dependant on concentration of degradation products with respect to one another. Since the exact order of the kinetic reactions cannot be determined without knowing concentration of the degradation products, the rate constant connot be determined.

Table 4-2. List of correlation coeffiencents and slopes for plot of Growth Factor versus test time shown in Figure 4-17(a).

Test ID	Correlation Coefficient (r^2)	Slope (m)
IN12NC	0.997	56.43
IN12C	0.985	53.60
IN85NC	0.993	57.84
IN85C	0.992	54.28
OX12NC	0.994	84.09
OX12C	0.998	87.25
OX92NC	0.996	79.94
OX92C	0.996	77.74

Further comparison can be made between the effects of catalyst, humidity, and atmosphere using the information shown in Figure 4-17(a) and Table 4-2. Although not supported by multiple data points, results show that the rate of formation of high molecular weight species increased with the presence of the M-50 steel catalyst and decreased for those samples tested in high humidity environments. Maximum growth factor values in non-oxidative environments were found to vary between 686 and 718. For the experiments performed in oxidative test environments, maximum growth factor values varied between 1160 and 1366.

In order to interpret how the formation of high molecular weight species affects lubricant performance, the interactions of the molecular weight species found in peak 1 must be related with viscosity results. Since all viscosity measurements reflected Newtonian behavior, the Einstein equation, Eq. (4-3), for particle content can be investigated as a plausible explanation for changes in both optical and viscoelastic behaviors.[Ein56,Hun93b]

$$\eta^* = \eta_o \cdot (1 + \frac{5}{2} \cdot \phi) \tag{4-3}$$

The η^* refers to the experimental viscosity, η_o refers to the as-received viscosity, and ϕ refers to the percent particle volume of the system. Particle volume values for all samples are shown in Table 4-3. In Figure 4-17(b), the calculated particle content is shown to correlate with changes in the high molecular weight degradation product represented by the growth factor. This correlation suggests that the degradation products are acting as particulate species with respect to physical changes shown by the viscosity results. The fitted curve for Figure 4-17(b) follows the parabolic relation $y = 0.036 - 1.82 \cdot x + 4.51 \cdot x^2$ and has a correlation coefficient of r^2=0.99.

Table 4-3. List of values for fractional particle volume (ϕ) calculated for the oil samples using Eq. 4-3.

Test\Sample	3 Hours	5 Hours	7 Hours	9 Hours	13 Hours
IN12NC	0.012	0.024	0.043	0.061	0.095
IN12C	0.004	0.026	0.051	0.062	0.106
IN85NC	0.010	0.030	0.040	0.061	0.111
IN85C	0.010	0.031	0.044	0.062	0.122
OX12NC	0.040	0.119	0.200	0.292	0.520
OX12C	0.065	0.139	0.223	0.346	0.687
OX92NC	0.038	0.076	0.141	0.211	0.408
OX92C	0.050	0.110	0.165	0.290	0.467

In order to understand the kinetic information generated and presented using the growth factor (Eq. (4-1)), a review of rate determining and limiting mechanisms by J.Th.G. Overbeek was incorporated.[0ve82] In his article, Overbeek gave definitions for rate of reactions when diffusion is and is not rate determining. Information was presented in terms of mean particle size and particle size distribution. In order to apply this information to the present work, calculations were made to estimate the particle size of the high molecular weight degradation products by calculating the radius of gyration:[Hie84]

$$r_g = \frac{l \cdot \sqrt{\frac{MW}{M_o}}}{\sqrt{6}} \qquad (4\text{-}4)$$

The symbols r_g refers to radius of gyration, l refers to the bond length, chain MW refers to molecular weight, and M_o refers to monomer molecular weight. Since the repeating units for the base ester structures shown in Figure 2-3 are ethylene and since the standard used to calibrate the GPC columns were polystyrene, the monomer weight of polyethylene (M_o=28) and bond length for polystyrene (l=0.53 nm), these values were used for the calculations to estimate the radius of gyration for the high molecular weight degradation products.

Figure 4-18 plots changes in the mean molecular weight values for the high molecular weight degradation product versus changes in the molecular weight distributions of the fitted Gaussian peaks taken to by the full width half maximum values. The estimated values for radius of gyration which correspond to the molecular weight changes are also presented, where $MW{\sim}r_g^2$. As shown during the initial stage of oil degradation (prior to antioxidant removal), changes in particulate size do not correlate with changes in particle size distribution and thus no information can be determined as for the rate limiting effects. After the antioxidant is removed (corresponding on Figure 4-18 to a mean molecular weight value of approximately 1300 MW), changes become linear. This relationship indicates the availability of rate determining information after antioxidant is depleted. From Figure 4-17(a), mean molecular weight (and thus particle radius squared) changes linearly with time, thus following the relationship:

$$a^2 = k \cdot t + b \tag{4-5}$$

where a refers to the particle size and k and b are constants. Integration of Eq. (4-5) shows that changes in mean molecular weight (particle size) follows the kinetic relation:

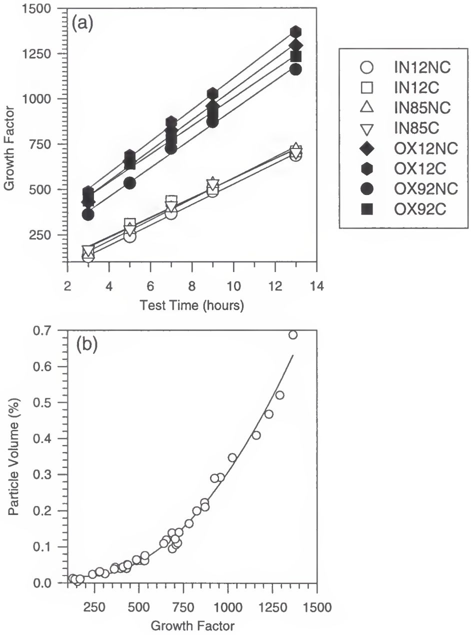

Figure 4-17. Rate of growth for high molecular weight degradation species (a) and viscosity versus growth of the high molecular weight species following parabolic equation $y = 0.036 - 1.82 \cdot x + 4.51 \cdot x^2$ (b) with r^2=0.99.

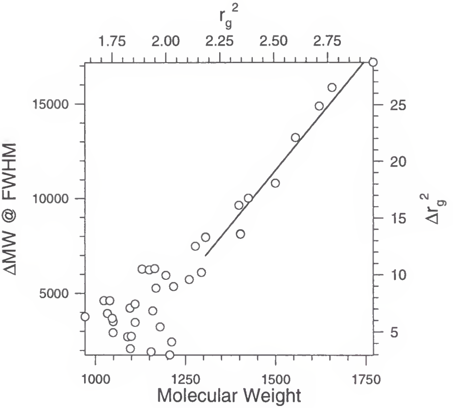

Figure 4-18. Changes in molecular weight distribution versus molecular weight and corresponding radius of gyration values for the high MW degradation product.

$$\frac{da}{dt} = k' \cdot a^{-1} \tag{4-6}$$

where *k'* is a constant. In accordance with the work presented by Overbeek, Eq. (4-6) follows the relation for diffusion limiting growth:

$$\frac{da}{dt} = \frac{D \cdot (c_\infty - c_o) \cdot V}{a^n} \tag{4-7}$$

where D is the diffusion coefficient, V is molar volume, $(c_\infty - c_o)$ is the change in concentration, and n can be 2, 1, 0, and -1. These result thus show that once the antioxidant is removed, degradation in the oil system is diffusion limited.

4.5. Conclusions

Results for tests designed to separate the individual effects of thermal and oxidative degradation mechanisms, as well as to determine the influence of high humidity and the effectiveness of M-50 steel as a catalyst material were performed at 250°C. For tests carried out in inert (non-oxidative) environments, the presence of the M-50 steel catalyst increased and high humidity decreased the rate of antioxidant removal. Although these results were not accompanied by significant changes in viscosity and TAN values, the limited effect of thermal degradation mechanisms on oil degradation for the various environments has been determined.

Results for tests performed in oxidative environments yielded similar results. The presence of the M-50 catalyst material and high humidity showed the same trends in the oxidative atmosphere as for the inert conditions. However, the resulting changes in viscosity, antioxidant content, total acid number, and molecular weight peak area/height were more extreme, showing that the combined effects of oxidative and thermal degradation act to increase the total degradation of the oil significantly more than for thermal degradation alone.

Analysis of volatiles recovered from the degradation tests were analyzed using FTIR and GPC. Results show water to be a primary degradation product. Along with results from Karl Fisher experiments which showed increased water content for the high humidity test environments, the formation of water as a degradation product is used to explain how the test condition of high humidity delayed the depletion of antioxidant and subsequent oil degradation: The degradation reaction which resulted in the formation of water and depletion of antioxidant was hindered by absorption of water by the oil in the high humidity environments.

Changes in concentration of the high molecular weight degradation products have been shown to follow a high order kinetic reaction. The actual order of the reaction is not able to be determined without more information on the degradation species. As for the physical changes in the oil, a direct correlation between the formation of high molecular weight species and viscosity was found using the Einstein equation for Newtonian fluids containing small particles. In this manner, the high molecular weight species are shown to act as particulate materials with respect to the physical behavior of the oil.

Further information on the nature of the oil degradation reaction was determined by relating changes in molecular weight to changes in particle size and distribution of the high molecular weight degradation product. Although no direct conclusions could be drawn for the oil system prior to antioxidant depletion, the knowledge of how free radicals act to degrade oil and how antioxidants act as scavengers to eliminate the free radicals suggests that variations in mean molecular weight and MW distribution are the result of a continuously changing concentrations of free radicals thus resulting in a low rate of degradation. Results showed that after the antioxidant was depleted, the reaction to form high molecular weight degradation products was diffusion limited.

The mechanism for the formation of high molecular weight degradation products may now be proposed. During the initial stages of degradation, the base ester chains degrade to form primary degradation products. The process is the result of reaction with and the formation of free radical molecules which are subsequently rendered inactive by the antioxidant. Once the antioxidant is depleted, primary degradation products continue to be formed, and these products react to form secondary degradation products which are of higher molecular weight. The formation of water suggests that the primary products undergo a polycondensation reaction mechanism, where water is a byproduct. This hypothesis is supported by the fact that high humidity environments, which would place water into the system and inhibit the polycondensation reaction, were shown to reduce the rate of degradation. As for results which show diffusion to be rate limiting after antioxidant depletion, the affect is attributed to the polycondensation reaction mechanism.

CHAPTER 5

THE USE OF UV/VIS SPECTROMETRY FOR OIL MONITORING

5.1. Introduction

Previous research presented in Chapter 3 suggests that the optical behavior of oil samples demonstrated by total loss edge values may be used for oil monitoring. In order to investigate this hypothesis, degraded oil samples were generated at 250°C under varying environmental conditions. Samples were characterized using viscosity, total acid number, antioxidant content, molecular weight, and ultraviolet/visible absorbance spectrometry. Results were used to determine the relationship between absorption data and oil degradation, and to determine the feasibility of utilizing this technique as a means of oil monitoring.

5.2. Background

One of the main goals for the research of hybrid bearing systems has been to determine an *in-situ* method in which component failure can be predicted and therefore prevented. Analysis of the synthetic oils used with these bearing systems is critical in attaining this goal for two reasons. First and foremost, each of the many oil lubricants used for gas turbine engines offer variable performance characteristics and degradation behavior due to proprietary additive packages which are unique to each vendor and military grade. In other words, along with the variable performance conditions which lubrication systems encounter due to differences in such areas as seal integrity, the actual lubricant can dictate lifetime performance. Second, analysis of the oil systems offers a unique opportunity to allow for *in-situ* monitoring of the oil condition by means of sampling and analysis, or by analysis during operation.

5.2.1. Oil Monitoring Techniques

In order to determine the condition of an engine's oil system at any given time, a select number of techniques are chosen. These test methods typically fall into two categories: the analysis of basic fluid parameters and off-line monitoring techniques.

Basic Fluid Parameters

As a first look at the extent of degradation in used oil samples, two basic techniques are used. To determine the extent to which degradation has affected the physical condition of the oil, viscosity testing is employed. To determine the extent to which the oil has chemically degraded, total acid number[1] is used. Total acid number (TAN) is a technique in which a small amount of the oil sample is dissolved in solvents and titrated using 0.1N alcoholic KOH. The amount of KOH solution needed to titrate the oil sample to a specific pH represents the concentration of base neutralized acidic sites on the various oil constituents and degradation products.

Off-line Techniques

Over the past decade, a number of techniques have been developed to determine the condition of degraded oil samples. Through the investigations of Kauffman et al., one particular technique has earned notable recognition. This technique is referred to as the remaining useful lubricant life evaluation rig[2] (RULLER) [Kau89,Kau95a,Kau95b]. A small sample of degraded oil is dissolved in a solvent and tested using a voltametric method to determine the antioxidant concentration in the oil sample. Taking into account the fact that the lubricant begins to degrade before the antioxidant content is completely depleted, the percent of antioxidant remaining is related to the remaining useful life of the used oil sample.

A second notable off-line technique is the complete oil breakdown rate analyzer[3] (COBRA). With this technique, changes in the electrochemical properties of oil samples are evaluated. Analysis is simple and quick, and results have been shown to correlate well with results from TAN analysis. Due to this correlation with TAN and due to faster analysis times, COBRA has been implemented as a technique to predict TAN results.

5.2.2. Ultraviolet/Visible Absorption Spectrometry

Ultraviolet and visible (UV/VIS) spectrometry is a commonly used technique for the identification of organic compounds [Mat86,Rab80,Sil91]. Absorbance of a particular molecule occurs when two criteria are met. The difference between two energy levels for a given macromolecule must be exactly equal to the energy associated with an incoming wavelength, and one energy level must contain an electron and the other a vacancy, as seen in Eq. (5-1):

$$\Delta E = h \cdot v = E_1 - E_2 \tag{5-1}$$

---

[1] ASTM 664-89.

[2] University of Dayton Research Institute, Dayton, OH 45469.

[3] COBRA Program, WPAFB, OH 45433.

where h is Plank's constant ($6.63\text{x}10^{-34}$ J•s), ν is frequency (s^{-1}), and E_1 and E_2 refer to the initial and final energies of the macromolecule respectively. Measurements are typically made between 200 and 900 nm, with added information available at larger wavelengths in the near-infrared region (NIR).

Performing qualitative analysis with UV/VIS spectrometry can be difficult. The vast numbers of absorbing species for each wavelength make the task of identification difficult without knowledge of the exact structures present [Mat86]. Application of ultraviolet spectroscopy (short λ's) is limited due to the large number of species which absorb in this region. Molecules must contain chromophoric groups in order to absorb, which include (poly)enes, molecules with aromatic rings, and molecules with carbonyl groups [Rab80].

Quantitative analysis using UV/VIS spectrometry is possible using the Beer-Lambert law as seen in Eq. (5-2) [Mat86, Rab80].

$$A = \log_{10}\left(\frac{Io}{I}\right) = \varepsilon \cdot c \cdot l \tag{5-2}$$

A is the absorbance, I_o is the intensity of the incident light (quanta/second), I is the intensity of the transmitted light (quanta/second), ε is the molar absorptivity or extinction coefficient ($liters \cdot mol^{-1} \cdot cm^{-1}$ or $m^3 \cdot kg^{-1} \cdot m^{-1}$), c is the concentration, and l is the optical path length. This equation yields a linear relationship between the concentration and absorptivity of a given species. For most accurate results in measuring the absorptivity of a given species, measurements of peak height should be made at absorbance maximum.

5.2.3. Objective

In this chapter, the absorption behavior of degraded oil samples in the ultraviolet and visible regions of the electromagnetic spectrum will be determined, thus evaluating this technique as a means for *in-situ* oil monitoring. Referred to as UV/VIS absorption spectrometry, this technique offers a unique opportunity in chemical analysis due to the fact that tests are quick and sensors can be manufactured to relatively small sizes. Results from Chapter 3 yielded a linear relation between total loss edge values and changes in viscosity. This linear relationship held for oil samples degraded to various times under different temperature treatments (210-300°C), showing total loss edge values to be independent of temperature variations. As a result, degradation of oil samples for this study will be limited to environmental variables only.

5.3. Materials and Methods

In order to determine the potential of using UV/VIS absorption spectrometry for oil monitoring, a series of oil degradation experiments was performed at 250°C under varying environmental conditions. As shown in Table 5-1, a total of eight experiments were performed while varying atmosphere, humidity, and the presence of M-50 steel surfaces. For each test, 750 ml of as-received ETO 2380 synthetic oil (MIL-L-23699) was placed in a Pyrex beaker on a hot plate (see Figure 5-1). The hot plate was connected to a constant temperature controller. The thermocouple from the controller was covered with a glass capillary tube sealed at one end with a H_2/O_2 torch, then placed into the oil bath. Gas flow was supplied to the oil bath using a flow meter set to 0.83 L/min and a glass dispersion tube placed into the bath. Finally, the beaker was wrapped in fiberglass insulation to aid in temperature control. In this manner, the oil was completely isolated from metallic surfaces which might act as catalysts. The hot plate was set to the highest setting and the temperature controller was set to 250°C, resulting in a heating rate of approximately 225°C/hour.

Table 5-1. List of degradation experiments used for UV/VIS spectrometry testing.

Test ID	Temperature	Atmosphere	Humidity	Catalyst
IN12NC	250°C	inert (Ar)	<12 %	None
IN12C	250°C	inert (Ar)	<12 %	M-50
IN85NC	250°C	inert (Ar)	~85 %	None
IN85C	250°C	inert (Ar)	~85 %	M-50
OX12NC	250°C	oxidative (Air)	<12 %	None
OX12C	250°C	oxidative (Air)	<12 %	M-50
OX92NC	250°C	oxidative (Air)	~92 %	None
OX92C	250°C	oxidative (Air)	~92 %	M-50

In accordance with Table 5-1, gas flow supplied to each experiment was either compressed argon, resulting in a mildly inert (non-oxidative) atmosphere which would promote thermal degradation without oxidative degradation, or compressed air which would promote both thermal and oxidative degradation. Samples of M-50 steel were supplied as catalyst surfaces for the designated tests in the form of 1/4" diameter bearing balls placed in the oil bath at the beginning of each of the experiments. The

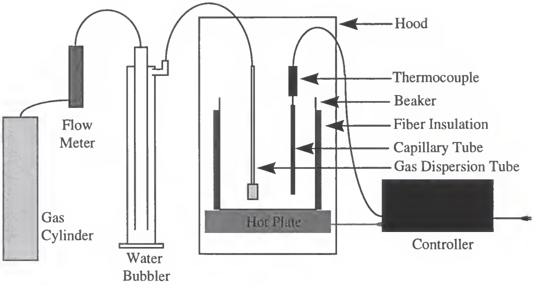

Figure 5-1. Assembly for degradation experiments. Water bubbler, presence of M-50 bearing balls placed in the beaker, and gas type dependent on individual test description.

resulting ratio of available surface area to oil was 3.6 mm^3/ml, which was kept constant for each of the appropriate tests. For tests performed under low humidities, gas flow for both compressed argon and air was determined with an on-line sensor[4] to be ≤12% RH. For the tests performed under high humidity, a liquid bubbler filled with distiller water was placed between the flow meter and the oil bath. The resulting relative humidities for the gas flow entering the bath were 85% for argon and 92% for air.

In order to analyze changes in oil condition with test time, 50 ml samples were taken during each experiment using a glass pipette. Sample times recorded from initial heatup were 3, 5, 7, 9, and 13 hours. Each sample was stored in a glass bottle with a Teflon lined lid to protect the oil samples from the environment and to prevent absorption of water, which might lead to further degradation.

In order to determine the effects of degradation on the physical behavior of the oil samples, viscosity tests were performed using a variable speed rheometer[5] with a 0.8° cone angle. Experiments were performed at 40±0.1°C using a constant temperature water bath, thereby producing results comparable with military specifications.

The extent to which oil degradation had occurred for each sample was determined using a number of analytical techniques. Antioxidant concentration for each sample was determined using a remaining useful lubricant life evaluation rig (RULLER) and the extent to which degradation had occurred was determined from the total acid number (TAN). For TAN determination, there were two modifications to the ASTM procedure, the use of aqueous based standards and titration to pH 11. These techniques are used in combination to predict when an oil is likely to degrade and the extent to which degradation has occurred.

---

[4] Implant Sciences Corporation, Wakefield, MA 01880.

In order to observe the formation of high molecular weight degradation products, size exclusion chromatography, also known as gel-permeation chromatography (GPC), was performed using an ultraviolet/visible (UV/VIS) wavelength detector.[6] A pre-filter and 50-1K, 5K-10K, 20K-300K and 100K-1000K molecular weight range columns[7] were used to determine the molecular weight distribution of each sample, with tetrahydrofuran as the solvent carrier. The columns were calibrated between 92 and 870,000 MW using polystyrene molecular weight standards and toluene. Approximately 20-30 mg of each sample was mixed with 10 ml of tetrahydrofuran and filtered three times through a 0.22 μm Teflon filter before injection. The flow rate was set to 0.4 ml/min, and the injection volume was 20 μl. UV/VIS data for the oil samples was processed at a constant wavelength of 216 nm. Data was calibrated against the polystyrene standards to generate molecular weight distributions from the measured elution times. In order to accurately compare results from each run, all data was corrected by normalizing the areas under each data curve. Evaluation of changes in peak intensity and location of the high molecular weight degradation products was performed using peak separation and analysis software[8] assuming Gaussian distributions.

---

[5] Brookfield RVDV III, Brookfield Engineering Laboratories, Inc., Stoughton, MA 02072.

[6] 600E System Controller, 610 Fluid Unit, 717 Auto Sampler, and 996 Photodiode Array Detector, Waters™ Chromatography Division, Millipore Corporation, Milford, MA 01757.

[7] Phenogel 4.6×300 mm columns, with 5 μm particles and 100, 500, 10^4 and 10^5 Å pore sizes, Phenomenex, Torrence, CA 90501.

[8] Peakfit™ V 4.0, Jandel Scientific Software, San Rafael, CA 94901.

Further tests were performed on these oil samples using UV/VIS spectrometry. Using a portable UV/VIS spectrometer[9], oil samples were placed in a constant path length cell and analyzed for transmittance with ±0.1% accuracy covering the ultraviolet and visible regions of the electromagnetic spectrum between 200 and 900 nm. In order to determine the total loss edge for each sample, the tangent of each spectra was generated and the intercept of the tangent to the x-axis was determined. Further analysis was performed in the near infrared spectrum by measuring absorbance characteristics of the oil samples using a high performance UV/VIS/NIR spectrometer[10] with ±0.1% accuracy between 350 and 2000 nm (2 μm). In order to analyze the absorption behavior of the degrading oil and to determine if the Beer-Lambert law was followed for the absorption behavior of concentrated samples, the 13 hour sample from test OX12NC was diluted in as-received oil and appropriately analyzed.

5.4. Results and Discussion

Oil samples used in this study were generated by degrading a conventional synthetic turbine oil (MIL-L-23699) under various environmental conditions as shown in Table 5-1. Characterization was performed using rheological measurements at 40°C, total acid number, antioxidant content using RULLER measurements, and molecular weight analysis using a UV/VIS detector at 216 nm. Analysis of the absorption characteristics of the oil samples was determined using UV/VIS/NIR spectrometry.

---

[9] Ultrospec III, Pharmacia LKB Biochrom LTD, Cambridge, England.

[10] Lambda 9 UV/VIS/NIR Spectrometer, Perkin-Elmer Corporation, Norwalk, CT 06856.

5.4.1. Sample Characterization

Results from viscosity measurements performed at 40°C showed all oil samples to yield Newtonian behavior without Bingham yield points. Oil viscosity (23.3 cP for the as-received sample) increased with increasing test time for each series of experiments, with more dramatic increases in viscosity changes for those experiments performed in oxidative environments (>100% maximum change) compared to non-oxidative environments (25-30% maximum change). The presence of the M-50 steel catalyst caused more extreme changes in viscosity and the effect of high humidity produced less extreme changes in viscosity, particularly for those samples tested in oxidative environments.

Results for total acid number and antioxidant content changes as a function of test time and environment showed changes similar to those for viscosity. As test time proceeded, the extent to which degradation had occurred increased, as indicated by increasing TAN values. The potential for continued degradation also increased, as indicated by decreasing antioxidant content. Variations in the rate of changes in TAN and antioxidant content with respect to catalyst and humidity were consistent with those for viscosity changes. Maximum changes for the 13 hour test samples yielded TAN and antioxidant values of 0.45 and 55% respectively for non-oxidative environments, and 4.0 and <40% respectively for oxidative test environments.

Molecular weight analysis performed on the oil samples showed the formation of a high molecular weight species above 1300 MW. With increasing test time, peak area determined by Gaussian curve fitting increased while maintaining the same mean molecular weight. Upon depletion of the antioxidant, peak analysis showed continual growth in peak area to be accompanied by an increasing shift in mean molecular weight. In order to incorporate changes in both peak area and mean molecular weight of the degradation product, a growth factor has been generated:

$$\text{Growth Factor} = \text{Mean Molecular Weight} \times \text{Peak Area Fraction} \qquad (5\text{-}3)$$

5.4.2. Total Loss Edge Analysis

In order to determine if the oil samples in this chapter exhibit the same linear relationship between total loss edge values and changes in viscosity as shown in Chapter 3, transmittance measurements were performed between 200 and 900 nm. As shown in Figure 5-2 for samples from tests IN12NC (a) and OX12NC (b), the transmittance behavior of the oil samples decreased and the loss edge increased to higher wavelengths as test time proceeded. Values for total loss edge were determined by extending the tangent for each spectra to the zero percent transmittance intercept. Total loss edge (TLE) values for all eight test series are plotted versus corresponding changes in viscosity in Figure 5-3. For the samples generated in non-oxidative environments, a linear relationship between the TLE values and viscosity changes is shown with a slope of 8.11. For samples generated in oxidative environments, the initial increase in TLE values with increasing viscosity follows the same slope as for samples tested in non-oxidative environments (m=8.11) until approximately 675 nm and 25% viscosity change, at which the viscosity begins to increase at a greater rate following the curve $y = 482.91 \cdot x^{0.10}$. For the as-received sample, a TLE value of 390 nm shows that the pristine oil does not correlate with the linear relation observed during the initial stages of degradation.

Deviations for experiments performed in oxidative environments from the linear relationship found for the non-oxidative environments can be explained by observing the chemical changes in the oil samples shown by total acid number (TAN) and antioxidant concentration changes. Figure 5-4(a) shows TAN values plotted against changes in antioxidant content for all test series. As degradation proceeded, antioxidant content fell below 40% and leveled off, an artifact of the RULLER test machine which interprets some degradation products to be antioxidant species. Since TAN values are not considered significant until above 1.0, Figure 5-4(a) shows that extensive oil degradation initiated when the antioxidant content fell below approximately 60%. Knowing the antioxidant concentration level at which significant degradation began (i.e. at the onset of antioxidant depletion), the plot of antioxidant content versus viscosity change (Figure 5-4(b)) can now be used to determine the corresponding viscosity change. A 60% antioxidant content corresponds to a 25% change in viscosity, the same value at which total loss edge began to deviate in Figure 5-3. Once the antioxidant level fell below approximately 60%, significant chemical changes occurred in the oil until approximately 40% antioxidant, at which point the chemical changes were accompanied by significant physical changes as indicated by the viscosity results. This region between 60-40% antioxidant content and 25-50% viscosity change is considered to be the region in which antioxidant content becomes critical. Thus, comparing these results with Figure 5-3, the TLE values accurately correspond to the physical changes in the oil samples until the antioxidant level reaches the critical concentration.

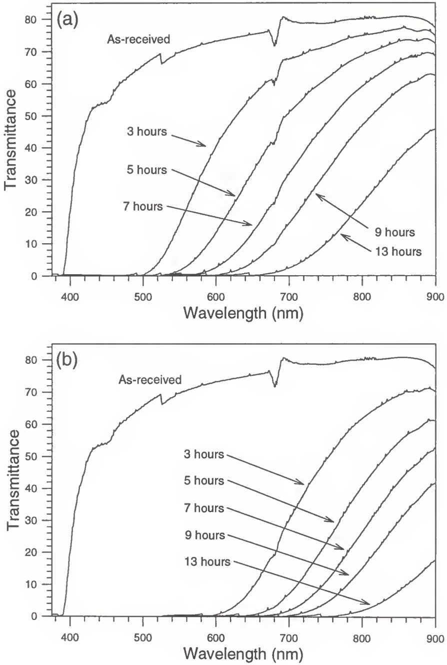

Figure 5-2. UV/VIS spectra for tests IN12NC (a) and OX12NC (b), plotted as transmittance versus Wavelength.

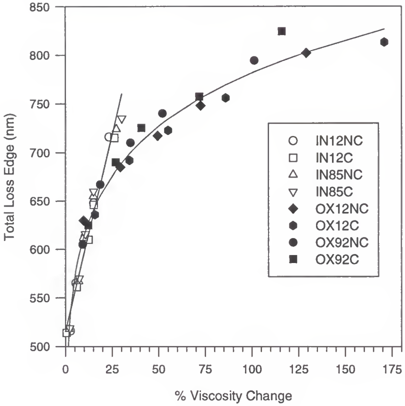

Figure 5-3. Total loss edge versus changes in viscosity. Lines reflect oxidative ($y = 482.91 \cdot x^{0.10}$) and non-oxidative environments ($y = 8.11 \cdot x + 515.13$) with correlation coefficients of r^2=0.96.

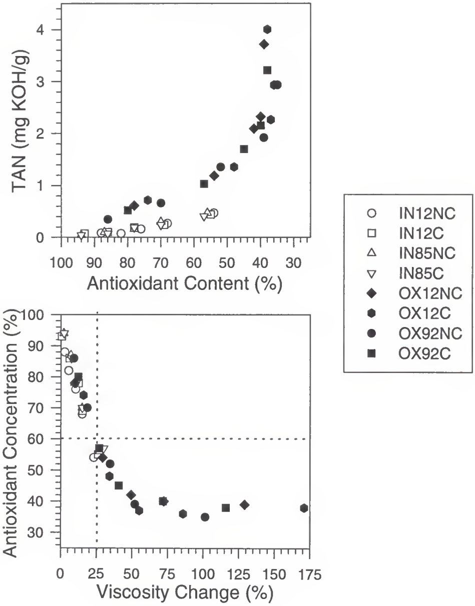

Figure 5-4. Total acid number results versus antioxidant content (a) and antioxidant content versus viscosity changes (b). Dotted lines indicate onset of chemical degradation in the oil samples.

5.4.3. Variations in Total Loss Edge Values in Chapters 3 and 5

Differences in the UV/VIS absorption results for this chapter's experiments and those from Chapter 3 include a different slope in TLE versus viscosity change behavior during initial degradation, and deviations from the linear behavior for samples which had undergone extensive degradation under oxidative environments. The significance of the differing slopes for results in Chapter 3 (m=5.44) and this chapter (m=8.11) can be explained by the test description. In Chapter 3, samples were generated by placing oil in a beaker and heating for specific times at various temperatures. In this chapter's experiments, oil samples were generated in a test setup which included compressed gas bubbling through the oil. Since gas flow would aid in removing low volatile oil species and degradation products, the concentration of high molecular weight degradation products would be increased. The optical behavior of the oil samples would be expected to change at a faster rate, as seen with results for experiments performed in this chapter with bubbling gas.

Deviations from the linear relationship between total loss edge values and changes in viscosity after antioxidant depletion can also be explained by the differences in degradation test methods. Heating synthetic oil samples above 200°C results in the generation of volatile species which prevent the adsorption of oxygen without the addition of gas as described for this chapter's degradation tests. Without this oxygen addition, the test setup in Chapter 3 was unable to supply oxygen to the heated oil and was the equivalent to a non-oxidative environment.

5.4.4. Absorption Behavior of the Degraded Oil Samples

In order to understand the correlation between total loss edge values and physical degradation effects reflected by viscosity changes, the absorption behavior of the oil samples generated for this study must be determined. This was accomplished using a high performance ultraviolet/visible spectrometer which was capable of detecting absorption characteristics in the near infrared spectra region. Samples were tested to higher wavelengths within the infrared region in order to discern absorption and scattering effects in the oil. Figure 5-5 shows absorbance behavior of samples from tests IN12NC (a) and OX12NC (b) to wavelength values of 1100 nm. As indicated by the direction of the arrows, the absorption behavior shifts in the same manner as the transmittance results shown in Figure 5-2. As degradation proceeds, both absorbance and loss edge shift to higher wavelengths.

In order to determine if spectra changes for the oil samples were the result of absorption rather than scattering, portions of the 13 hour sample from test OX12NC were diluted in as-received oil to concentrations shown in Table 5-2. These solutions were mixed and then tested using the high performance UV/VIS/NIR spectrometer. The results are shown in Figure 5-6(a). The absorbance of the solutions increased and loss edge shifted to higher wavelengths with increasing concentration, as indicated by the arrow.

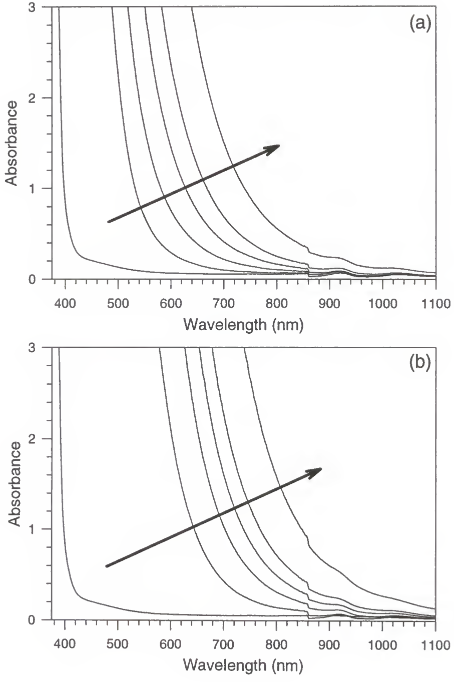

Figure 5-5. Absorbance spectra for tests IN12NC (a) and OX12NC (b).

Table 5-2. List of concentrations (weight percent) and normalized absorbance peak areas (given in percent change) for OX12NC 13 hour test sample diluted in as-received oil.

Concentration (weight %)	Area Peak 1 (355 nm)	Area Peak 2 (415 nm)	Area Peak 3 (500 nm)
0.36%	-28%	86%	200%
0.54%	-32%	136%	220%
0.66%	-40%	157%	300%
0.85%	-44%	176%	520%
2.09%	-50%	597%	900%
4.95%	NA	1610%	2650%
9.45%	NA	3189%	4100%
29.12%	NA	7400%	6900%
50.00%	NA	13,058%	14,900%
75.00%	NA	19,637%	19,900%
100.00%	NA	23,584%	21,900%

The changes in absorption behavior have been attributed to the presence of three absorption peaks, located at 355, 415 and 500 nm and referred to as peaks 1 though 3 respectively. Peaks were fitted for Gaussian distributions and as shown in Figure 5-6(b). Peak 1 is initially highly absorbing and decreases in intensity as concentration of the degraded oil increases. Peaks 2 and 3 initially are not strongly absorbing, however increase in absorbance with increasing concentration of the degraded oil. In Figure 5-6(b), the most absorbing peak for the given concentrations are identified. For dilutions of 2.09% and below, peak 1 is dominant and thus dictates the location of the total loss edge (extrapolated to an absorption value of 5 corresponding to 0 transmittance). For concentrations of 9.45 and above, peak 2 is most absorbing and dictates the location of the loss edge. These results show that the absorbance spectra (and associated total loss edge values) will reflect the extent of oil degradation, but only after a certain amount of degradation has occurred and a large enough concentration of degradation species exist.

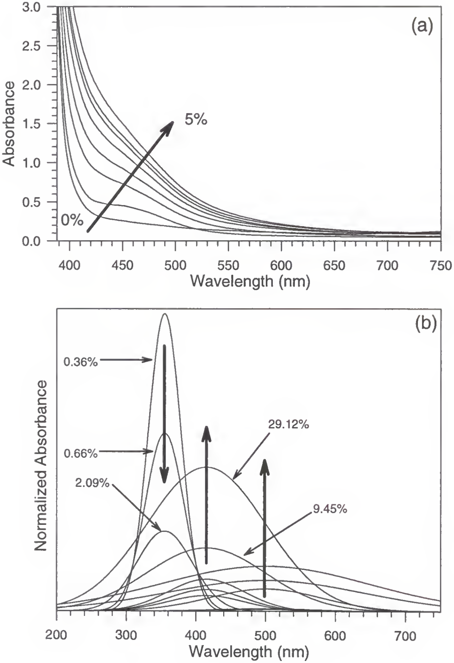

Figure 5-6. Changes in the absorbance spectra for the OX12NC, 13 hour sample diluted in as-received oil as a function of concentration (a), and changes in intensities for 355, 415, and 500 nm peaks with changes in concentration (b).

Evident from these results is the explanation as to why the as-received oil sample does not correspond with the linear relationship observed during the initial stages of degradation between TLE values and viscosity changes: The initial TLE value for the as-received sample reflects the absorption behavior of the base ester and does not reflect degradation until the absorbance of peaks 1 and 2 decrease and increase respectively to the point in which peak 2 predominates.

5.4.5. Absorption Behavior and Degradation Product Concentration

Results of changes in the absorption behavior of the degraded oil sample diluted in as-received oil (shown in Figure 5-6) suggests that absorption characteristics are directly related to the concentration of the degradation products. In order to test this hypothesis, the Beer-Lambert law (Eq. (5-2)) for this oil system must be confirmed. Changes in peak area as a function of concentration were calculated from fitted Gaussian distributions and used for absorbance values (listed in Table 5-2). Figure 5-7 shows changes in absorbance peak area as a function of concentration for peaks 2 and 3. Both peaks yield linear results, and thus confirm to the Beer-Lambert law.

Results shown in Figure 5-7 yielded slopes for both peaks which are approximately equal (m= 4.07 and 4.16 for peaks 2 and 3 respectively), suggesting that both peaks are due to the same degradation product. In order to determine if the absorbing species are the high molecular weight products observed in gel permeation chromatography (GPC) analysis, the absorbance characteristics for test samples from all eight degradation experiments must be determined. Figure 5-8(a) shows the absorption characteristic for peak 2 area ($y = 0.86 \cdot x^{1.34}$) and peak 3 ($y = 0.14 \cdot x^{1.68}$) plotted versus changes in peak area for the high molecular weight degradation product. Both absorption peaks follow the same general trend until approximately 45% peak area, at which the absorbance values for peak 3 undergo positive deviation with respect to peak 2. To understand the significance of this change in absorbance behavior, Figure 5-8(b) shows the changes in peak area for the high molecular weight species versus changes in viscosity for the oil samples. At values of approximately 45%, peak 3 area for experiments performed in oxidative environments deviate from the initially linear relationship between peak 2 area and viscosity change. This deviation signifies the onset of physical changes which result from extreme oil degradation. Relating this data to the results for absorbance changes in Figure 5-8(a) show that deviations for both plots occur at 45%, thus signifying that the absorbance characteristics for peak 2 and 3 do not reflect the same behavior.

Further comparisons can be made between absorbance values and the growth factor (Eq. (5-3)) associated with the high molecular weight species, shown in Figure 5-9. Absorbance values for peaks 2 and 3 increase at the same rate until the mean molecular weight values for the high molecular weight peak begins to increase. The absorbance values for peak 3 then undergoes positive deviation with respect to peak 2. This behavior shows that peak 2 represents the increasing molecular weight peak area associated with the degradation product, and that absorbance peak 3 represents both increases in area and mean molecular weight values for the degradation product. Thus the absorbance behavior of peak 3 is more representative of oil condition.

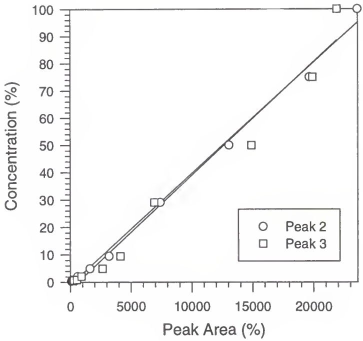

Figure 5-7. Absorbance values for peaks 2 and 3 for the OX12NC, 13 hour test sample diluted in as-received oil to concentrations listed in Table 5-2. Linear regression coefficients and slopes for peaks 2 and 3 are $r^2=0.99$, m=4.07 and $r^2=0.98$, m=4.16 respectively.

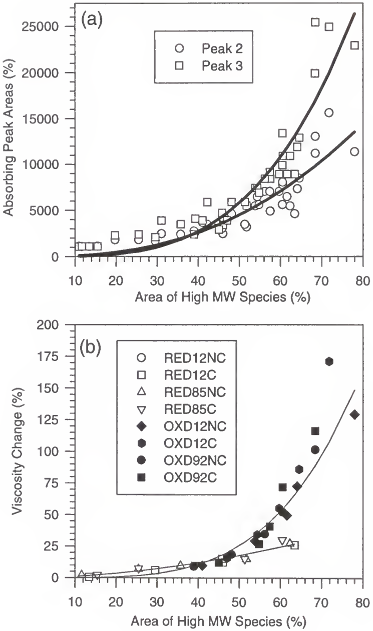

Figure 5-8. Changes in absorbance (a) for peak 2 ($y = 0.86 \cdot x^{1.34}$) area and peak 3 ($y = 0.14 \cdot x^{1.68}$) area with correlation coefficients of r^2=0.93 and 0.95 respectively , and changes in viscosity (b) versus changes in area of the high moleular weight species. with coefficients of r^2=0.82 and 0.93 for the oxidative and inert environments respectively.

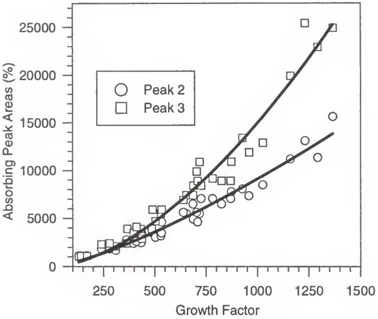

Figure 5-9. Changes in absorbance peak 2 and 3 areas versus changes in growth factor for the high molecular weight degradation species with correlation coefficients of $r^2=0.96$.

5.4.6. Degradation Product Concentration Versus Particle Volume

From the absorbance information generated for the oil samples, relative concentration of the absorbing species can be determined by normalizing the absorbance area for a given peak with respect to the most degraded test sample. Although this normalization method does not allow for determination of the extinction coefficient associated with the absorbing species, the method does allow for a general description of the extent to which the quantity of degradation product affects the overall absorbance properties of the test samples. Further comparisons can be made with the physical changes associated with oil degradation by treating the high molecular weight degradation product as particulates. Since all viscosity measurements reflected Newtonian behavior, the Einstein equation, Eq. (5-4), for particle content can be investigated as a plausible cause for both optical and viscoelastic behaviors.[Ein56,Hun93b]

$$\eta^* = \eta_o \cdot \left(1 + \frac{5}{2} \cdot \phi\right) \tag{5-4}$$

The η^* refers to the experimental viscosity, η_o refers to the as-received viscosity, and ϕ refers to the particle volume fraction of the system. Values for the particle content are shown in Table 5-3. Assuming that viscosity changes in the oil samples are the result of high molecular weight degradation products acting as particulate species, the estimated particle content determined using Eq. (5-4) may be compared with absorbance data. Figure 5-10 shows the relationship between particle volume as calculated using Eq. (5-4) and the relative concentration of the degradation species determined for absorbance peaks 2 (a) and 3 (b). Particle volume calculations yielded maximum values of 0.69%. Concentrations associated with the absorption peaks show linear relationships, with slope and correlation coefficients of m=1.34 and r^2=0.93 for peak 2 and m=1.55 and r^2=0.92 for peak 3. The differences in slopes may in fact signify that the two absorbance peaks do not reflect the same behavior. Furthermore, the linear relationships shown in Figure 5-10 support the hypothesis that the high molecular weight degradation products behave as particulate species.

Table 5-3. List of values for fractional particle volume (ϕ) calculated for the oil samples using Eq. 5-4.

Test\Sample	3 Hours	5 Hours	7 Hours	9 Hours	13 Hours
IN12NC	0.012	0.024	0.043	0.061	0.095
IN12C	0.004	0.026	0.051	0.062	0.106
IN85NC	0.010	0.030	0.040	0.061	0.111
IN85C	0.010	0.031	0.044	0.062	0.122
OX12NC	0.040	0.119	0.200	0.292	0.520
OX12C	0.065	0.139	0.223	0.346	0.687
OX92NC	0.038	0.076	0.141	0.211	0.408
OX92C	0.050	0.110	0.165	0.290	0.467

5.4.7. Association of Absorbance Peaks

Identification of the absorbing species reflected by peaks 1 through 3 has not been accomplished. Possible degradation products for synthetic oil systems and the lack of absorption information on each product makes identification impossible at this time. However, knowing that absorption peaks 1 and 2 are in the ultraviolet spectra, that only compounds with chromophoric groups (e.g. poly(enes) and species with carbonyl and aromatic rings) absorb in this region, and that ester compounds are the primary constituent (>90%) in the as-received oil allows for a general association of the probable absorbing species. Since peak 1 decreases and peak 2 increases in, peak 1 can be attributed to the original base ester(s), which decrease in concentration during reaction to form degradation products, and peak 2 can be attributed to the high molecular weight degradation product which contains carbonyl groups.

Since results have shown that the absorption characteristics of both peaks 2 and 3 correlate with the formation of the high molecular weight degradation product, peak 3 must also be associated with this species. However, since peak 3 shows effects from the movement of the degradation product to higher molecular weight values after the antioxidant is depleted (Figure 5-9) and since the slope for concentration versus particle volume (m=1.55) is greater than for peak 2 (m=1.34), peak 3 is attributed to an absorbance property of the degradation product which is dependent on chain length and/or polymer crosslinking. Therefore, the absorbance behavior of peak 3 (rather than peak 2) is most representative of the oil condition in terms of degradation product concentration and size.

5.4.8. Comparison of Peak Area and Total Loss Edge Analysis

This chapter has shown that the technique of using total loss edge (TLE) values to predict the physical changes associate with oil degradation is plausible, and that the TLE values actually reflect the absorbance behavior of peaks associated with the base ester and degradation products. Although the analysis of the absorption peaks has been shown to be an accurate method for observing oil condition, we will now compare information from both absorption peaks area and TLE values in order to determine which technique is more representative of the overall oil condition.

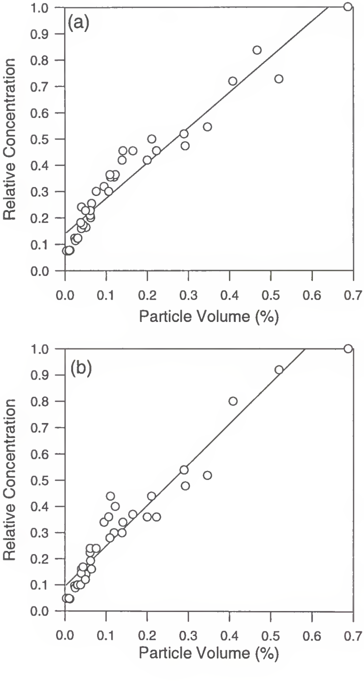

Figure 5-10. Relative concentration of high molecular weight species versus particle volume for absorbance peak 2 (a) where r^2=0.93 and m=1.34, and for peak 3 (b) where r^2=0.92 and m=1.55.

Since the absorbance behavior of peaks 2 and 3 have been shown in Figure 5-7 to confirm the Beer-Lambert law, the area under each absorbance curve can be related to the concentration of degradation product. In Chapter 4, the rate of product generation was shown to follow a high order kinetic reaction by the linear relationship between growth factor and test time (Figure 4-17(a)). To confirm the same behavior for the absorptivity of peaks 2 and 3, Figure 5-11 shows a linear relationship between absorbance and test time. Values for correlation coefficients and slopes are shown in Table 5-4. Comparison of this data with the results for growth factor analysis shown in Table 4-2 shows lower correlation coefficients for the absorption peaks, an indication of less accurate measurements which is attributed to human error involved in absorbance peak fitting. Further comparison of slope values shown in Tables 4-2 and 5-4 yield linear correlation coefficients ≥0.92, confirming that the absorbance peak information accurately reflects the concentration of high molecular weight degradation products.

In order to compare the total loss edge (TLE) technique with absorbance peak results, changes in TLE values are plotted versus test time for all eight test series in Figure 5-12. Results for absorbance peak analysis (Figure 5-11) show that both peaks 2 and 3 reflect linear growth versus test time, whereas TLE values shown in Figure 5-12 do not hold a linear relationship. This comparison shows that the TLE values do not accurately represent the absorption data and therefore is not indicative of changes in degradation product concentration. Furthermore, initially high rates of TLE change with test time are attributed to the fact that the TLE values initially reflect base ester

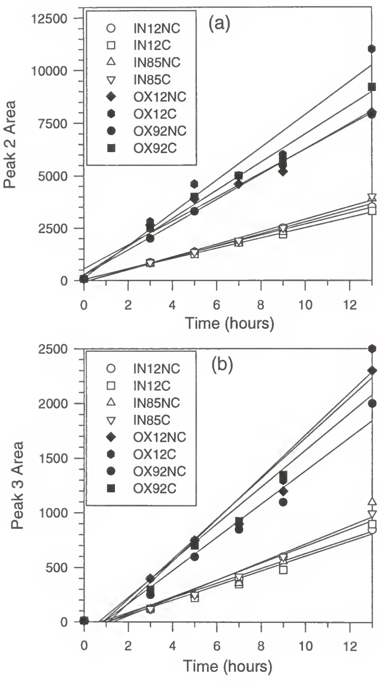

Figure 5-11. Changes in absorbance peaks 2 and 3 as a function of test time with linear regression for each test series.

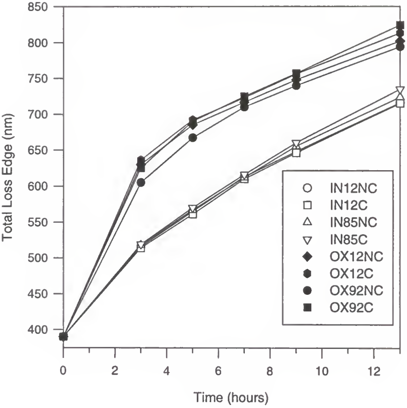

Figure 5-12. Total loss edge versus test time for degraded oil samples.

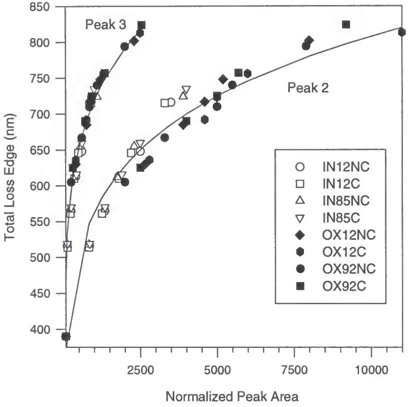

Figure 5-13. Total loss edge versus absorbing peaks 2 and 3 areas. Fitted curves reflect ($y = 190.59 \cdot x^{0.16}$) for peak 2 and ($y = 273.68 \cdot x^{0.14}$) for peak 3 with correlation coefficients of r^2=0.98 and 0.99 respectively.

absorbance properties and do not reflect degradation until the concentration of degradation species is significant.

Table 5-4. List of correlation coefficients and slopes for linear regression analysis performed on absorbance versus time plots shown in Figure 5-11.

Test ID	Peak 2: r^2	Peak 2: Slope	Peak 3: r^2	Peak 3: Slope
IN12NC	0.998	265.2	0.980	68.1
IN12C	0.998	245.9	0.951	67.7
IN85NC	0.982	286.2	0.931	82.2
IN85C	0.991	298.6	0.970	77.7
OX12NC	0.975	571.0	0.957	186.5
OX12C	0.960	779.0	0.949	184.2
OX92NC	0.990	602.1	0.970	152.0
OX92C	0.987	669.3	0.952	192.6

Direct comparison of total loss edge values with results for the two absorbance peaks is shown in Figure 5-13. Data follows the relations $y = 190.59 \cdot x^{0.16}$ for peak 2 (r^2=0.98) and $y = 273.68 \cdot x^{0.14}$ for peak 3 (r^2=0.99). Values of absorbance peaks increase at higher rates with increasing degradation in comparison to TLE values. This shows that the sensitivity of the TLE technique in measuring extent of degradation is lost as more severe degradation occurs. Also evident is the fact that changes in absorbance values for peak 2, although proportional to peak 3 (Figure 5-7), are greater with respect to peak 3 and therefore more sensitive to small changes in degradation behavior.

5.5. Conclusions

This chapter has presented data supporting the use of absorbance characteristics of synthetic oil samples to determine degradation behavior and oil condition. Two techniques have been investigated: the use of absorbance changes characteristic of the base ester and degradation products, and the use of total loss edge (TLE) values determined by the changes in absorbance peak intensities. The investigations were centered on oil samples generated at 250°C under various environments.

The changes in absorbance spectra for the oil samples were shown to be the result of changes in the behavior of three absorption peaks located at 355, 415, and 500 nm. Total loss edge values determined for the oil samples are a direct reflection of the absorbance peak which predominates for a given sample. As degradation proceeded, the 355 nm peak decreased in intensity and is thus attributed to the base esters. The absorbance of the 415 and 500 nm peaks increased with increasing degradation, thus these peaks are attributed to the degradation products. As degradation proceeds, TLE values are determined by the 355 nm peak and thus represent the base esters until the absorptivity of the degradation products predominate, at which point the TLE values are represented by the 415 and 500 nm peaks and increase at a somewhat linear rate with time. However, comparison of TLE values with absorbance changes for these three peaks has shown that changes in peak area are more representative and sensitive to changes in degradation behavior.

Further relations have been shown between the formation of the high molecular weight degradation products and changes in the absorption characteristics of peaks at 415 and 500 nm. The 415 nm peak has been attributed to an absorbance characteristic of the degradation product which reflects concentration, whereas the 500 nm peak has been attributed to an absorbance characteristic which represents product concentration and size. By relating the formation of the high molecular weight products to the formation of particulate species using the Einstein Eq. (5-4), results have shown that the relative concentration of degradation products correlated with the formation of particulate species.

In reference to using these techniques for monitoring oil condition and the extent to which degradation has proceeded, values for both the 415 and 500 nm absorbance peaks have been shown to correlate with concentration results presented in Chapter 4 for the high molecular weight degradation product. Information gained from absorbance results can be used to relate concentration and estimate mean molecular weight for the degradation products.

CHAPTER 6

CONCLUSIONS AND SUGGESTED FUTURE WORK

6.1. Overview

Increasing requirements in the performance characteristics of load bearing systems calls for a better understanding of system behavior. Specifically for applications under extreme environments, knowledge of the interactions between various components is critical. Without advances in understanding how such systems operate and fail, improvements in design and implementation are limited.

Work presented in this thesis was the direct result of endeavors motivated by the lack of understanding in the failure behavior of hybrid bearing systems utilized in gas turbine engines. The approach was specifically designed to develop a more complete understanding of performance and failure characteristics through the analysis of the lubrication systems employed with these bearings. Objectives included developing an understanding of how the lubricants degrade, determining the influences of degradation on the performance characteristics of bearing system, and developing a means of monitoring performance and predicting failure.

Oil degradation experiments were performed using Exxon turbine oil ETO 2380, a commercially available ester-based synthetic lubricant meeting military specifications MIL-L-23699. Advantages to using a conventional lubrication system include the direct application to industry. Disadvantages result from the proprietary nature of the base stock, additives, and mixing ratios, resulting in limited interpretation of chemical changes which result from degradation.

6.2. Conclusions

6.2.1. Oil Degradation and Resulting Effects on Friction and Wear

Characterization of thermally degraded samples of a conventional synthetic oil (MIL-L-23699) was performed using viscosity, spectroscopy, molecular weight, total acid number, and antioxidant content. Rheology results showed viscosity changes to be between -2.3% and 49.4% relative to the as-received oil. Results of molecular weight analysis of the samples for the most extreme testing conditions showed the formation of high molecular weight species, which were subsequently removed as test time proceeded, suggesting coking behavior. In correlation with infrared spectrometry results which showed peak broadening effects, the degradation mechanism for the system at hand could not be determined, as the formation of carboxylic acids, ketones, and esters (via transesterification) were all possible reaction products.

A linear relationship was found to exist between total loss edge values and changes in viscosity. This observation suggested that changes in the optical behavior of the oil was dependent on physical changes which result during degradation. These results initiated the investigation into the use of this technique for oil analysis and monitoring in Chapter 5.

Friction and wear testing of the previously degraded oil samples was performed in order to determine effects of oil degradation on the tribological properties of the silicon nitride/M50 steel system. Results from testing under boundary lubrication conditions showed the coefficient of friction to increase with respect to oil condition. Results for wear measurements showed no correlation between the rate of wear for both the silicon nitride and M-50 surfaces with oil condition.

6.2.2. A Kinetic Study of Oil Degradation

Results for tests designed to separate the individual effects of thermal and oxidative degradation mechanisms, as well as to determine the influence of high humidities and the effectiveness of M-50 steel as a catalyst material were performed at 250°C. For tests performed in inert (non-oxidative) environments, the presence of the M-50 steel catalyst increased and high humidity decreased the rate of antioxidant removal. Although these results were not accompanied by significant changes in viscosity and TAN values for the degraded oil samples, the limited effect of thermal degradation mechanisms on oil degradation for the various environments was determined.

Results for tests performed in oxidative environments yielded similar results. The presence of the M-50 steel catalyst material and high humidity environments showed the same trends in the oxidative atmosphere as for the reducing conditions. However, the resulting changes in viscosity, antioxidant content, total acid number, and peak area/height were more extreme, showing that the combined effects of oxidative and thermal degradation act to increase the total degradation of the oil significantly more than for thermal degradation alone.

Chemical analysis performed using FTIR showed peak broadening for the carbonyl (1743 cm^{-1}) peak, thus corresponding to the formation of new ester, carboxylic acid, and ketone structures. Changes in concentration of the ester species was not possible due to the fact that the lactone peak was not distinguishable. Furthermore, after antioxidant depletion, hydroxyl (-OH) information was generated, thus confirming that TAN results which showed carboxylic acid to be a primary degradation product. As for an overall view of the degradation process observed using this synthetic oil system and test conditions, viscosity results which show the oil samples to remain Newtonian during degradation suggests transesterification to be the dominant reaction prior to antioxidant depletion. After antioxidant is effectively removed from the oil samples, TAN and FTIR results show carboxylic acid to increase in concentration, thus suggesting the degradation of ester species into carboxylic acid species to predominate after antioxidant removal.

Analysis of volatiles recovered from the degradation tests were analyzed using FTIR and GPC. Results showed water to be a primary degradation product. Along with results from Karl Fisher experiments which showed increased water content for high humidity test environments, the formation of water as a degradation product explained how the high humidity test environments delayed the depletion of antioxidant and subsequent oil degradation: The degradation reaction, which resulted in the formation of water and depletion of antioxidant, was hindered by absorption of water by the oil in the high humidity environments.

As for the physical changes in the oil, a direct correlation between the formation of high molecular weight species and viscosity was found using the Einstein equation for Newtonian fluids containing small particles. In this manner, the high molecular weight species were shown to act as particulate materials with respect to the physical behavior of the degraded oil. Further analysis of changes in degradation product concentration and size distribution showed the reaction for the formation of these products to be diffusion limited after antioxidant depletion.

The mechanism for the formation of high molecular weight degradation products is proposed. During the initial stages of degradation, the base ester chains degrade to form primary degradation products. The process is the result of reaction with and the formation of free radical molecules which are subsequently rendered inactive by the antioxidant. Once the antioxidant is depleted, primary degradation products continue to be formed, and these products react to form secondary degradation products which are of higher molecular weight. The formation of water suggests that the primary products undergo a polycondensation reaction mechanism, where water is a byproduct. This hypothesis is supported by the fact that high humidity environments, which would place water into the system and inhibit the polycondensation reaction, were shown to reduce the rate of degradation. As for results which show diffusion to be rate limiting after antioxidant depletion, the affect is attributed to the polycondensation reaction mechanism.

6.2.3. The Use of UV/VIS Spectrometry for Oil Monitoring

The use of absorbance characteristics in determining the degradation behavior and condition of synthetic oil samples was investigated. Absorbance changes characteristic of the base ester and degradation products, and total loss edge (TLE) values generated from the transmittance spectra were compared. The investigation centered on degraded oil samples generated at 250°C under various environments.

Results showed that the changes in absorbance spectra for the oil samples was the result of changes in the intensities of absorption peaks located at 355, 415, and 500 nm. Total loss edge values determined for the oil samples were a direct reflection of the absorbance peak which predominated for a given sample. As degradation proceeded, the 355 nm peak decreased in intensity and was thus attributed to the base esters. The absorbance of the 415 and 500 nm peaks increased with increasing degradation, thus these peaks were attributed to the degradation products. As degradation proceeded, TLE values were determined by the 355 nm peak and thus represent the base esters until the absorptivity of the degradation products predominate, at which point the TLE values were represented by the 415 and 500 nm peaks. However, comparison of TLE values with absorbance changes for the three peaks showed that changes in peak area were more representative and sensitive to changes in degradation behavior.

Further relations were shown between the formation of the high molecular weight degradation products and changes in the absorption characteristics of peaks at 415 and 500 nm. The 415 nm peak was attributed to an absorbance characteristic of the degradation product which reflected concentration, whereas the 500 nm peak was attributed to an absorbance characteristic which represented product concentration and size. By relating the formation of the high molecular weight products to the formation of particulate species using the Einstein relation (Eq. (5-4)), results showed that the relative concentration of degradation products correlated with the formation of particulate species.

In reference to implementing UV/VIS absorption spectrometry for monitoring oil condition and the extent to which degradation proceeds, values for the 415 and 500 nm absorbance peaks have been shown to directly related to the concentration of high molecular weight degradation product. Also shown was that information gained from absorbance results could be used to predict degradation product concentration and estimate mean molecular weight for the degradation products.

6.3. Suggested Future Work

Results presented in this study yield an understanding as to how degradation of synthetic oil lubricants affects the performance of the silicon nitride/M-50 steel system, how degradation of the lubricants affects by test environment, and how the absorption characteristics of the degradation products may be used to predict oil condition. Many questions still remain unanswered, and this section discusses future endeavors which may be undertaken.

6.3.1. Effects of Oil Degradation on Wear Properties

Results for experiments on the wear behavior of the silicon nitride/M-50 steel system with degraded oil lubricants showed no correlation to oil condition. However, measurement of wear for the disk surfaces was limited by the low rate of wear for the silicon nitride/M-50 steel sliding couple and time limitations for test runs. In order to determine more accurate data for these systems, rolling contact fatigue (RCF) testing may be implemented. This test method would allow for much higher rates of wear and result in more accurate wear measurements. Furthermore, since RCF testing reflects elastohydrodynamic lubrication conditions, further analysis of the physical changes which occur during oil degradation can be measured by testing oil samples with varying viscosities, thus controlling the thickness of the separatory film between raceway and rolling element.

6.3.2. Confirmation of Polycondensation Reaction Mechanism

The formation high molecular weight degradation product after antioxidant depletion has been hypothesized as a polycondensation reaction mechanism. Confirmation of this reaction mechanism, as well as the identification of methods for hindering the reaction, is a significant contribution to the scientific community.

In order to confirm the polycondensation reaction mechanism, identification of the degradation products must be achieved. Since synthetic lubricants are composed of multiple base esters and complex additive packages, analysis would have to include separation of oil constituents and degradation products using a method such as high performance liquid chromatography (HPLC). Identification of individual compounds could then be performed using a combination of techniques such as nuclear magnetic resonance spectrometry (NMR), gas chromatography (GC) with mass spectrometry, and infrared spectrometry.

Further experimental analysis of oil degradation mechanisms may be accomplished by comparing the performance of branched versus non-branched ester molecules. Carbon atoms located at the branch points are most susceptible to free radical and carbon-carbon scission attack [Jon85a,Jon85b]. Once decomposed into primary degradation products, secondary products formed by polycondensation mechanisms can be generated. Comparing degradation behavior and product formation of branched esters to those for non-branched esters may allow for the understanding of how to prevent degradation by eliminating materials susceptible to the initial degradation mechanisms.

As for the identification of methods for preventing the polycondensation reaction mechanism in a lubricant, only one avenue exists. Development of additives which hinder the condensation reaction between primary degradation products would allow for better control of oil breakdown. An example condensation reaction between two primary degradation products is as follows [Bak92]:

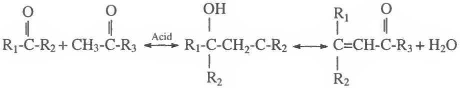

$$R_1\text{-}\overset{O}{\overset{\|}{C}}\text{-}R_2 + CH_3\text{-}\overset{O}{\overset{\|}{C}}\text{-}R_3 \xleftrightarrow{\text{Acid}} R_1\text{-}\underset{\underset{R_2}{|}}{\overset{\overset{OH}{|}}{C}}\text{-}CH_2\text{-}C\text{-}R_2 \longleftrightarrow \underset{\underset{R_2}{|}}{\overset{\overset{R_1}{|}}{C}}\text{=}CH\text{-}\overset{O}{\overset{\|}{C}}\text{-}R_3 + H_2O$$

[6.1]

Any additive which would act to retard this reaction would have to protect the carbonyl groups from acid attack (i.e., solvolysis) [Sch81]. As this type of attack only occurs in neutral to acidic environments ($pH \leq 7$), one such means of preventing the reaction would be to maintain a pH greater than 7.

6.3.3. UV/VIS Absorption Spectrometry for Oil Monitoring

In order to determine if UV/VIS spectrometry can be implemented as a method for the in-situ testing of lubrication systems, further experiments must be performed in order to confirm that the behavior reported in Chapter 5 is followed for all oils under more representative operating conditions. Each synthetic oil, designated by military grade and vendor, contains significantly different additive packages which influence lubricant behavior and lifetime. The use of UV/VIS spectrometry must be confirmed for multiple oil systems, under experimental conditions which more accurately reflect turbine engine environments.

6.4. Summary

Investigations into the degradation behavior of synthetic lubricants used in hybrid bearing systems have been performed. Analysis has included determination of changes in the performance characteristics of the silicon nitride/M-50 steel system with lubricant degradation, and analysis of ultraviolet/visible absorption spectrometry as a technique for oil monitoring.

Results have yielded a better insight into the behavior and interactions of the components in hybrid bearing systems. Although many questions such as the exact degradation reactions and associated products have not been answered, the general effects of various operating conditions on the rate of oil degradation and formation of degradation products have been shown. Furthermore, results from the investigation into using absorption spectrometry for oil analysis have demonstrated that this technique can be used for oil condition monitoring.

LIST OF REFERENCES

Aja92	Ajayi, O.O., Erdemir, A., Hsieh, J.H., Erck, R.A., and Fenske, G.R., "Combined Solid and Liquid Lubrication of Silicon Nitride under Boundary Conditions," Lubrication Engineering, 48, 7, 584-591, 1992.
Aka90	Akagaki, T. and Kato, K., "Effects of Hardness on the Wear Mode Diagram in Lubricated Sliding Friction of Carbon Steels," Wear, 141, 1-15, 1990.
And84	Andrievskii, R.A., and Leontev, M.A., "Phase Composition and Infrared Spectra of Silicon Nitride Powders," Izvestiya Akademii Nauk SSSR, Neorganicheskie Materialy, 20, 12, 2053-2055, 1984.
Ara88	Aramaki, H., Shoda, Y., Morishita, Y., and Sawamoto, T., "The Performance of Ball Bearings With Silicon Nitride Ceramic Balls in High Speed Spindles for Machine Tools." Journal of Tribology, 110, 693-698, 1988.
Bak92	Bakunin, V.N., and Parenago, O.P., "A Mechanism of Thermo-Oxidative Degradation of Polyol Ester Lubricants," Journal of Synthetic Lubrication, 9, 2, 127-143, 1992.
Bel86	Belman, H.M., "Oil Debris Monitoring," Avionics Magazine, February 1986.
Ber89	Bergstrom, L., and Pugh, R.J., "Interfacial Characterization of Silicon Nitride Powders," Journal of the American Ceramic Society, 72, 1, 1989.
Ber90	Bergstrom, L., and Bostedt, E., "Surface Chemistry of Silicon Nitride Powders: Electrokinetic Behavior and ESCA Studies," Colliods and Surfaces, 49, 183-197, 1990.
Bla92	Blau, P.J., "Effects of Surface Preparation on the Friction and Wear Behavior of Silicon Nitride/Silicon Carbide Sliding Pairs," Journal of Materials Science, 27, 4732-4740, 1992.

Boh93	Bohmer, H.J., "Residual Stresses and Material Behavior of M50NiL and RBD," Creative Use of Bearing Steels, ASTM STP 1195, J.J.C. Hoo, Ed., American Society for Testing and Materials, Philadelphia, 34-48, 1993.
Bra92	Braza, J.F., "Rolling Contact Fatigue and Sliding Wear Performance of Ferritic Nitrocarburized M-50 Steel," Tribology Transactions, 35, 1, 89-97, 1992.
Braz89	Braza, J.F., and Fine, M.E., "Silicon Nitride Wear Mechanisms: Rolling and Sliding Contact," Tribology Transactions, 32, 4, 439-446, 1989.
Bro90	Brown, S.F., "21st Century Hot Jet Engines," Popular Science, 83-89, June 1990.
But90	Bunting, R.G., "Wear in Dry-Lubricated, Silicon Nitride, Angular Contact Ball Bearings," Lubrication Engineering, 46, 11, 745-751, 1990.
Car86	Carre, D.J., "Perfluoropolyalkylether Oil degredation: Inference of FeF3 Formation on Stel Surfaces under Boundary Lubrication," ASLE Transactions, 29, 2, 121-125, 1986.
Coa86	Coates, J.P., and Setti, L.C., "Infrared Spectroscopy as a Tool for Monitoring Oil Degradation," Aspects of Lubricant Oxidation, ASTM STP 916, W.H. Stadtmiller and A.N. Smith, Eds., American Society for Testing and Materials, Philadelphia, 57-78, 1986.
Cra88	Cranmer, D.C., "Wear Surface Analysis of Silicon Nitride," Lubrication Engineering, 44, 12, 975-980, 1988.
Dan91	Danyluk, S., Park, D.S., and McNallan, M., "Scanning Electron Microscopy of Tribochemical Films on Si_3N_4 to H_2O at High Temperatures," Ultramicroscopy, 37, 239-246, 1991.
Del94	Del Pesco, T., "Perfluoroalkylpolyethers," CRC Handbook of Lubrication and Technology, Volume III, Booser, E.R., CRC Press, Boca Raton, Florida, US, 287-303, 1994.
Den95	Denape, J., Masri, T., and Petit, J-A., "Influence of Surface Roughness and Oil Aging on Various Ceramic-Steel Contacts Under Boundary Lubrication," Journal of Engineering Tribology, 209, 173, 182, 1995.
Dup95	"Dupont Preformance Lubricants, Krytox®,", E.I. du Pont de Nemours and Company, Deleware, 1995.

Ein56	Einstein, A., "Investigations on the Theory of the Brownian Movement, " Dover Publications, Inc., USA, 1956.
Fag90	FAG Kugelfischer Georg Schafer KGaA, "High-Performance Ceramics in FAG Rolling Bearings, " Publ. No. WL 40 204 EA, 1990.
Fei92	Fein, Richard S., "Liquid Lubricants," ASM Handbook Volume 18, Friction, Lubrication, and Wear Technology, ASM International, 81-88, 1992.
Fie50	Fieser, L.F. and Fieser, M., "Organic Chemistry," D. C. Heath and Company, New York, 1950.
Gala95	Galassi, C., Rastelli, E., Roncari, E., Ardizzone, S., and Cattania, M.G., "Characterization and Stabilization of Si_3N_4 Suspensions," J. Mater. Res., 10, 2, 339-344, 1995.
Galb92	Galbato, A.T., Cundill, R.T., and Harris, T.A., "Fatigue Life of Silicon Nitride Balls," STLE Preprint No. 92-Am-8A-2.
Gat91	Gates, R.S., and Hsu, S.M., "Effect of Selected Chemical Compounds on the Lubrication of Silicon Nitride," Tribology Transactions, 34, 417-425, 1991.
Gee94	Gee, M.G., "Wear Testing and Ceramics," Journal of Engineering Tribology, 208, 153-166, 1994.
Gen94	Gentle, C.R., "Bearings with Ceramic Balls - The Effect of Reduced Lubricant Supply on the Minimum Load," Prec. Instn. Mech. Engrs., 20, 253-256, 1994.
God95	Goddard, K.N., and Maisaac, B.D., "The Use of Oil Born Debris as a Failure Criterion for Roller Element Bearings," Lubrication Engineering, 51, 6, 481-487, 1995.
Gun62	Gunderson, R. C., and Heart, A. W., "Synthetic Lubricants," Reinhold Publishing Corporation, New York, 1962.
Ham85	Hamrock, B.J., "Elastrohydrodynamic Lubrication - Status of Understanding," New Directions in Materials, Wear, and Surface Interactions, Tribology in the 80's, Edited by W. R. Loomis, Noyes Publications, 484-505, 1985.
Ham94	Hamrock, B.J., "Fundamentals of Fluid Film Lubrication," McGraw-Hill, Inc., New York, 1994.

Han88 Hannoosh, J.G., "Ceramic Bearings Enter the Mainstream, A growing need for tougher bearings prompts two U.S. companies to produce non-metallic rolling elements that can take the heat," Design News, 224-227, November 21, 1988

Hie84 Hiemenz, P.C., Polymer Chemistry, Marcel Dekker Inc., New York, 1984.

Hos91 Hosang, G.W., "Experimental and Computed Performance Characteristics of High-Speed Silicon Nitride Hybrid Ball Bearings," Journal of Engineering for Gas Turbnes and Power, 113, 635-643, 1991.

Hsu86 Hsu, S.M., Ku, C.S., and Pei, P.T., "Oxidative Degradation Mechanisms of Lubricants," Aspects of Lubricant Oxidation, ASTM STP 916, W.H. Stadtmiller and A.N. Smith, Eds., American Society for Testing and Materials, Philadelphia, 27-48, 1986.

Hun93a Hunter, M., Klaus, E.E., and Duda, J.L., "A Kinetic Study of Antioxidant Mechanisms," Lubrication Engineeering, 49, 6, 492-498, 1993.

Hun93b Hunter, R.J., "Foundations of Colloid Science Volume I," Oxford University Press Inc., New York, 1993.

Jac91 Jackson, A., "Elastrohydrodynamic Lubrication (EHL)," Lubrication Engineering, 833-835, 1991.

Jah94 Jahanmir, S., "Advanced Ceramics in Tribological Applications," Friction and Wear of Ceramics, Ed. Jahanmir, S., Marcel Dekker, Inc., 3-12, 1994.

Jon85a Jones, W.R. Jr, "Thermal and Oxidative Stabilities of Liquid Lubricants," New Directions in Lubrication, Materials, Wear, and Surface Interactions, Tribology in the 80's," Loomis, W.R. Jr, Ed., Noyes Publications, 1985.

Jon85b Jones, W.R., "The Furture for Liquid Lubricants and Additives, Thermal and Oxidative Stabilities of Liquid Lubricants," New Directions in Lubrication, Materials, Wear, and Surface Interactions, Tribology in the 80's," Ed. Loomis, W.R., Noyes Publications, Park Ridge, NJ, 810-813, 1985.

Kas91a Kasai, P.H., Tang, W.T., and Wheeler, P., "Degradation of Perfluoropolyethers Catalyzed by Aluminum Oxide," Applied Surface Science, 51, 201-211, 1991.

Kas91b Kasai, P.H., and Wheeler, P., “Degradation of Perfluoropolyethers Catalyzed by Aluminum Chloride,” Applied Surface Science, 52, 91-106, 1991.

Kas92 Kasai, P.H., “Perfluoropolyethers: Intramolecular Disproportionation,” Macromolecules, 25, 6791-6799, 1992.

Kat90 Kato, K. “Tribology in Ceramics,” Wear, 136, 117-133, 1990.

Kau85 Kauffman, R.E., Saba, C.S., Rhine, W.E., and Eisentraut, K.J., “Chemical Nature of Wear Debris,” ASLE Transactions, 28, 3, 400-406, 1985.

Kau89 Kauffman, R.E., “Developement of a Remaining Useful Life of a Lubricant Evaluation Technique. Part III: Cyclic Voltammetric Methods,” Lubrication Engineering, 45, 11, 709-716, 1995.

Kau95a Kauffman, R.E., “On-Line and Off-Line Techniques for Monitoring the Thermal and Oxidative Degradations of Aircraft Turbine Engine Oils - Part I: Laboratory Evaluations,” Lubrication Engineering, 51, 11, 914-921, 1995.

Kau95b Kauffman, R.E., “Remaining Useful Life Measurements of Deisel Engine Oils, Automotive Engine Oils, Hydraulic Fluids, and Greases Using Cyclic Voltammetric Methods,” Lubrication Engineering, 51, 3, 223-229, 1995.

Kir85 Kirk-Othmer, Concise Encyclopedia of Chemical Technology, John Wiley & Sons, New York, 708, 1985.

Kla85 Klaus, E.E., ”Status of New Directions of Liquid Lubricants,” New Directions in Materials, Wear, and Surface Interactions, Tribology in the 80’s, William R. Loomis, Noyes Publications, 354-375, 1985.

Kla91 Klaus, E.E., Duda, J.L., and Wu, W.T., “Lubricated Wear of Silicon Nitride,” Lubrication Engineering, 47, 8, 679-684, 1991.

Kop75 Kopylova, V.P., and Nazarchuk, T.N., “Chemical Stability of Silicon Nitride and Oxynitride Powders,” Poroshkovaya Metallurgiya, 10, 154, 38-43, 1975.

Lin94 Lin, J.F., and Chen, Y.N., “Tribological Reaction Generated on Ceramic-Stellite Couples Under Dry Sliding Contact and Water- and Oil-Lubricated Conditions,” Wear, 177, 139-149, 1994.

Loc92 Lockwood, F.E., Dalley, R., "Lubricant Analysis," ASM Handbook Volume 18, Friction, Lubrication, and Wear Technology, ASM International, 299-312, 1992.

Luc92 Lucek, J.W., and Hannoosh, J.G., "Field Experience in Ceramic Bearings," Cerbec, Inc., East Granby, CT, 1992.

Lut94 Luther, E.P., Kramer, T.M., Lange, F.F., and Pearson, D.S., "Developement of Short-Range Repulsive Potentials in Aqueous, Silicon Nitride," Journal of the American Ceramic Society, 77, 4, 1047-51, 1994.

Lyc91 Lyckfeldt, O., Bostedt, E., Persson, M., and Carlsson, R., "Stabilization and Slip Casting of Silicon and Silicon Nitride in a Non-Aqueous Media," Ceramics Today - Tomarrow's Ceramics, 1991.

Mat86 "Materials Characterization," Metals Handbook Ninth Edition, 10, American Society for Metals, 1986.

Mor89 Mori, S., and Morales, W., "Tribological Reaction of Perfluoroalkyl Polyether Oils with Stainless Steel Under Ultrahigh Vacuum Conditions at Room Temperature," Wear, 132, 111-121, 1989.

Ove82 Overbeek, J.Th.G., "Monodisperse Colloidal Systems, Fascinating and Useful," Advances in Colloid and Interface Science, 15, 251-277, 1982.

Pac89 Pachuta, D.G., Thich, J.A., Knipple, R.W., and Stephanic, D.A., "Experiences with an Analytical Montioring Program Designed for Commercial Flight Tests of Advanced Mil-23699 Turbine Fluids," Turbine Oil Monitoring, ASTM STP 1021, W.C. Young and R.S. Robertson, Eds., American Society for Testing and Materials, Philadelphia, 1989, 54-76, 1989.

Par75 Park, D.S., Danyluk, S., and McNallan, M.J., "Influence of Tribochemical Reaction Products on Friction and Wear of Silicon Nitride at Elevated Temperatures in Reactive Environments," Journal of the American Ceramic Society, 75, 11, 3033-3039, 1992.

Pow93 Powel, J. R.,Compton, D. A. C., "Automated FTIR Spectrometry for Monitoring Hydrocarbon-Based Engine Oils," Lubrication Engineering, 49, 3, 233-239, March 1993.

Rab80 Rabek, J.F., "Experimental Methods in Polymer Chemistry, " John Wiley & Sons, New York, 1980.

Sch81 Schnabel, W., "Polymer Degradation, Principles and Practical Applications," Macmillan Publishing Co., Inc., New York, 1981.

Sei72 Seifert, W.W., and Westcott, V.C., "A method for the Study of Wear Particles in Lubricating Oil," Wear, 21, 1972, 27-42, 1972.

Sek92 Seki, K., and Nishimura, M., "Lubrication Characteristics of Oils and Greases Applied to Ball Bearings for Use in Vacuo," Journal of Synthetic Lubricants, 9, 1, 17-21, April 1992.

Sha94 Shankwalker, S., and Placek, D., "Oxidation Kinetics of Tricresyl Phosphate (TCP) Using Differential Scanning Calorimetry (DSC)," Lubrication Engineer, 50, 3, 261-264, 1994.

Sil81 Silverson, R.M., Bassler, G.C., and Morrill, T.C., "Spectrometric Identification of Organic Compounds," John Wiley & Sons, 1981.

Sil91 Silverson, R.M., Bassler, G.C., and Morrill, T.C., "Spectrometric Identification of Organic Compounds," John Wiley & Sons, 1991.

Sil90 "Silicon Nitride for High-Performance Bearings," Ceramic Bulletin, 69, 7, 1990, 1113-1115, 1990.

Sli92 Sliney, Harold E., "Solid Lubricants," ASM Handbook Volume 18, Friction, Lubrication, and Wear Technology, ASM International, 113-122, 1992.

Sli94 Sliney, H.E., and Dellacorte, C., "The Friction and Wear of Ceramic/Ceramic and Ceramic/Metal Combinations in Sliding Contact," Lubrication Engineering, 50, 7, 571-576, 1994.

Ste89 Steinfeld, J.I., Francisco, J.S., and Hase, W.L., "Chemical Kinetics and Dynamics," Prentice Hall, New Jersey, 1989.

Ste90 Steinmann, D., "Silicon Nitride Ceramics for Balls and Ball Bearings," Cfi/Ber. DKG, 67, 12, 1990.

Uni88 United Technologies Pratt & Whitney, "The Aircraft Gas Turbine Engine and its Operation," Part No. P&W 182408, August 1988.

Wak74 Wakelin, R.J., "Tribology: The Friction, Lubrication, and Wear of Moving Parts," Annual Reveiw of Materials Science, Huggins, R.A., Bube, R.H., and Roberts, R.W., Eds., 4, 1974.

Wed87 Wedeven, L. D., and Harris, T. A., "Rolling Element," Machine Design, 72-76, August 1987.

Yao95 Yao, D. and Shang, J.K., "Lubricant Enhanced Fatigue Crack Growth in Silicon Nitride," Tribology Transactions, 38, 4, 973-979, 1995.

Zut94 Zutshi, A., Haber, R.A., Niesz, D.E., Adams, J.W., Wachtman, J.B., Ferber, M.K., and Hsu, S.M., "Processing, Microstructure, and Wear Behavior of Silicon Nitride Hot-Pressing with Alumina and Yttria," Journal of the American Ceramic Society, 77, 4, 883-890, 1994.

BIOGRAPHICAL SKETCH

Robert Sabia was born on October 19, 1970 in Red Bank, New Jersey, to Regina and Raffaele Sabia. Though raised in Atlanta, Georgia, his undergraduate career was spent in New Jersey at Rutgers University's College of Engineering, where he majored in ceramic engineering. After graduating with his bachelors degree in May of 1993, the author began his graduate studies in materials science and engineering at the University of Florida. He is currently a member of the American Ceramic Society and the Society for Tribologists and Lubrication Engineers.

I certify that I have read this study and that in my opinion it conforms to acceptable standards of scholarly presentation and is fully adequate, in scope and quality, as a dissertation for the degree of Doctor of Philosophy.

James H. Adair, Chair
Associate Professor of Materials Science and Engineering

I certify that I have read this study and that in my opinion it conforms to acceptable standards of scholarly presentation and is fully adequate, in scope and quality, as a dissertation for the degree of Doctor of Philosophy.

Paul H. Holloway
Professor of Materials Science and Engineering

I certify that I have read this study and that in my opinion it conforms to acceptable standards of scholarly presentation and is fully adequate, in scope and quality, as a dissertation for the degree of Doctor of Philosophy.

John J. Mecholsky, Jr.
Professor of Materials Science and Engineering

I certify that I have read this study and that in my opinion it conforms to acceptable standards of scholarly presentation and is fully adequate, in scope and quality, as a dissertation for the degree of Doctor of Philosophy.

E. Dow Whitney
Professor of Materials Science and Engineering

I certify that I have read this study and that in my opinion it conforms to acceptable standards of scholarly presentation and is fully adequate, in scope and quality, as a dissertation for the degree of Doctor of Philosophy.

James D. Winefordner
Graduate Research Professor of Chemistry

This dissertation was submitted to the Graduate Faculty of the College of Engineering and to the Graduate School and was accepted as partial fulfillment of the requirements for the degree of Doctor of Philosophy.

May, 1997

Winfred M. Phillips
Dean, College of Engineering

Karen A. Holbrook
Dean, Graduate School